COMILLAS
UNIVERSIDAD PONTIFICIA
ICAI

GRADO EN INGENIERÍA EN TECNOLOGÍAS INDUSTRIALES

TRABAJO FIN DE GRADO

DISEÑO Y SIMULACIÓN DE UN CHASIS MONOCASCO PARA UN COCHE DE FORMULA STUDENT

Autor: Miguel Ángel Medina Lazcano
Director: Ángel Rubio López

Madrid

Declaro, bajo mi responsabilidad, que el Proyecto presentado con el título

Diseño y simulación de un chasis monocasco para un coche de Formula Student

en la ETS de Ingeniería - ICAI de la Universidad Pontificia Comillas en el

curso académico 2024/25 es de mi autoría, original e inédito y

no ha sido presentado con anterioridad a otros efectos.

El Proyecto no es plagio de otro, ni total ni parcialmente y la información que ha sido

tomada de otros documentos está debidamente referenciada.

Fdo.: Miguel Ángel Medina Lazcano Fecha: ……/ ……/ ……

Autorizada la entrega del proyecto

EL DIRECTOR DEL PROYECTO

Fdo.: Ángel Rubio López Fecha: 16 / Enero / 2026

COMILLAS
UNIVERSIDAD PONTIFICIA
ICAI

GRADO EN INGENIERÍA EN TECNOLOGÍAS INDUSTRIALES

TRABAJO FIN DE GRADO

DESIGN AND SIMULATION OF A MONOCOQUE CHASSIS FOR A FORMULA STUDENT CAR.

Autor: Miguel Ángel Medina Lazcano

Director: Ángel Rubio López

Madrid

Agradecimientos

Me gustaría agradecer al ISC FS Racing Team por el apoyo y lo que me ha ayudado a crecer. También a mi familia por apoyarme y a Angel Rubio por ayudarme a hacer este trabajo posible.

DISEÑO Y SIMULACIÓN DE UN CHASIS MONOCASCO PARA UN COCHE DE FORMULA STUDENT

Autor: Medina Lazcano, Miguel Ángel.
Director: Rubio López, Ángel.
Entidad Colaboradora: ICAI – Universidad Pontificia Comillas

RESUMEN

Este Proyecto ha sido desarrollado en colaboración con el equipo ISC FS Racing Team. En la competición de Formula Student, los equipos diseñan, fabrican y compiten con coches tipo formula. Este Proyecto muestra el diseño de un chasis monocasco. El objetivo es enfocarse en la optimización del laminado del material compuesto de un chasis base. El proceso de optimización consigue reducir la masa del chasis actual del equipo en un total de 19kg aproximadamente y doblando la rigidez torsional a 4000 Nm /deg

Palabras clave: chasis, rigidez, dinámica, simulación, estructura

1. **Introducción:**

   El chasis es la estructura principal del coche, protege al piloto de colisiones y aloja todos los componentes del coche. En este proyecto se realiza el diseño y la simulación de un chasis monocasco utilizando Altair Hypermesh como herramienta. Los conocimientos adquiridos, así como los resultados del proyecto, servirán al equipo ISC FS Racing Team en temporadas futuras en el Desarrollo del chasis del equipo.

   El objetivo principal es crear un monocasco virtual ligero y rígido en el poco tiempo en el que la temporada de Formula Student deja para diseñar un chasis. El proyecto se completará en la primera mitad del semestre y no implicará ningún proceso de fabricación. El objetivo técnico es reducir la masa a la mitad y doblar la rigidez torsional. En la Figura 1 se puede observar la diferencia entre un chasis tubular y un monocasco de fibra de carbono, ambos plantean distintos enfoques al diseño que se tendrán en cuenta.

Figura 1. Superposición de un chasis tubular y un monocasco

2. Metodología

El monoplaza actual del ISC FS Racing Team, el IFS-07 de la temporada 2024-2025, lleva un chasis tubular de acero el cual pesa unos 38,5 kg y tiene una rigidez torsional de alrededor de 2300 Nm/deg. Estos parámetros serán claves para posteriormente analizar la mejora del diseño y de las simulaciones. El monocasco estará formado a partir de estructuras a modo sándwich con pieles o *plies* de fibra de carbono y un núcleo de honeycomb de aluminio.

Antes de empezar con el proceso de simulación, se diseña el chasis en función de la normativa de Formula Student [1]. El diseño final (Figura 2) tiene en cuenta las limitaciones establecidas por la normativa y las especificaciones técnicas establecidas por componentes como la suspensión [2] y la batería.

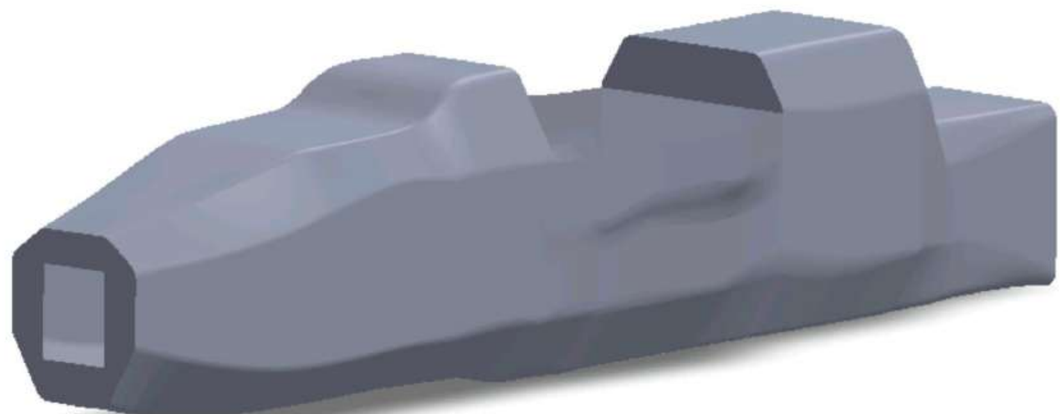

Figura 2. Diseño final del chasis

3. Proceso de simulación

El proceso de simulación combina dos pasos. Un primer paso de optimización de las capas de fibra de carbono, en el cual se consigue la forma óptima de cada capa en función de los esfuerzos y el orden del laminado, se puede observar en la Figura 2 un resultado de las simulaciones. En la Segunda parte, se analiza el laminado comprobando que cumple con los requerimientos que establece la normativa. Además, se estudia la teoría de los laminados de materiales compuestos para tener un entendimiento completo sobre su funcionamiento y el cálculo de los mismos.[3]

Figura 3. Ejemplo del resultado de la optimización

4. Resultado

El proceso de optimización consigue obtener los objetivos deseados. El laminad final consigue un monocasco optimizado de 19,78 kg y una rigidez torsional de 4089 Nm/deg según las simulaciones. Estos resultados representan una mejora considerable sobre los parámetros base que se extrajeron del ISC IFS-07 (Figura 4), sobre los cuales se ha reducido en un 48,7% y se consigue aumentar la rigidez torsional del 77,7%.

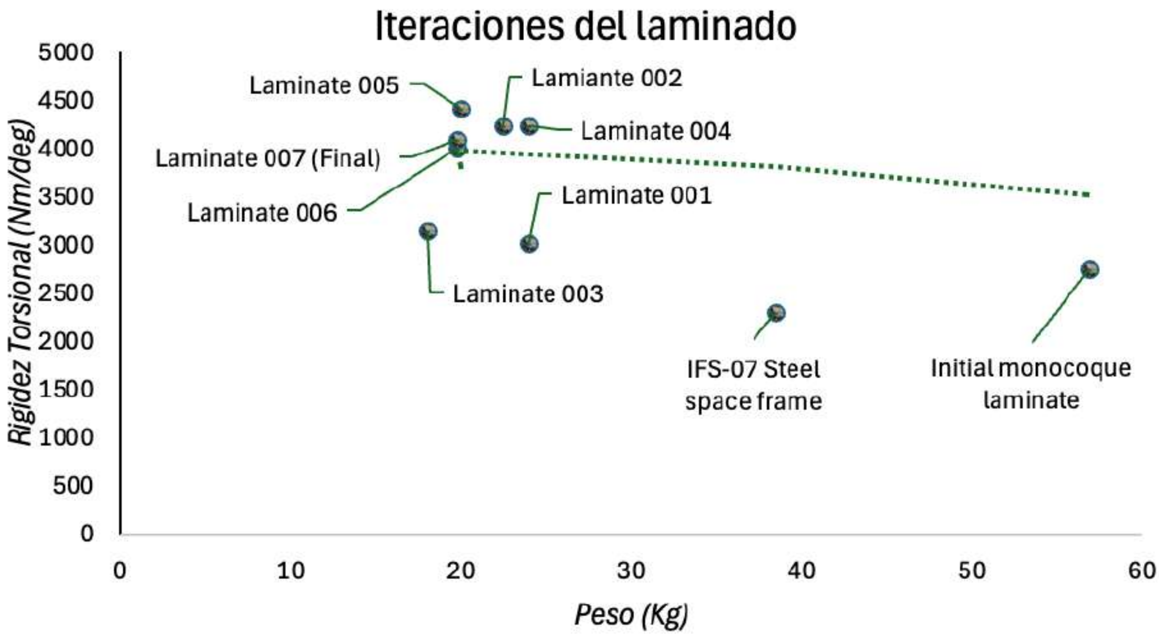

Figura 4. Resultado de las iteraciones de laminados.

La mejora dinámica del chasis se obtiene gracias al laminado optimizado. El laminado está compuesto por 31 capas distribuidas con 7 tipos de formas distintos como se puede observar en la Figura 5.

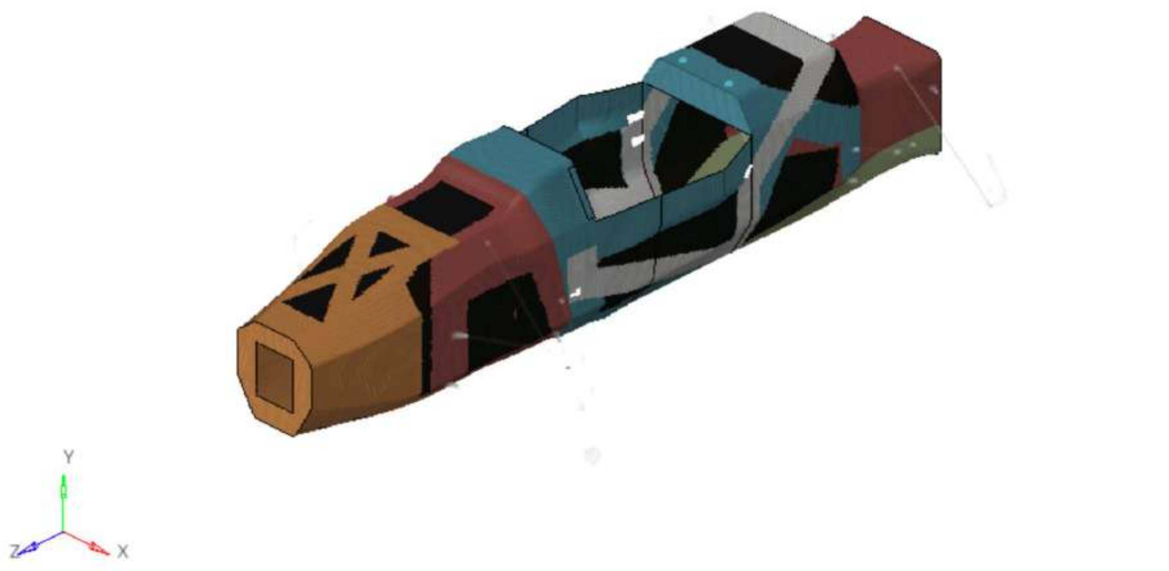

Figura 5. Distribución final del laminado

5. Conclusiones

Este proyecto muestra el flujo de trabajo del diseño de un monocasco de Formula Student. La aplicación de la teoría de los materiales compuestos junto con procedimientos de optimización ha permitido el desarrollo de una estructura que cumple con los requisitos y objetivos propuestos al inicio del proyecto.

El proyecto demuestra la capacidad para implementar la optimización del laminado a una de las piezas más importantes del monoplaza. Además, este trabajo necesitará una evaluación para determinar la viabilidad de laminado desde el punto de vista de la fabricabilidad, dado a que no se ha realizado un estudio intensivo de este aspecto, aunque se ha tenido en cuenta a la hora de realizar la forma de las capas y el diseño de este.

6. Referencias

[1]«Formula Student Rules 2026, Version: 1.1, Rev-15f99a7». Disponible en: https://www.formulastudent.de/fileadmin/user_upload/all/2026/rules/FS-Rules_2026_v1.1.pdf

[2]W. F. Milliken y D. L. Milliken, *Race car vehicle dynamics*. en R, no. 146. Warrendale, PA: Society of Automotive Engineers Internat, 1995.

[3]A. K. Kaw, *Mechanics of composite materials*, 2. ed. en Mechanical engineering series, no. 29. Boca Raton, FL: CRC Taylor & Francis, 2006.

DESIGN AND SIMULATION OF A MONOCOQUE CHASSIS FOR A FORMULA STUDENT CAR.

Author: Medina Lazcano, Miguel Ángel.
Supervisor: Rubio López, Ángel.
Collaborating Entity: ICAI – Universidad Pontificia Comillas)

ABSTRACT

This Project has been developed in collaboration with the ISC FS Racing Team. In the Formula Student competition, teams design, manufacture, and compete with formula-type cars. This Project shows the design of a monocoque chassis. The objective is to focus on the optimization of the composite material laminate of a base chassis. The optimization process manages to reduce the mass of the team's current chassis by a total of approximately 19 kg and doubling the torsional stiffness to 4000 Nm/deg.

Keywords: Bluetooth, Mobile, Indoor

1. **Introduction:**

The chassis is the main structure of the car, protects the driver from collisions, and houses all the components of the car. In this project, the design and simulation of a monocoque chassis are carried out using Altair Hypermesh as a tool. The knowledge acquired, as well as the results of the project, will serve the ISC FS Racing Team in future seasons in the development of the team's chassis.

The main objective is to create a lightweight and rigid virtual monocoque in the short time that the Formula Student season allows to design a chassis. The project will be completed in the first half of the semester and will not involve any manufacturing process. The technical objective is to reduce the mass by half and double the torsional stiffness. Figure 5 shows the difference between a tubular chassis and a carbon fibre monocoque, both of which represent different design approaches that will be considered.

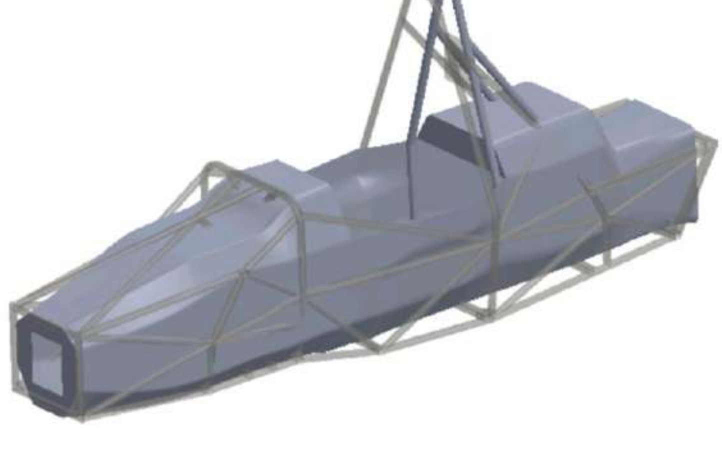

Figure 5. Overlay of a tubular steel frame and the monocoque.

2. Methodology

The current single-seater of the ISC FS Racing Team, the IFS-07 from the 2024–2025 season, features a steel tubular chassis that weighs approximately 38.5 kg and has a torsional stiffness of around 2300 Nm/deg. These parameters will be key for subsequently analyzing the improvement of the design and the simulations. The monocoque will be formed from sandwich-type structures with carbon fiber skins or plies and an aluminum honeycomb core.

Before starting the simulation process, the chassis is designed according to the Formula Student regulations [1]. The final design considers the limitations established by the regulations and the technical specifications set by components such as the suspension [2] and the battery.

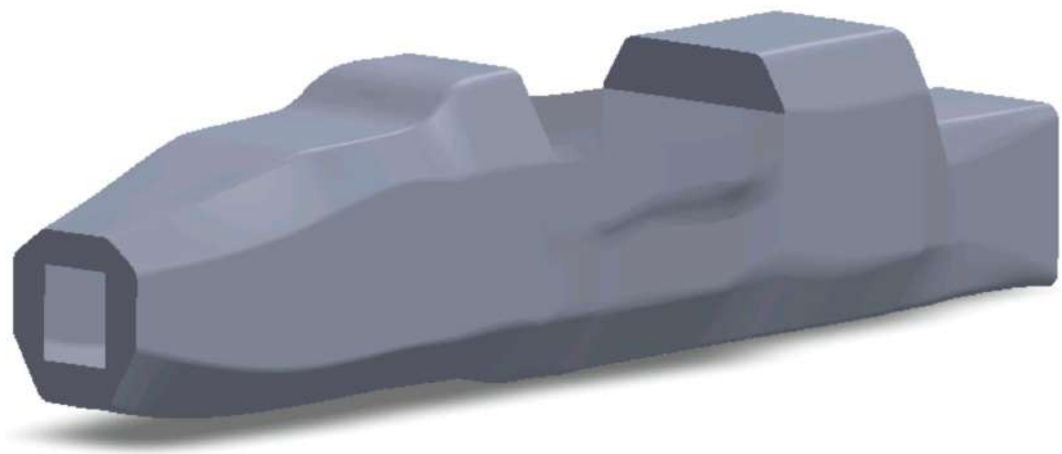

Figure 6. Final chassis design

3. Simulation process

The simulation process combines two steps. A first step of optimization of the carbon fiber layers, in which we obtain the optimal shape of each layer as a function of the loads and the layup sequence, a result of the simulation can be observed in Figure 6. In the second part, the laminate is analyzed by checking that it meets the requirements established by the regulations. In addition, composite laminate theory is studied to have a complete understanding of their behavior and their calculation [3].

Figure 6. Example of the optimization result

4. Results

The optimization process manages to achieve the desired objectives. The final laminate results in an optimized monocoque of 19.78 kg and a torsional stiffness of 4089 Nm/deg. These results represent a considerable improvement over the baseline parameters extracted from the ISC IFS-07 (Figure 7), with a mass reduction of 48.7% and an increase in torsional stiffness of 77.7%.

The dynamic improvement of the chassis is obtained thanks to the achieved laminate. The laminate is composed of 31 layers distributed with 7 types of layer shapes.

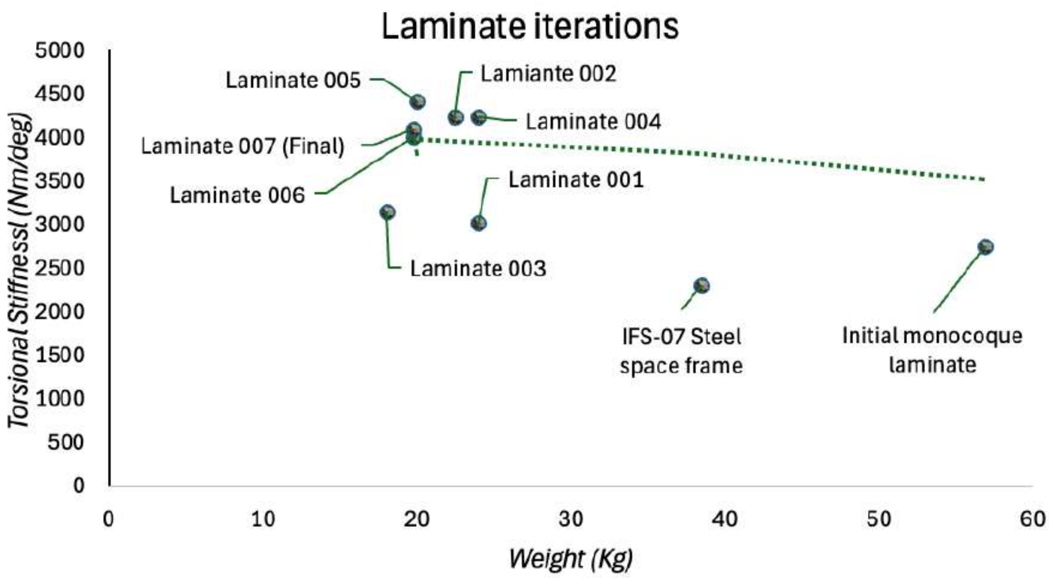

Figure 7. Laminate iteration results

The dynamic improvement of the chassis is achieved because of the optimized laminate. The laminate is composed of 31 plies distributed in 7 different layup types as shown in Figure 8.

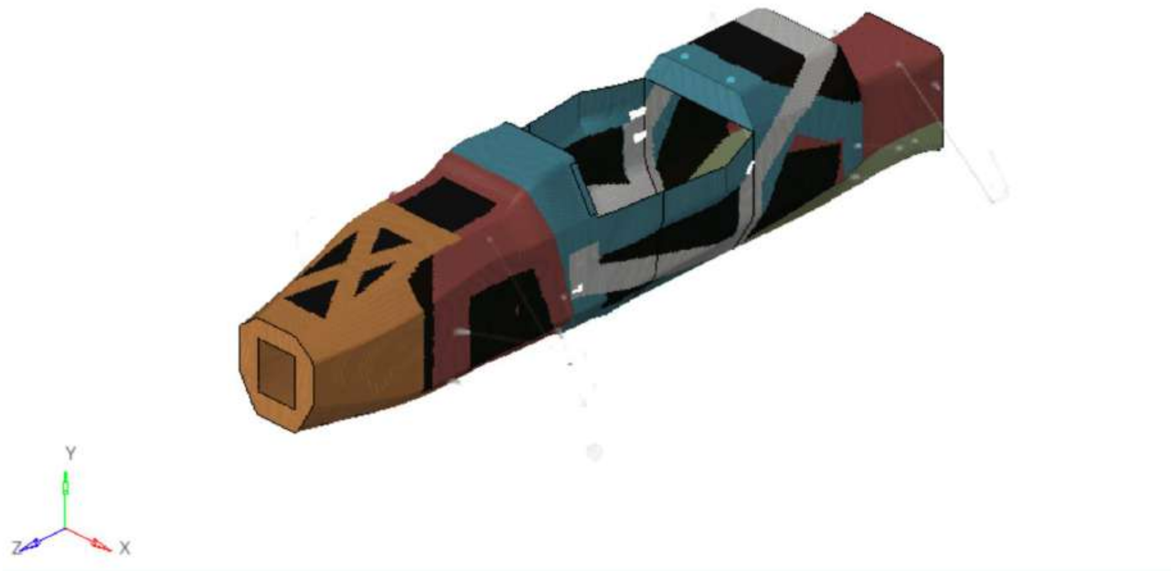

Figure 8. Final laminate

5. Conclusions

This project demonstrates the workflow of the design of a Formula Student monocoque. Through the application of composite materials theory together with optimization procedures, a structure has been developed that meets the requirements and objectives proposed at the beginning of the project.

The project demonstrates the capability to implement shape and laminate optimizations on one of the most important parts of the single seater. In addition, this work will require an evaluation of the manufacturing of this laminate, since no study has been carried out on its feasibility, although it has been considered when defining the layer shapes and the design itself.

6. References

[1]«Formula Student Rules 2026, Version: 1.1, Rev-15f99a7». Disponible en: https://www.formulastudent.de/fileadmin/user_upload/all/2026/rules/FS-Rules_2026_v1.1.pdf

[2]W. F. Milliken y D. L. Milliken, *Race car vehicle dynamics*. en R, no. 146. Warrendale, PA: Society of Automotive Engineers Internat, 1995.

[3]A. K. Kaw, *Mechanics of composite materials*, 2. ed. en Mechanical engineering series, no. 29. Boca Raton, FL: CRC Taylor & Francis, 2006.

Contents

List of figures

List of tables

Chapter 1. INTRODUCTION

In this project, the work is carried out in collaboration with the ISC FS Racing Team. The objective of the project is to illustrate the design and development of a monocoque-type chassis within the context of Formula Student. This chassis must comply with the requirements established by the competition regulations, as well as those defined by the team for the specific structure.

1.1 FORMULA STUDENT

Formula Student is an international competition in which students from all over the world compete in a series of static and dynamic events. There are different categories within Formula Student (Figures 9 and 10), divided according to the type of propulsion system installed in the vehicle. These types include combustion, electric, hybrid, and hydrogen powertrains. The Formula Student regulations, established annually by Formula Student Germany, cover all these categories. In the case of this project, we will focus exclusively on the electric category.

The competition consists of eight events in total. There are three static events: Business Plan, Design Report, and Cost Report. Together, these static events account for 300 out of the 1000 total points that determine the overall competition results. The remaining points are awarded in the dynamic events, which will be the focus of this project. Throughout this project, these different events will be referenced, as each of them imposes distinct requirements that lead to specific analyses of the chassis geometry.

Figure 9. ISC IFS-07 during testing.

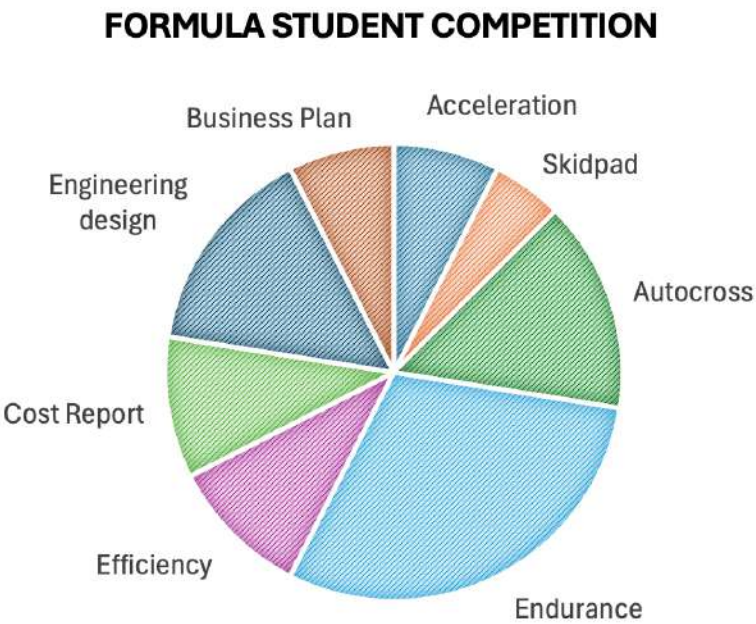

Figure 10. Formula Student Competition Events.

1.2 MOTIVATION

This is my fourth year as a team lead at the ISC FS Racing Team (Figure 9). As my time with the team is coming to an end, I want to leave a lasting contribution to the team's technical knowledge. Over the last three years, several final degree projects have been carried out covering this topic. This project aims to serve as the culmination of that research, providing the team with a comprehensive knowledge base for the development of a monocoque chassis.

Furthermore, the application of composite material optimization to vehicle performance represents a valuable tool for my professional career.

The main motivation behind the design of this monocoque chassis is to enhance both the team's knowledge and my own understanding of composite material optimization. Improvements in the vehicle chassis can directly contribute to better performance in competition events.

1.3 OBJECTIVE

The ISC runs a steel tubular space frame chassis for many years now. The development of in house CFRP monocoque is an expensive and time-consuming project that the team has not been able to carry out. For 4 years, many final degree projects have approached the team to this possibility by attacking the critical features of this kind of chassis. This project aims to end this cycle and provide the team with the ideal tools for this development.

The main objective is to create a light and stiff virtual monocoque in the small-time gap that the formula student season leaves to design a monocoque chassis. The project will be completed in the first half of the semester and will not involve any kind of fabrication processes. As of 2025, the ISC IFS-07 has a 38,5 kg steel chassis with approximately 2300 Nm/deg torsional stiffness. The objective is to reduce the mass by half and improve the torsional stiffness by double. To resume these main objectives:

1. Design a stylised and rule compliant monocoque chassis following the formula student rules.

2. Improve torsional stiffness to 4000Nm/deg and reduce total mass to approximately 20kg.

2. Provide new knowledge in composite optimization to the ISC FS Racing Team.

1.4 RESOURCES

To develop the project as planned, these different tools have been used:

1. CAD software: All CAD designs were created using Dassault Systèmes Solidworks 2025 Student edition.
2. FEA software: ALTAIR Hypermesh has been used for the optimization of the carbon fibre layers.
3. Solver: Optistruct has been used for its support for linear static cases, which were required to evaluate the relationship between stresses and displacements under applied loads.
4. Suspension analysis: Optimum Kinematics has been used for the suspension geometry analyses.
5. Notion: Is a productivity application that was used for note taking, planning and tracking during the whole Project.

Chapter 2. STATE OF THE ART

In this chapter, the different types of chassis and requirements used in formula student. Each team uses a different type of chassis with different objectives.

2.1 FORMULA STUDENT

The competition in Europe is governed by the Formula Student Rules published by Formula Student Germany (FSG) every year. These rules establish the distinct aspects that any car competing at any event must have.

The rules are divided in different sections which deal with:

- Administrative regulations
- General technical requirements
- Internal combustión engine vehicles
- Electric vehicles
- Technical inspections, static disciplines and Dynamic disciplines

This project is focused on the general technical requirement stablished by the rules. These requirements review the different measurements, stiffnesses and safety related to the design of the car.

2.1.1 GENERAL TECHNICAL REQUIREMENTS

In this section, the rules state that the car must be an open-wheeled, single seat (formula style body) with four wheels that are not in a straight line. The car needs a minimum ground clearance of 30mm, which affects us in the suspension geometry and height. General guidelines for all basic automotive parts are given in a general sense.

2.1.2 GENERAL CHASSIS DESIGN

The initial design of the monocoque chassis starts here. First, the chassis design starts with the size constraints revealing the main dimensions of the chassis. During this phase, the spaces left for the different templates are taken into account and measurements are imposed[1]. Three templates define the inside section of the chassis:

- Cockpit section Template (Figure 11): This template establishes the minimum cockpit opening that the car needs. [1]

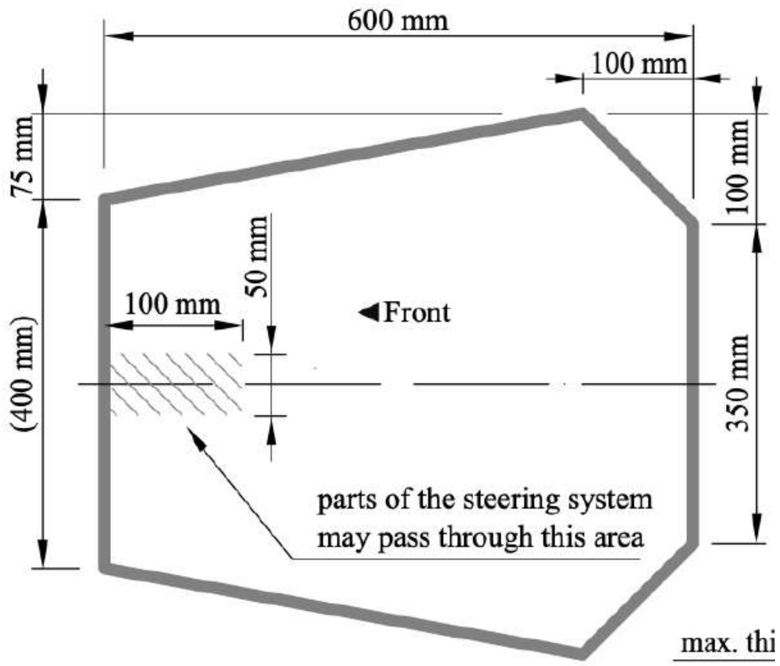

Figure 11 Cockpit cross-section template

- Cockpit internal cross section (Figure 12): This template defines the mínimum space that the driver legs need. In this case, exceptions are made for steering systems that pass through the middle of the template.[1]

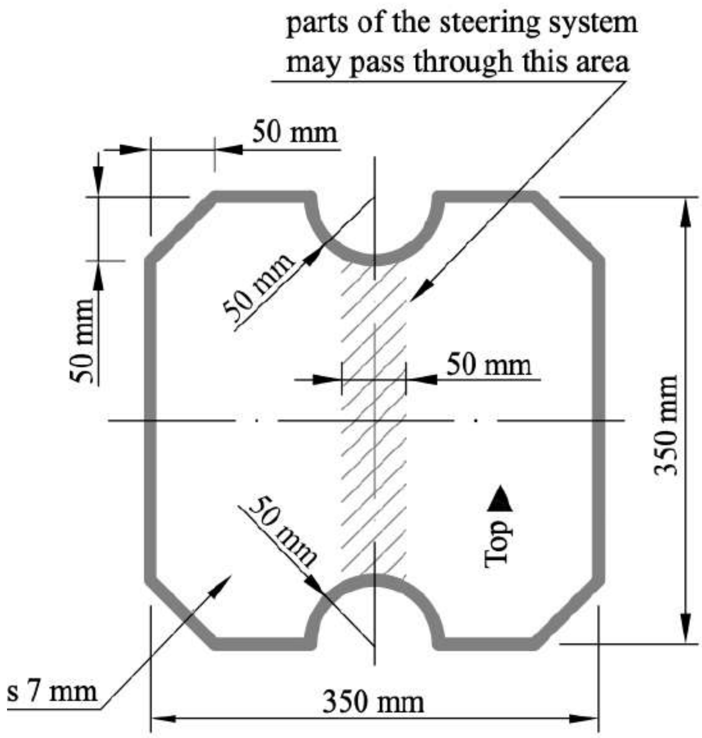

Figure 12 Internal cross-section template

- Percy (Figure 13): This template represents the 95th percentile men. When seated normally and restrained by the by the driver restrained system the helmet of the Percy and all other drivers must:[1]

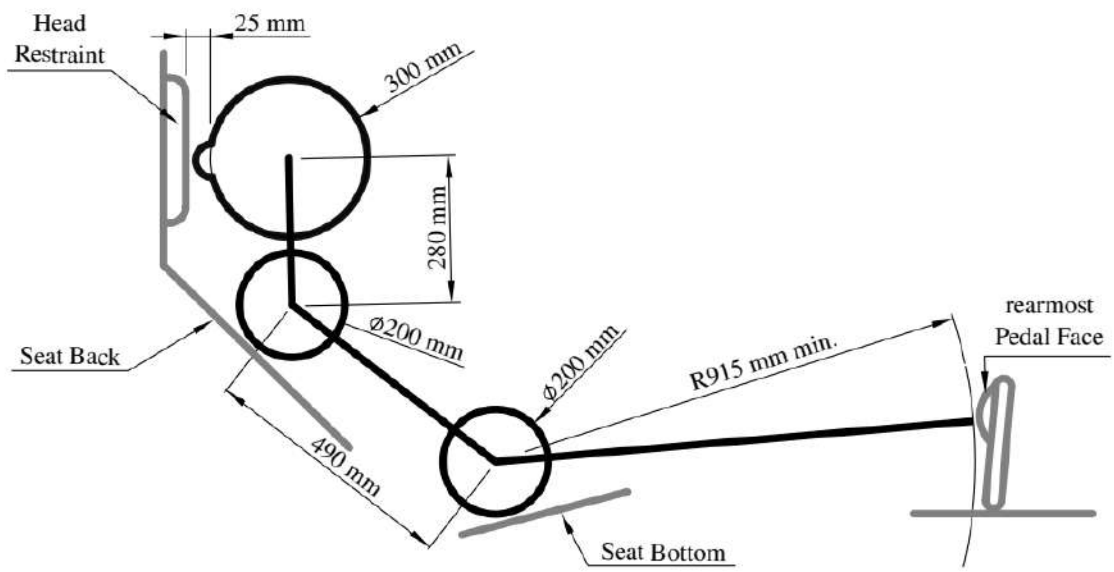

Figure 13 Percy placement

2.2 INTRODUCTION TO VEHICLE CHASSIS

The chassis is the pivotal structure of any vehicle as it suffers all the loads and houses all the systems inside the car. The different materials and fabrication methods create various type of chassis which vary in performance and use. Also, key parameters like torsional stiffness, determine which chassis is best in each case. In addition, weight is a critical parameter in motorsport racing that must be taken into consideration while designing a chassis.

The structural stiffness of a chassis is defined by two elements:

- Torsional stiffness: Is the resistance of a structure or component to twisting when torque is applied.
- Bending stiffness: The resistance of the chassis to bending. It shows the amount of force that needs to be applied to produce a certain amount of vertical deflection.

Is important to have these parameters at hand as calculations for suspension systems and vehicle dynamics are usually done under the assumption that the chassis is rigid. In every performance vehicle, a Formula Student car in this case, must have right torsional stiffness around the longitudinal axis of the car (usually the x axis). Later, this paper we will discuss the effects of a low torsional stiffness value. Each type of chassis has different ranges of these parameters.

2.2.1 SPACE FRAME CHASSIS

A space frame chassis is a structure composed of steel tubes arranged in triangular formations, a design that has been employed in motorsport since the earliest days of racing. The chassis is engineered around the vehicle's primary components, such as the powertrain and suspension systems, to achieve optimal triangulation.

The most significant forces, coming from the suspension and powertrain, are transmitted through the chassis nodes, while the tubes themselves are subjected only to tension or compression. This configuration helps to reduce fatigue and improve stiffness, although the stiffness achieved is generally lower than that of composite structures. For instance, the most recent chassis developed by the ISC FS Racing Team demonstrated lower simulated stiffness compared to that of composite alternatives (Figure 14).

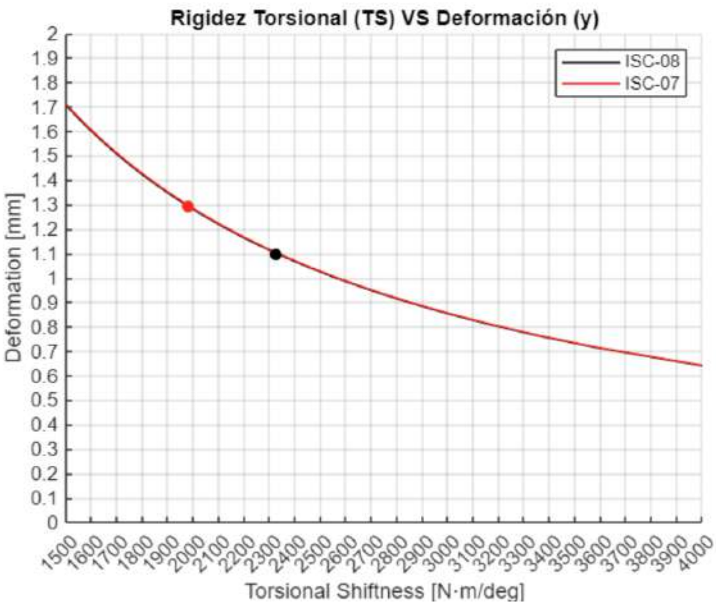

Figure 14 Difference in torsional stiffness of the IFS-07 and IFS-08

2.2.2 MONOCOQUE

The monocoque chassis was introduced in motorsport with the McLaren MP4 Formula 1 car during the 1981 season (Figure 15). This innovative technology consists of a tub constructed from sandwich panels, typically composed of carbon fibre reinforced polymer and aluminium honeycomb. The sandwich panel design generates a beam effect whereby, according to materials science principles, increasing the distance between the outer skins enhances the section modulus. This characteristic significantly improves the panel's resistance to bending making it highly suitable for motorsport applications. The geometry of a monocoque chassis differs markedly from that of a traditional space frame chassis. The tub encloses the driver, providing enhanced protection and improved aerodynamic efficiency. Additionally, monocoque structures exhibit greater torsional stiffness compared to tubular space frame chassis. The crucial factor is the weight-to-torsional stiffness ratio, which is substantially superior in monocoque designs.

Due to its safety benefits, high torsional stiffness-to-weight ratio, and excellent integration with the vehicle's systems, the monocoque chassis is predominantly employed across all forms of racing.

Figure 15: First Formula 1 monocoque in the Mclaren MP4-1

2.2.3 HYBRID

Hybrid chassis combine both technologies mentioned above (Figure 16). They divide the car into two parts: the cockpit made from a monocoque structure and the powertrain support which is made from tubular space frame chassis. The best example of this is formula 1 cars, their whole powertrain assembly (transmission, differential and rear suspension) is attached to the tub. This way they optimize the space behind the driver, obtaining the most out of the car.

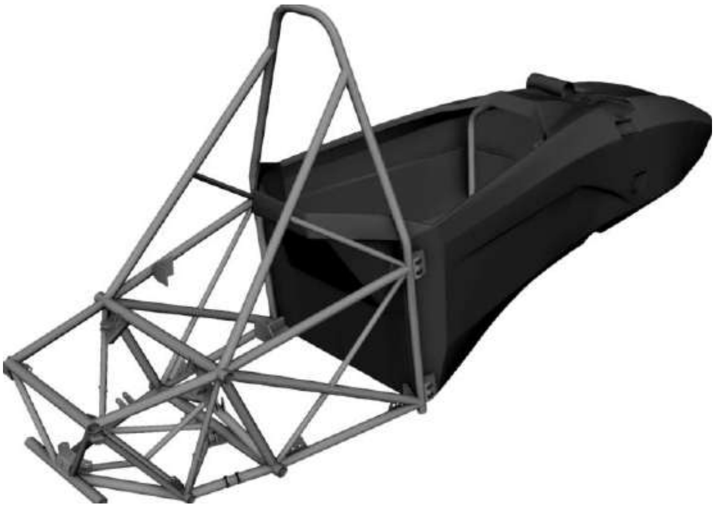

Figure 16: Hybrid Formula Student chassis.

2.3 INTRODUCTION TO VEHICLE DYNAMICS

The design of the chassis has one key objective, which is to obtain the optimal equilibrium in between torsional stiffness, weight and structural safety, while all this guaranty an efficient and controllable dynamic performance. Torsional stiffness plays a significant role when designing race cars. Suspension kinematics and compliance, handling, steering and ride behaviour all are affected by the variation of torsional stiffness.

During suspension kinematics analyses the chassis is considered a rigid body, so excessive chassis flexibility will cause problems for example in tuning lateral load transfer distribution with roll stiffness distribution. The whole body of the car can be modelled as three torsional springs: One spring being the front suspension, one being the body and the last one being the rear suspension. If the body spring stiffness is low, the spring that represents the body will alter the effect that roll stiffness distribution has on lateral load transfer distribution (Equation 1). This means that it will be hard to control the resistance to roll moment between the front and the rear axle. This yields to the inability of modifying the car behaviour while modifying suspension parameters.[4]

$$\frac{1}{k_{eq}} = \frac{1}{k_1} + \frac{1}{k_2}$$

Equation 1. Relationship between two springs torsional stiffness in series.[4]

When a car corners, the sprung mass rotates about a roll axis between the axles and rolls. Therefore, the body of the car rolls at an angle while both wheels are in contact with the ground causing a change in ride height.

We know that for a certain vertical displacement of the wheel, it will experience a certain amount of spring force. For a given amount of a body roll, much spring force is generated. With the coil spring wheel rate and the antiroll bar wheel rate for both axles, we can calculate the needed torsional stiffness of the chassis or either way, the suspension stiffness which should be the 10% of the chassis stiffness approximately.

Chapter 3. CHASSIS DESIGN

The chassis design will be imposed by the competition regulations, stablished by the Formula Student Germany competition. The chassis is divided in different parts according to the regulations. These parts are (Figure 17):

- Impact attenuator: A deformable material able to absorb the energy from a frontal impact located before the front bulkhead.
- Front bulkhead: A planar structure that defines the forward plane of the chassis and provides protection for the driver's feet. It is supported by the front bulkhead support.
- Front bulkhead support: Structure that is the side of the chassis from the drivers' feet to the front hoop. It covers from the bottom of the front hoop to the top of the side impact structure.
- Front hoop: A continuous roll bar located over the driver's legs. The steering system I usually attached to this steering system.
- Main hoop: A roll bar covering the driver's head. It creates an imaginary line to protect the driver from hitting the floor in case of roll over.
- Roll hoops bracing: A structure supporting both the front hoop and the main hoop.
- Side impact structure: The side of the chassis covering the cockpit protecting the driver from side impacts.

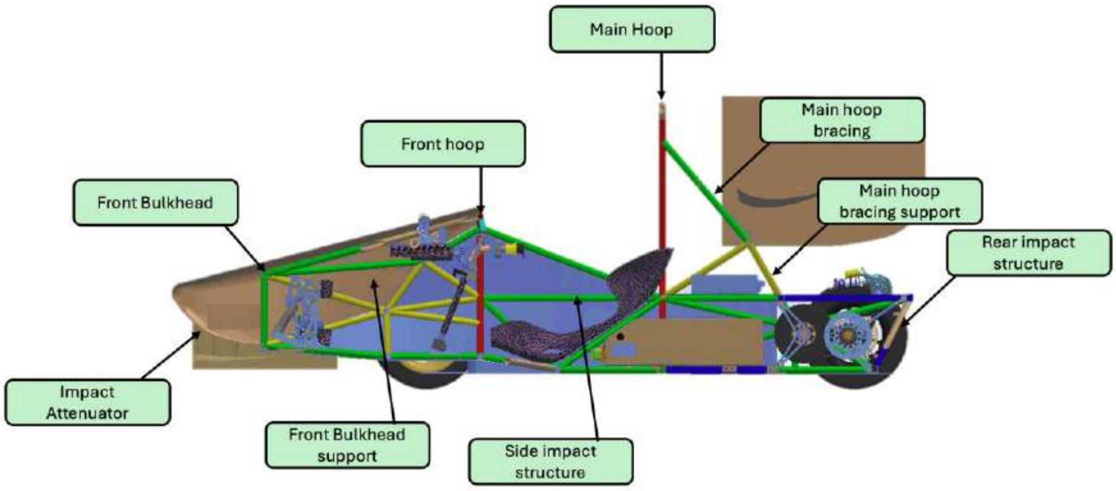

Figure 17 Chassis parts on a Formula Student

3.1 CHASSIS DESIGN BASIS

The aim of this project is to serve as template for future monocoque chassis of the ISC FS Racing Team. For this purpose, no specific dimensions have been shown of critical components of the car. The critical dimensions that have been followed are the one stated by the Formula Student Rules. Driver placement, hoops and bracing structures have not been placed in specific places as they are not a constraint in the important part of this project, the simulation. For this reason, the geometry serves as an example, so all dimensions are virtual.

After these templates are put in place, the design of the monocoque starts. In this case, the only element that we need for the FEM analyses is the surface geometry. First, we start with the sketches grouping templates and suspension points.

This sketch represents the baseline dimensions stablished by the suspension points and the three templates. From this sketch, the surface is created. This process took time as some operations created some zero thickness surfaces and strange edges.

In the design, it must be implementing the roll hoops as they are another design constraint in this process. The final design is the following (Figure 18 – 20):

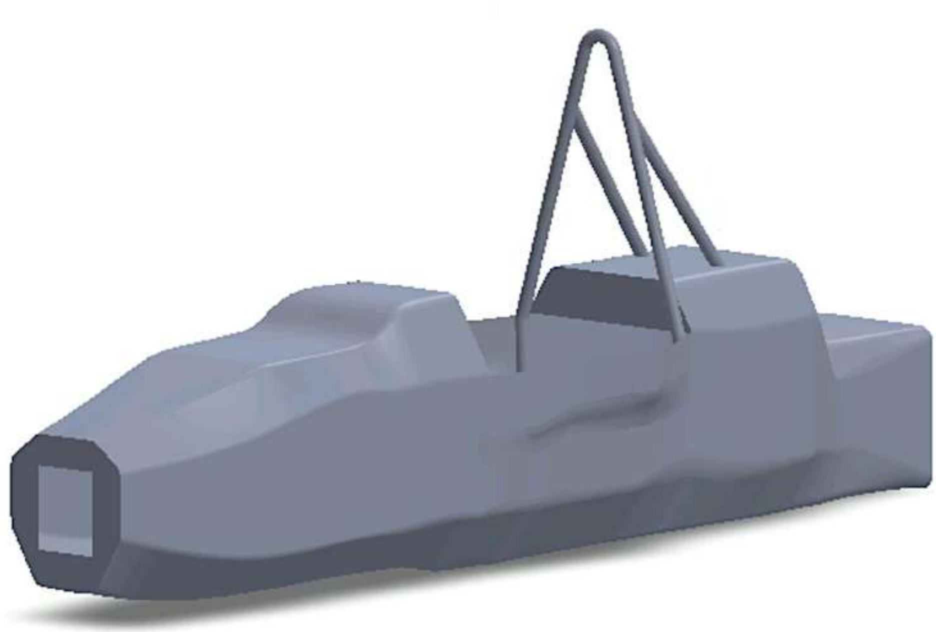

Figure 18 Monocoque surface 3D view

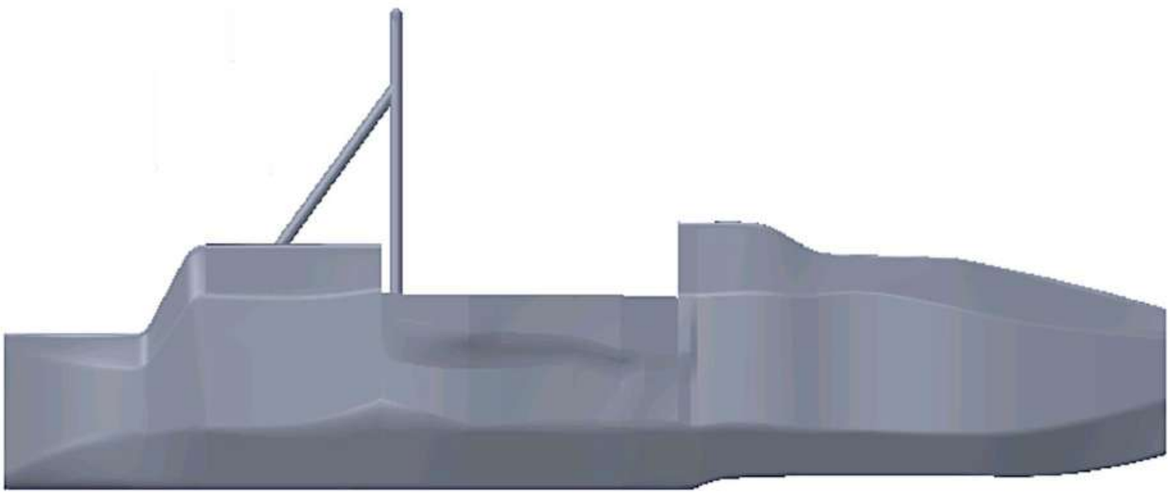

Figure 20 Monocoque surface side view

Figure 19 Monocoque surface front view

3.2 COMPOSITE MATERIALS

Composite materials are composed of at least to distinct elements that collaborate to achieve material properties unattainable by the elements on their own. The architecture consists of a primary material, known as the matrix, combined with reinforcement elements, typically polymer-based fibres to increase strength and stiffness characteristics. These materials are maintaining their distinctiveness and remain separable allowing for precise control over composite properties through proportion management during manufacturing.

The resin systems, usually used epoxies and polyesters, don't have good material properties but they have good adaptability to all different shapes and can be mixed easily. The reinforcements, such as glass, carbon and aramid fibres, exhibit excellent tensile and strength performance. However, individual fibres can only exhibit their properties along their longitudinal axis, like the tensile behaviour of rope fibres, limiting their multidirectional load capability.

The breakthrough with this technology occurs when the resin matrix is combined with the reinforcing fibres. The resin matrix It distributes applied loads among individual reinforcing fibres, ensuring load sharing across the entire composite structure. The resulting polymer matrix composite (PMC's) combines remarkable properties including high strength-to-weight ratios, stiffness characteristics, ability to form complex shapes, all while maintaining significantly lower densities compared to metallic alternatives.

Material	Observaciones	Rm (MPa)	E (GPa)	Densidad (g/cm³)	Resistencia específica (MPa/g/cm³)
Aluminio 2024	Sin endurecimiento	190	75	2,76	68,8
Aluminio 2024 T3	Endurecido térmicamente	420	72	2,76	152
Aluminio 6061 T6	Endurecido térmicamente	310	68	2,71	114
Aluminio 5251 H	Endurecido por acritud	230	72	2,69	85,5
Acero C20 Normalizado	Sin tratamiento térmico	490	210	7,85	62,4
Acero C80 Normalizado	Sin tratamiento térmico	1000	207	7,85	127
Acero C80 T+R	Templado en aceite + revenido a 300ºC	1300	207	7,85	166
CFRP-Epoxi (UN) Fibra Unidireccional	65% Fibra carbono	1950	140	1,55	1258
CFRP-Epoxi (Woven) Fibra en tejido	60% Fibra carbono	650	62	1,52	428
GRP-Epoxi (UN) Fibra Unidireccional	45% Fibra vidrio	700	40	1,77	395
GRP-Epoxi (Woven) Fibra en tejido	45% Fibra vidrio	445	26	1,84	242
Epoxi-Kevlar (UN) Fibra Unidireccional	45% Fibra de Aramida (Kevlar)	1240	70	1,38	899

Table 1. Comparison of mechanical properties of composite material versus metallic alternatives [5]

3.3 LAMINATE THEORY

Reinforced polymers are used because of their excellent ratio between their mechanical properties and their weight. When manufactured correctly, CFRP presents excellent mechanical properties.

Classical laminate theory perceives a composite material as a material build with a matrix, some kind of resin) and fibres. When the matrix and the fibres are loaded in the same direction, they present greater stiffness and strength than in the transversal direction (Figure 21).

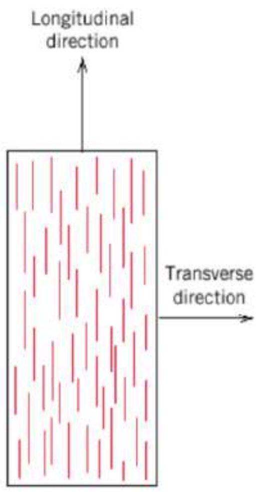

Figure 21 Distribution of the fibre composition in a composite material

The Voigt model for load application in the longitudinal direction states that when a strong union between the fibre and the matrix, the material enters an isodeformation state where the material deforms as an isotropic material like steel. In the equations stated in this model, some parameters are very important and will be used in the optimization process: [5]

- Vf: Volume fraction of the fibre
- Vm: Volume fraction of the resin matrix

$$
\begin{aligned}
&F_c = F_m + F_f \\
&\sigma_c A_c = \sigma_m A_m + \sigma_f A_f \\
&(\varepsilon_c = \varepsilon_m = \varepsilon_f) \\
&E_c \varepsilon_c A_c = E_m \varepsilon_m A_m + E_f \varepsilon_f A_f \\
&E_c = E_m \frac{A_m}{A_c} + E_f \frac{A_f}{A_c} \\
&E_c = v_m E_m + v_f E_f
\end{aligned}
$$

Equation 2 Voigt's composite model

The mix of mechanical properties make fibre reinforced polymers superior to their metallic counterparts if the forces are applied in the correct way and they are manufactured correctly. Classic laminate theory determines the strains and stresses that each ply of a laminate will see under specific conditions.[6]

A laminate is formed by the stacking of multiple plies under specific conditions: Orientation, material properties and vertical position. When the laminate is under load, each ply has a different stress variation when the strain variation is somewhat constant (Figure 22). This effect can cause individual ply failure which can ultimately lead to the complete laminate failure.

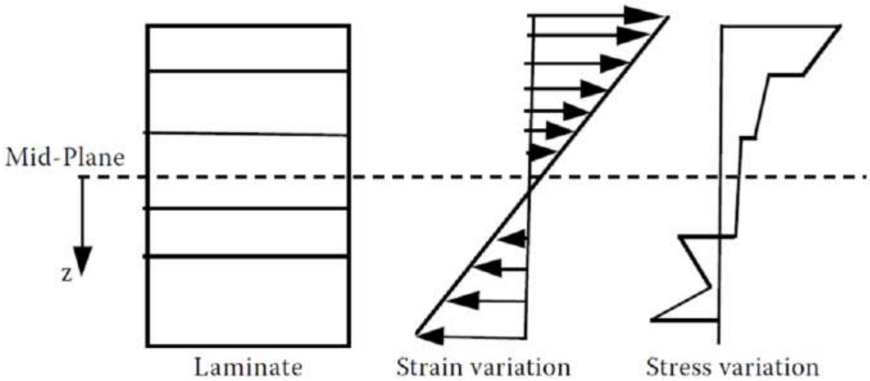

Figure 22 Strain and stress distribution along a laminate thickness[6]

Material properties are essential for good mechanical properties. The Young modulus of the material and the shear modulus are considered on the calculation of the stresses through the strains.

A laminate usually doesn't have all unidirectional plies because their low stiffness and strength properties on the transverse direction[6]. This creates a need to stack some plies at an angle, which leads us to analyse the strain-stress relation of thus laminates. For this analysis, we will use the coordinate system pictured in figure 23. Axis 1 will be the longitudinal axis of the lamina and axis 2 will be the transverse axis. The separation between the global coordinate system and this local coordinate system requires a transformation matrix dependent on the angle between the longitudinal axes.

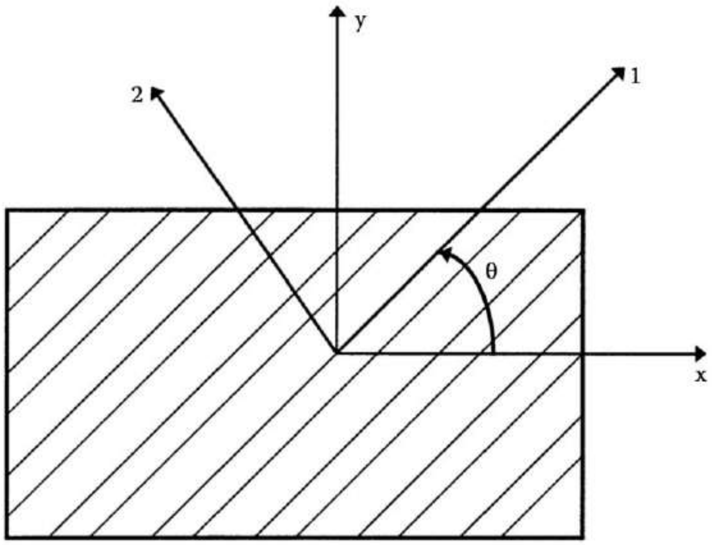

Figure 23 Coordinate system of an angled ply[6]

$$[T]=\begin{bmatrix} c^2 & s^2 & 2sc \\ s^2 & c^2 & -2sc \\ -sc & sc & c^2-s^2 \end{bmatrix},$$

$$c = \text{Cos}(\theta),$$

$$s = \text{Sin}(\theta).$$

Equation 2 Transformation matrix [6]

Lamina orientation creates a drastic change in the effect of each young modulus related to the x and y axis. There is an inverted correlation between the elastic modulus and the angle of the lamina as shown on the Figures 24 and 25.

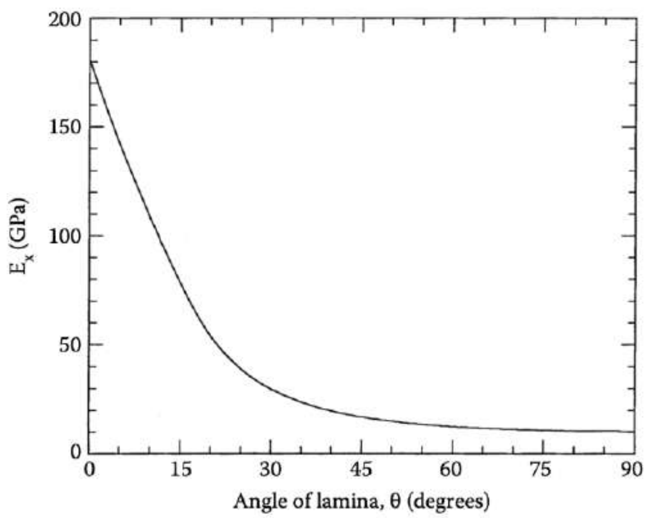

Figure 24 Change in Ex as a function of the lamina angle[6]

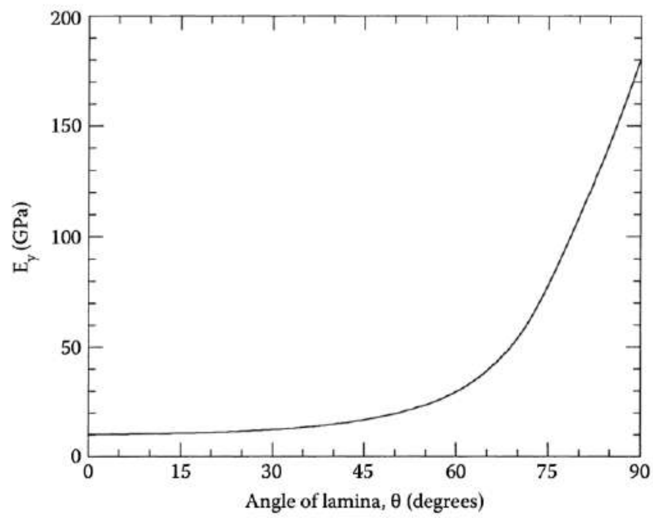

Figure 25 Change of Ey as a function of the lamina angle[6]

This change in lamina angle creates a gradual increase in shear modulus of the lamina, which leads to the increase in torsional stiffness of the chassis as this is the stress that the chassis is put through during this test. As we can see in Figure 26, the peak shear modulus is achieved at an angle of 45º. This consideration will directly affect the final laminate of the chassis.

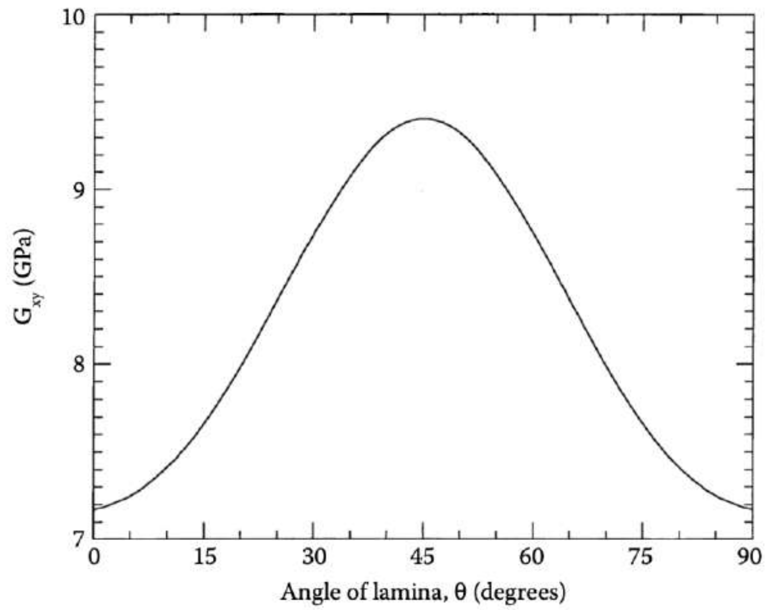

Figure 26 Relationship between in plane shear modulus and lamina angle

LAMINATE ANALYSYS:

The laminate analysis starts with the calculation of the stiffness matrix of each lamina. We can consider that a carbon fibre lamina is an orthotropic material that has different material properties in three directions. Also, we will assume place stress loads and that the lamina does not carry any out-of-plane stresses.

Taking this consideration, and the stress problem can be expressed with the equation:

$$\begin{bmatrix} \varepsilon_1 \\ \varepsilon_2 \\ \gamma_{12} \end{bmatrix} = \begin{bmatrix} S_{11} & S_{12} & 0 \\ S_{12} & S_{22} & 0 \\ 0 & 0 & S_{66} \end{bmatrix} \begin{bmatrix} \sigma_1 \\ \sigma_2 \\ \tau_{12} \end{bmatrix}.$$

Equation 3: Strain – stress relationship[6]

By inverting this equation, the stress – strain relation is expressed with the reduced stiffness coefficients:

$$\begin{bmatrix} \sigma_1 \\ \sigma_2 \\ \tau_{12} \end{bmatrix} = \begin{bmatrix} Q_{11} & Q_{12} & 0 \\ Q_{12} & Q_{22} & 0 \\ 0 & 0 & Q_{66} \end{bmatrix} \begin{bmatrix} \varepsilon_1 \\ \varepsilon_2 \\ \gamma_{12} \end{bmatrix}$$

Equation 4 Stress – strain relationship[6]

Generally, the stress – strain relation is stablished through the engineering elastic constants. In this case, the nomenclature that will be used is:

$$E_1 = Longitudinal\ Young\ Modulus$$

$$E_2 = Transversal\ Young\ Modulus$$

$$G_{12} = Shear\ modulus$$

$$v_{12} = Poisson\ mayor\ ratio$$

v_{ij}= is defined as the ratio of the negative of the normal strain in direction j to the normal strain in direction I, when the only normal load is applied in direction i

The next step is to determine the coordinates of the top and bottom surfaces of each ply of the laminate consisting in n plies. The thickness of each ply is known.

$$Ply\ 1:\ h_o = -\frac{h}{2}\ (Top\ surface);\quad -\frac{h}{2} + T_1\ (bottom\ surface)$$

$$Ply\ k:\ h_{k-1} = -\frac{h}{2} + \sum_{K=1}^{K-1} T\ (Top\ surface);\quad -\frac{h}{2} + \sum_{K=1}^{K} T\ (Top\ surface)$$

Equation 5 Ply coordinate calculations in a laminate

Calculations for the reduced stiffness matrix [Q] are the following:

$$Q_{11} = \frac{E_1}{1 - v_{21} * v_{12}};\ Q_{12} = \frac{v_{12} * E_2}{1 - v_{21} * v_{12}};\ Q_{22} = \frac{E_2}{1 - v_{21} * v_{12}};\ Q_{66} = G_{12}$$

Equation 6 Reduced stiffness matrix elements calculations[6]

These elements are on the local system of the plies, so by using the transformation matrix the elements on the global systems can be obtained.

$$\bar{Q}_{11} = Q_{11}c^4 + Q_{22}s^4 + 2(Q_{12} + 2Q_{66})\, s^2c^2$$

$$\bar{Q}_{12} = (Q_{11} + Q_{22} - 4Q_{66})\, s^2c^2 + Q_{12}\,(c^4 + s^4)$$

$$\bar{Q}_{22} = Q_{11}s^4 + Q_{22}c^4 + 2(Q_{12} + 2Q_{66})\, s^2c^2$$

$$\bar{Q}_{16} = (Q_{11} - Q_{12} - 2Q_{66})\, c^3s - (Q_{22} - Q_{12} - 2Q_{66})\, s^3c$$

$$\bar{Q}_{26} = (Q_{11} - Q_{12} - 2Q_{66})\, c^3s - (Q_{22} - Q_{12} - 2Q_{66})\, s^3c$$

$$\bar{Q}_{66} = (Q_{11} + Q_{22} - 2Q_{12} - 2Q_{66})\, s^2c^2 + Q_{66}\,(s^4 + c^4)$$

Equation 7 Transformation matrix applied to the reduced stiffness matrix terms

Then we generate the ABD matrix (Appendix 1), that is the extensional [A], coupling[B] and bending [D] matrix. The extensional matrix [A] relates the resultant in-plane forces to the in-plane strains, and the bending [D] stiffness matrix relates the resultant bending moments to the plate curvature. The coupling stiffness matrix [B] couples the force and moment terms to the midplane strains and midplane curvatures.[6]

3.4 FAILURE CRITERIA

Composite materials are made from different layers bonded together. This build provides an uneven distribution of stresses when they are subjected to different forces.

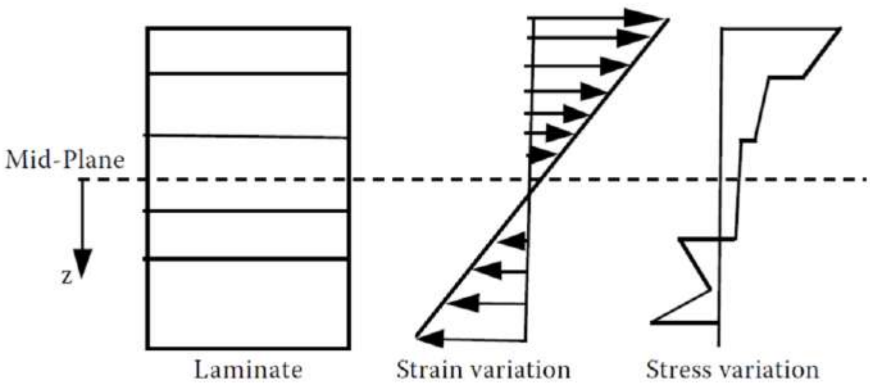

Numerous failure criteria can be considered when working with composite materials. The criterion used in this project is the Tsai-Hill failure criterion, which accounts for the interactions between different stresses, laminate orientations, and material coefficients to establish a failure threshold. After calculating the coefficients and applying the formula to each case, a numerical result is obtained. If this result exceeds 1, the composite will fail. This method was selected to enable easier verification through hand calculations.

$$F_{index} = \frac{\sigma_1^2}{X^2} - \frac{\sigma_1 * \sigma_2}{X^2} + \frac{\sigma_2^2}{Y^2} + \frac{\tau_{12}^2}{S^2}$$

Equation 8 TSAI Hill Criterion

The failure parameters X and Y in the Tsai-Hill criterion are not constant values; instead, they depend on the stress state of the composite material. These parameters change based on which quadrant of the stress coordinate plane is being analysed.

When dealing with longitudinal stress (σ_1), the failure parameter X is selected based on the sign of the stress. If the material experiences tensile stress ($\sigma_1 > 0$), the tensile strength X_T is used. However, if the material is subjected to compressive stress ($\sigma_1 < 0$), the compressive strength X_C is used instead.

The same logic applies to the transverse stress direction (σ_2). The material's failure parameter Y is determined by whether the stress is tensile or compressive, using Y_T for tension and Y_C for compression.

Chapter 4. ANALYSIS

4.1 SIMULATION PROCESS

The simulation process is composed of 2 phases: the optimization phase in which the laminate parameters and layers are determined, and the analyses phase where the optimization result is tested and simplified for it to be manufacturable.

4.1.1 OPTIMIZATION PHASE

The optimization stage starts from a basic laminate composed of all laminate alternatives from the selected materials. In this case, the start ply laminate of the first stage simulation was (Table 2):

First stage optimization laminate		
Material type	Thickness (mm)	Fibre orientation
Gurit IMC UNI	2	0º
Gurit RC200T 0ºx90º	2	0º
Gurit XC411 45ºx45º	2	0º
Gurit RC200T 0ºx90º	2	45º
Gurit XC411 45ºx45º	2	45º
ALU Honeycomb DURA-CORE-II-5052	30	-

Table 2 First stage optimization Ply laminate

The laminate groups all the possible combinations of the different type of fibre cloths.

4.2 GEOMETRY SIMPLIFICATION AND MODELLING

The model used for simulation represented the basic surface of the monocoque, because with the ALTAIR Hypermesh optimization we will stablish the thickness of every ply, number of plies and orientation. The suspension systems have been included in the simulation with their own material properties as efforts on the chassis are transmitted to the suspension and viceversa (Figure 27).

As the aim of the project is directed towards the shape optimization of the laminate, inserts for the monocoque have not been taking in consideration for the simulations. For this load transfer to be the most realistic, rigid bodies (RBE2) have been used to transmit the forces to the monocoque.

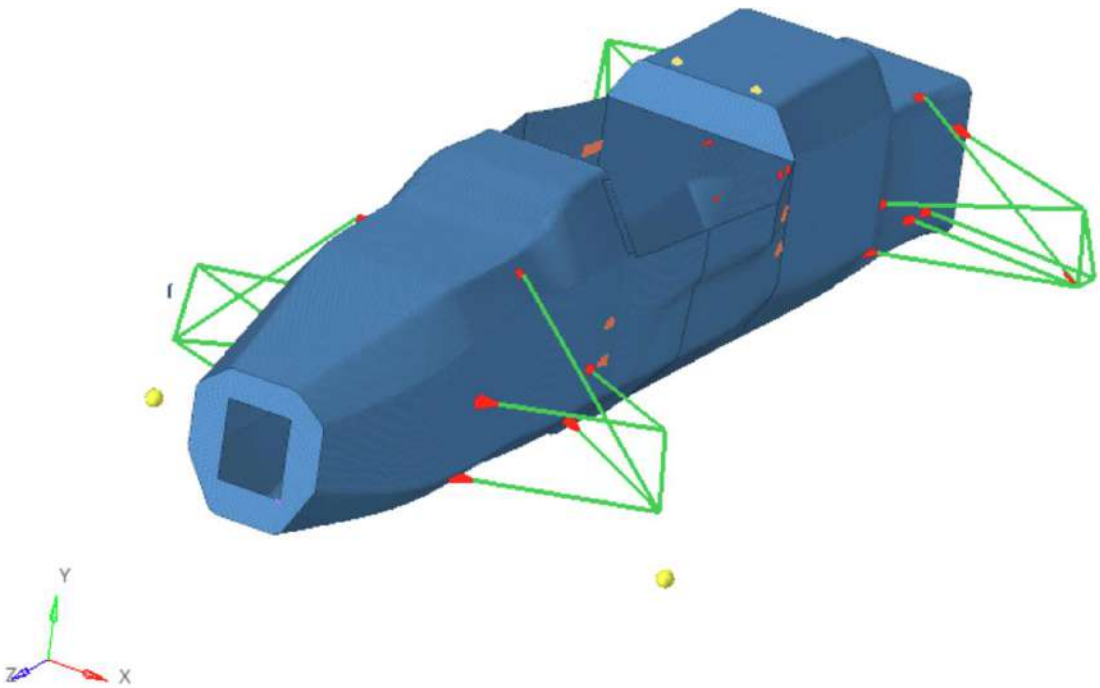

Figure 27: Monocoque Hypermesh Model

4.2.1 SUSPENSION MODELLING

Chassis development is directly correlated to the suspension geometry. Because of this, the suspension geometry was redesigned with minor changes to fit a more discrete chassis compared to a tubular steel frame chassis. The objective of this redesign was to maintain the suspension parameters as close as the original design.

This process was done using Optimun Kinematics by Optimum G. This software permits the user design, simulate and test bench suspension systems. The main changes on the suspension where the change on the rocker pick up points change in height. This change created a possibility to make the chassis more compact and to adapt the suspension from a tubular steel frame chassis to a monocoque structure.

The final geometry suspension points after various iterations are the following for the front and rear suspension (Table 3-4).

FRONT AXLE				NEW COORDINATES		
SUSPENSION PICK UP POINTS:	x (mm)	y (mm)	z (mm)	x (mm)	y (mm)	z (mm)
Lower Wishbone Front pivot	14,2	229,1	230	3,3	212,9	230,0
Lower Wishbone Rear pivot	346,7	229,1	230	353,3	210,8	230,0
Lower Wishbone outer ball joint	148,1	550	230	148,1	550,0	230,0
Upper wishbone Front pivot	14,2	263	400	4,3	245,6	400,7
Upper wishbone Rear Pivot	332,7	263	360,3	343,3	246,1	358,4
Upper Wishbone outer ball joint	165,5	530	390	165,5	530,0	390,0
Push Rod wishbone	148,1	515,5	250	148,1	515,5	250,0
Push Rod rocker end	148,1	268,3	773,7	148,1	263,3	650,0
Outer track rod ball joint	221.75	505,2	265,1	221.75	505,2	265,1
inner track rod ball joint	221,75	234,5	264	221,8	234,5	264,0
Damper to body	148,1	25	755,1	148,1	25,0	650,0
Damper to rocker	148,1	188,2	818,2	148,1	188,2	90,0
Rocker 1º axis point	128,1	205	755,1	128,1	205,0	611,4
Rocker 2º axis point	168,1	205	755,1	168,1	205,0	611,4
Wheel center point	160	600	310	160,0	600,0	310,0
Wheel spindle point	160	638	311,7	160,0	638,0	311,7

Table 3 Front axle suspension points

REAR AXLE				NEW COORDINATES		
SUSPENSION PICK UP POINTS	x (mm)	y (mm)	z (mm)	x (mm)	y (mm)	z (mm)
Lower Wishbone Front pivot	1523,3	240	230	1571,1	187,2	229,6
Lower Wishbone Rear pivot	1756	240	230	1762,7	159,6	230,0
Lower Wishbone outer ball joint	1730	550	230	1730,0	550,0	230,0
Upper wishbone Front pivot	1529,1	259	347	1551,2	193,8	345,1
Upper wishbone Rear Pivot	1895	259	390	1879,8	190,6	383,5
Upper Wishbone outer ball joint	1730	540	390	1570,0	540,0	390,0
Push Rod wishbone	1725	515	250	1725,0	515,0	250,0
Push Rod rocker end	1858,9	279,5	485,8	1841,1	149,8	459,3
Outer track rod ball joint	1790	550	230	1790,0	550,0	230,0
inner track rod ball joint	1816	240	230	1822,7	160,3	230,0
Damper to body	1640,8	231,1	512,4	1625,7	72,2	510,0
Damper to rocker	1811,8	213,5	545,1	1810,1	75,2	507,6
Rocker 1º axis point	1816,2	274,2	514,9	1806,7	108,5	433,3
Rocker 2º axis point	1818,8	246,6	486,1	1778,5	147,7	516,1
Wheel center point	1730	600	310	1730,0	600,0	310,0
Wheel pindle point	1730	650	311,9	1730,0	650,0	311,9

Table 4 Rear axle suspension points

The suspension arms characteristics that have been changed are the wishbones lengths and the position of the rocker and push rod. The main goal was to maintain as much as possible the suspension parameters, this was achieved by reducing the lengths of the suspension rods with the direction vector of each rod. The push rod / rocker changes in height maintained the designed motion ratio, 1.2.

4.3 SIMULATION PARAMETERS

4.3.1 MESHING & MODEL GEOMETRY

In simulation analyses, the stages of model geometry preparation and meshing constitute foundational aspects in achieving accurate and efficient analyses. Altair Hypermesh provides robust tools to clean, discretize and mesh geometries. For my model I have used the batchmester tool, which allows the user to create a surface mesh with an easy-use-interface (Table 5).

Mesh elements	
1D	
Element type	Number of elements
BEAM	1980
RIGID	43
2D	
Element type	Number of elements
Quad4	140367
Tria3	589

Table 5 Mesh elements type

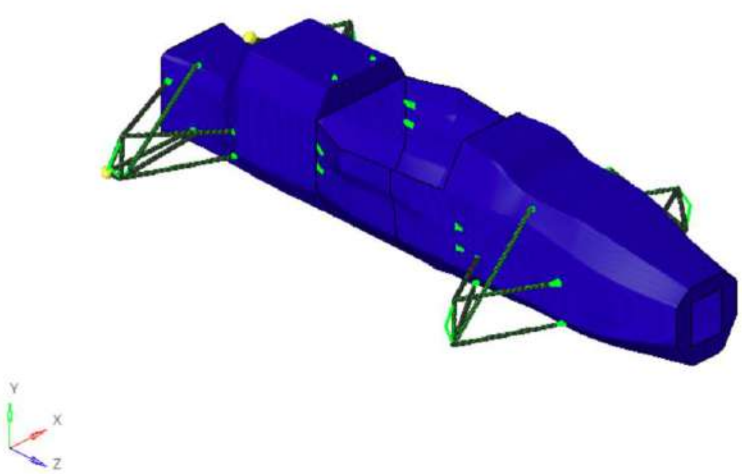

Figure 28 2D elements (Blue) 1D elements (Green)

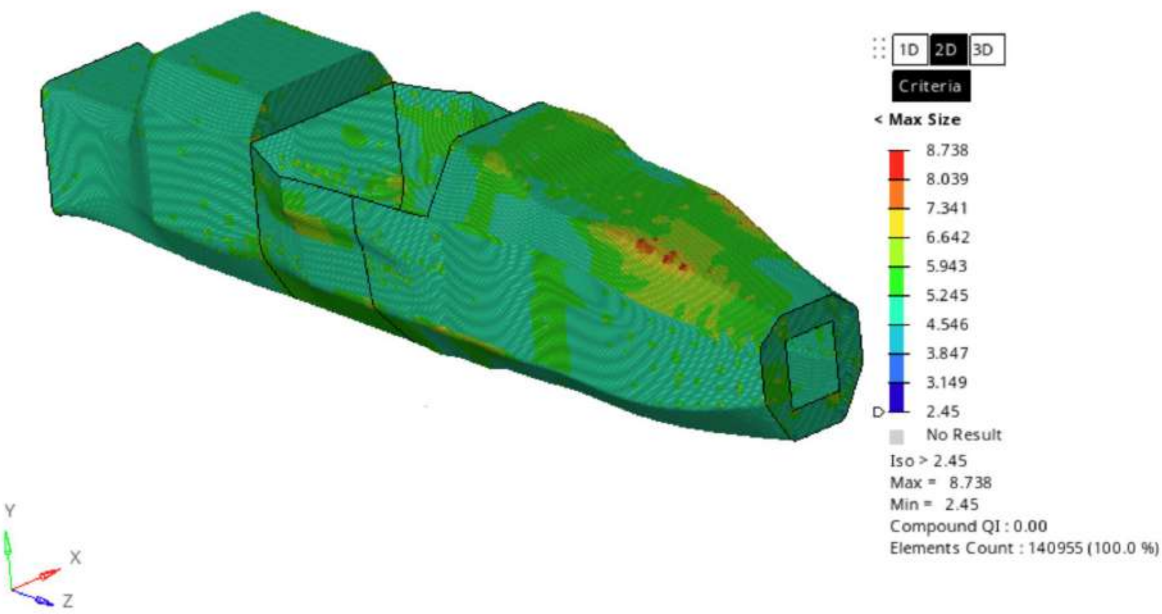

Figure 29 2D element size heat map

The initial mesh of the model has been set to 5mm length elements. The meshing operation using the batchmesher tool creates the mesh with a target element size and cleans up the mesh (Figure 29). This tool has been adjusted with the following parameters to create the mesh:

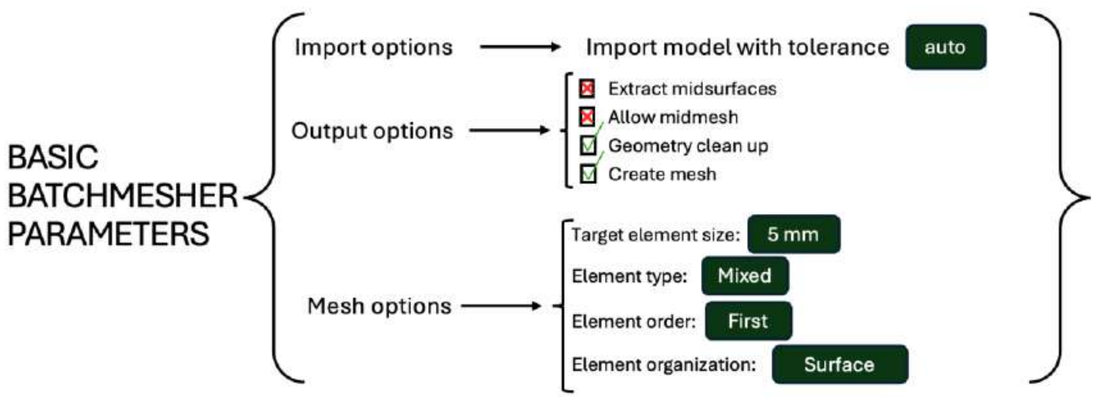

Figure 30 Basic batchmesher parameters

After creating the meshing, some check needs to be done to complete the meshing operation. First, each element normal must be pointing in the same direction as the element normals of the elements next to it. In the case of this project, the positive side of the element normal, where the laminate will grow towards, is the inside of the monocoque (Figure 31).

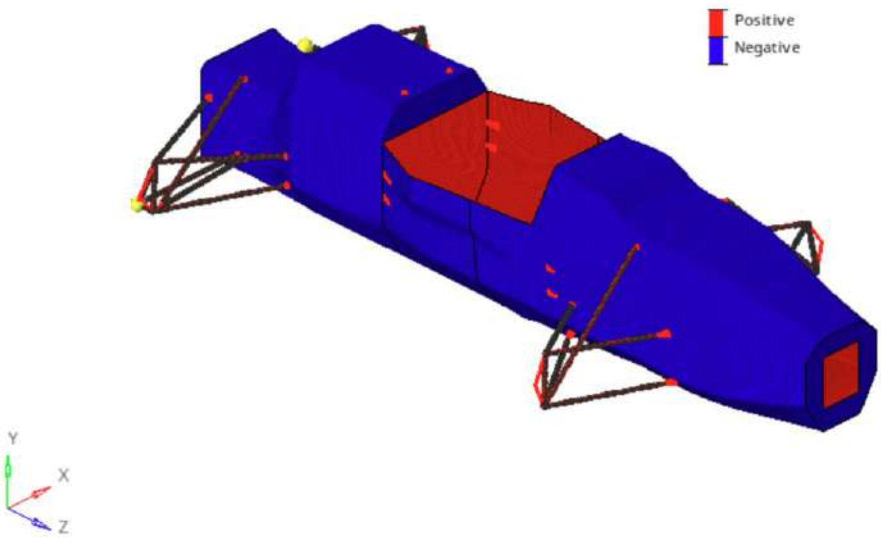

Figure 31 Element normal distribution

After the element normals check, each element local system must be aligned with the global system chosen at the start of the meshing operation (Figure 32).

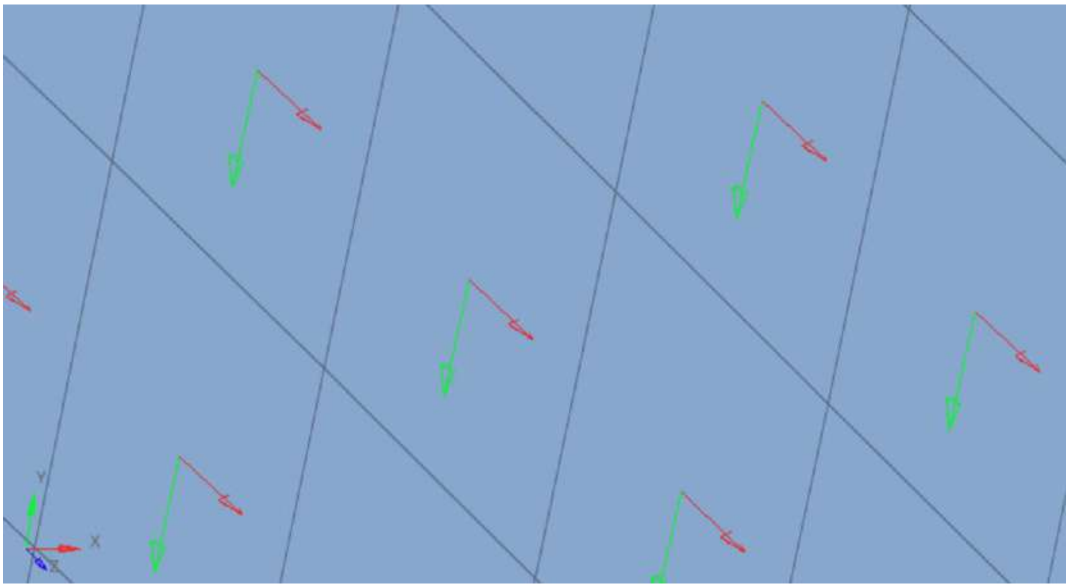

Figure 32 Mesh orientation detailed

The objective of the simulation is to be as real as possible with a base chassis model. For this to be maintained, the suspension arms have been modelled in the simulation following the real geometry and parameters that would be on the real car.

First, the suspension was modelled with nodes and lines following the edited suspension pick up points coordinates determined on Optimum Kinematics (Figure 33).

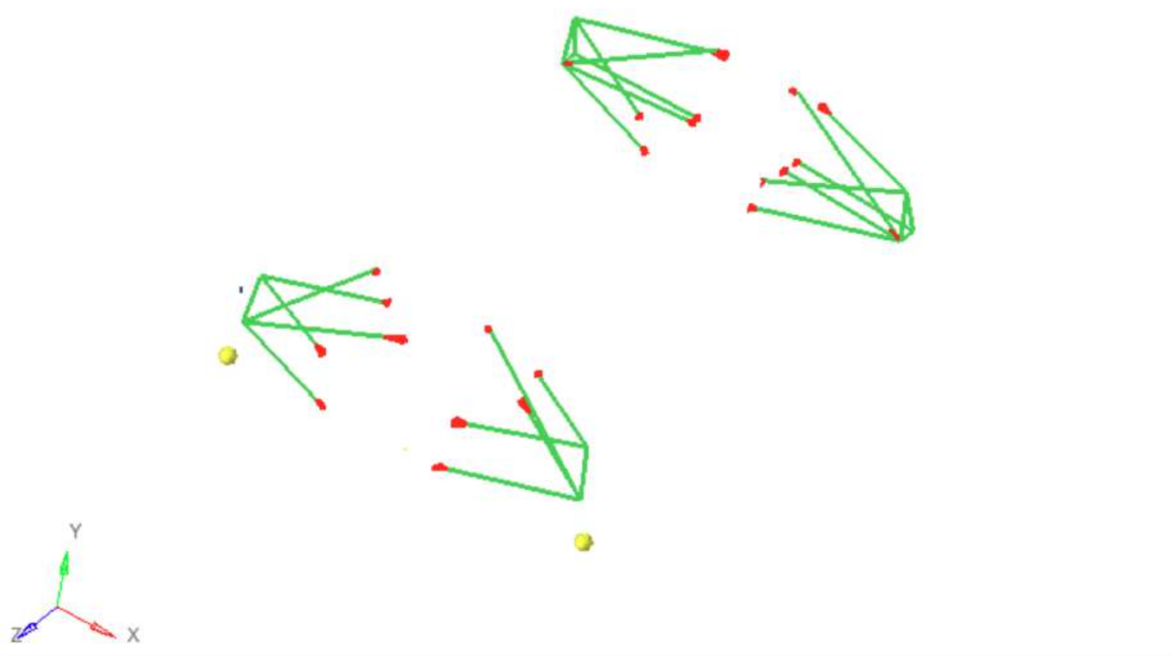

Figure 33 Suspension geometry model

This model serves as a sketch for the 1D meshing. This meshing was carried out with the line mesh tool on the software, which stablished the number of elements per suspension arm relative to the length of this one. The meshed model adds up 1980 1D elements all for the suspension modelling (Figure 34 - 36).

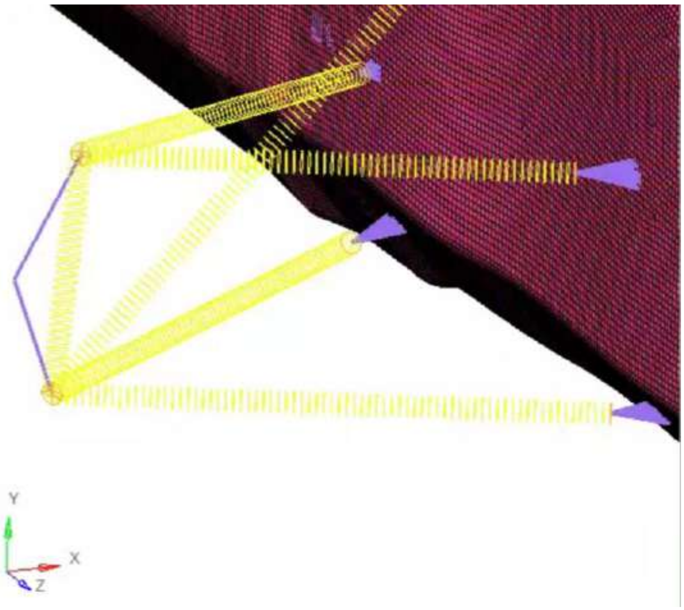

Figure 34 Front suspension detailed mesh

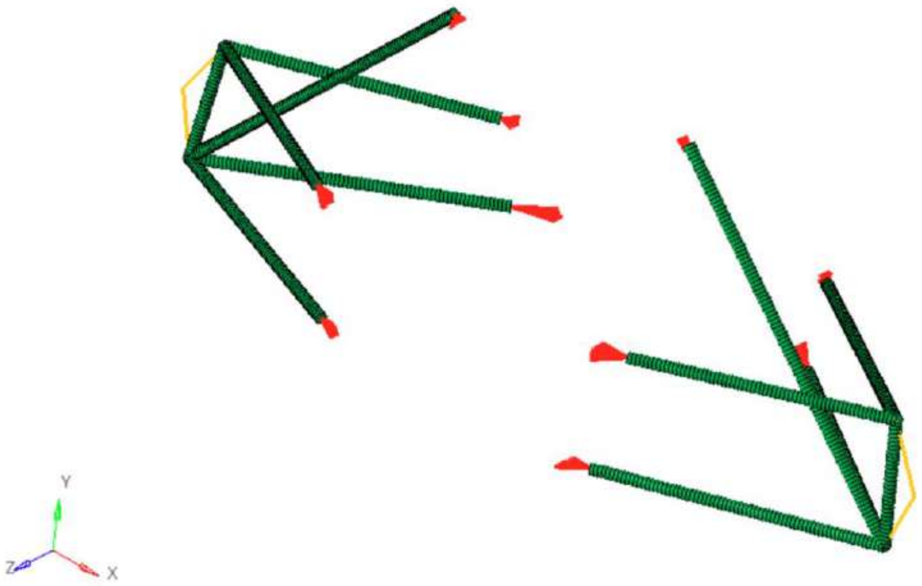

Figure 35 Front suspension meshing

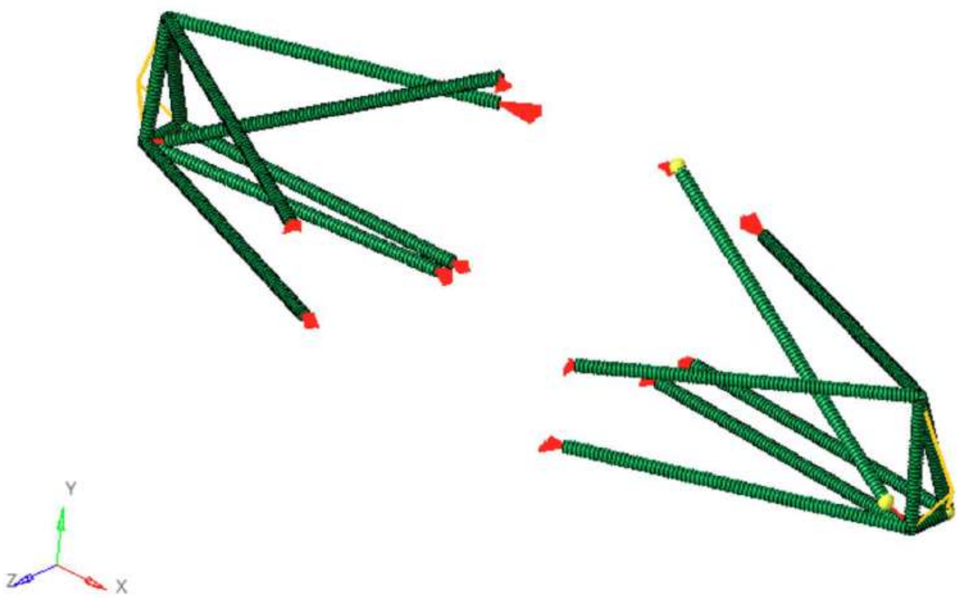

Figure 36 Rear suspension Meshing

4.3.1.1 PROPERTIES:

Properties are assigned to each component for the solver to identify their physical properties. They determine the physical behaviour in the simulation. The properties that we will be using for the suspension systems is PBEAM and for the composite parts we will be using the PCOMPP property.

PBEAM:

The PBEAM property is defined by the section of the suspension tube and the material type. For this case a steel suspension system has been used for the simplicity on the modelling of the material. For further implementations, the suspension can be modelled with carbon fibre tubes. The section of the suspension rod is a basic circular section; in this field further implementations can be made.

PCOMPP:

PCOMPP is a property card used to define composite laminates for panel-based composite optimization. This property is essential to perform free size and sizing optimization. In PCOMPP it's important to identify the Z0 parameter. This parameter establishes the offset of the shell mid-surface from the actual mesh surface. In this model, the Z0 offset is not needed so this parameter is not filled, and the option is set to real.

4.3.2 SYSTEMS

In the Hypermesh model the global coordinate system was defined by:

X axis: Transversal to the tub's longitudinal direction.

Y axis: vertical direction to the tub's longitudinal direction.

Z axis: Parallel to the tub's longitudinal direction.

This system has been stablished from the SolidWorks model; in the automotive industry the X axis is parallel to the tub's the longitudinal direction and the Z axis is the vertical one (Figure 37).

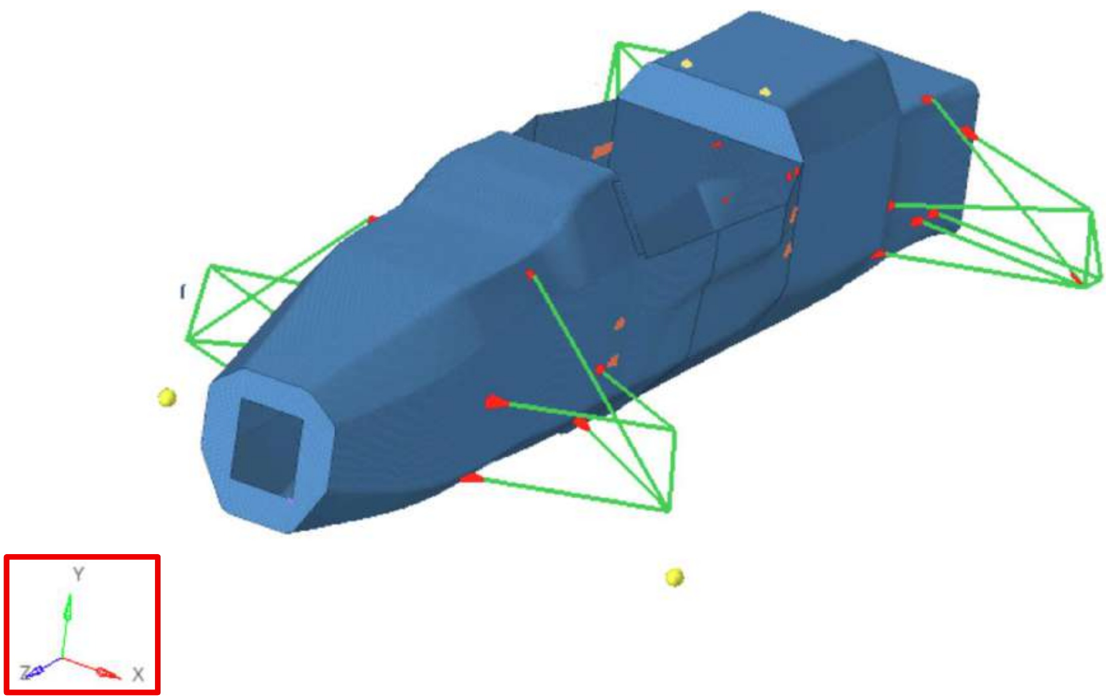

Figure 37 Definition of the global coordinate system

In my Hypermesh model there are also 2 more independent coordinate systems that serve as reference for the plies orientation and for the suspension nodes. The plies orientation coordinate system is situated just below the driver's legs. This system helps with the 0º baseline for ply orientation and the normal vectors baseline for the laminate sequence (Figure 38).

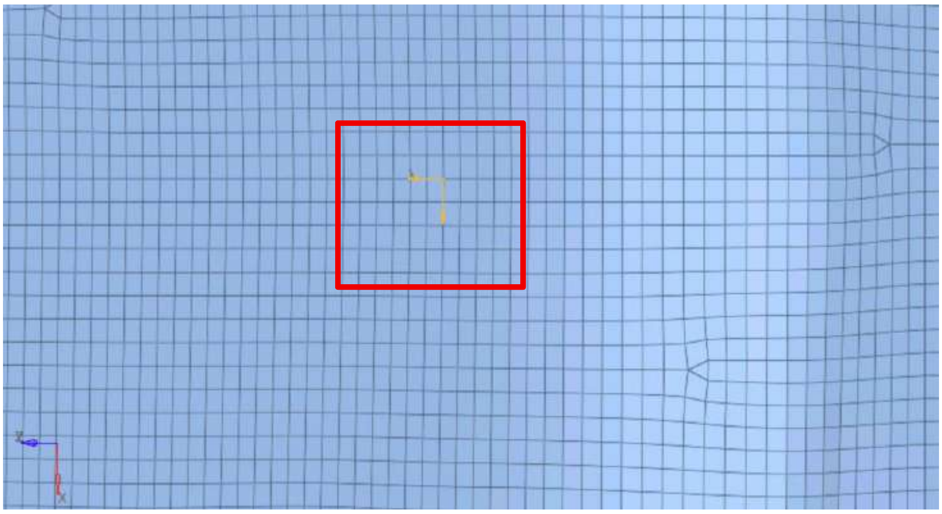

Figure 38 Ply orientation coordinate system in the Hypermesh model

The last coordinate system helps to establish a relationship between the solidworks model and the Hypermesh model. The placement of this coordinate system has been the left-hand side (drivers view) from the AIP maintenance hole. All suspension nodes have that reference which makes it easier to trespass the suspension coordinates from Solidworks to Hypermesh. Figure 39 shows the positioning of the suspension points reference system (Figure 39).

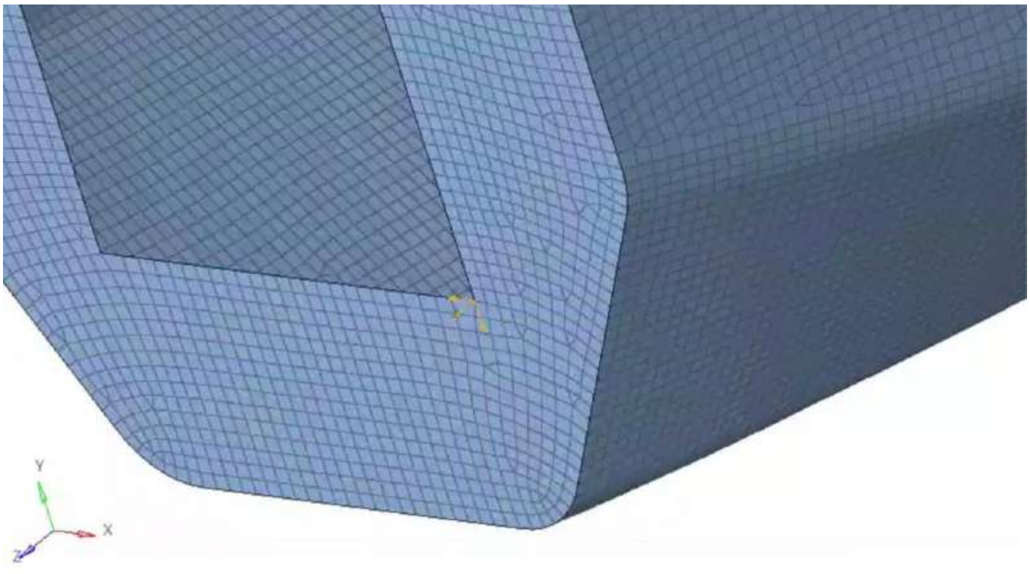

Figure 39 Suspension nodes coordinate system

DEGREES OF FREEDOM

In Hypermesh each node has 6 D.O.F, for the simulation constraints theses parameters will be used:

1. Translational degree of freedom on the x axis
2. Translational degree of freedom on the y axis
3. Translational degree of freedom on the z axis
4. Rotational degree of freedom on the x axis
5. Rotational degree of freedom on the y axis
6. Rotational degree of freedom on the z axis

4.3.3 MATERIALS

Materials in Altair Hypermesh are first designated because of their mechanical properties. In this model MAT8 and MAT1 type materials are the ones used, MAT8 defines a linear elastic orthotropic material for 2D elements (surface mesh elements) and MAT 1 defines a linear static, isotropic material where mechanical properties are the same in all directions. The MAT 8 designation was used for all the CFRP plies and MAT 1 was used for the suspension geometry and the torsion rig.

CARBON FIBRE LAMINATES:

The material selection consists of a range of commercially available carbon fibre pre-impregnated (pre-preg) materials. Three types of carbon laminates from Gurit are considered, as they are commonly used in advanced engineering applications and in the design of lightweight, high-strength structures. The Gurit IMC Fiber UNI material corresponds to a unidirectional carbon fibre laminate, providing maximum strength and stiffness along the fibre direction, which is particularly suitable for applications where the primary loads are concentrated along a single axis.

In addition, the Gurit RC200T 0°/90° laminate is a bidirectional fabric that offers load-carrying capability in two perpendicular directions, enabling improved load distribution in components subjected to multiaxial stresses. Finally, the Gurit XC411 ±45° laminate is a diagonal fabric optimized for shear load absorption and enhanced structural response under torsional or inclined loading conditions. These materials are combined to exploit their complementary mechanical properties and to optimize the overall structural performance and weight of the model. [7]

The mechanical properties of each type of material are contemplated on the following table (Table 6):

PROPERTIES	Units	IMC Unidirectional fibre	RC 200T 0ºx90º fibre	XC411 45ºx45º
Volume fraction	%	55.5	47-53	47-59
Density	ton/m^3	1,50E-09	1,50E-09	47-59
Cured ply thickness	mm	0.23*	0.23	0.43
E11 (Young modulus at 0º)	MPa	170000	60900	63800
E22 (Young modulus at 90º)	MPa	8400	61600	64500
v12 (Poisson ratio)	-	0.3	0.06	0.06
G12 (shear modulus)	MPa	3000	4136,856	4136,856
G1Z (out-of-plane shear modulus)	MPa	4136,856	2757,904	2757,904
G2Z (out-of-plane shear modulus)	MPa	2757,904	2757,904	2757,904
σ_11 (Tensile strength X_t)	Mpa	2874	1124	1124
σ_22 (Tensile strength Y_t)	Mpa	33.2	662	1237
Ec_11 (Young modulus at 0º)	MPa	153000	58300	62000
Ec_22 (Young modulus at 90º)	MPa	-	59000	62000
σ_11 (Compresive strength X_c)	Mpa	1354	759	595
σ_22 (Compresive strength Y_c)	Mpa	-	731	645

Table 6 Mechanical properties of all fibres[7]

Furthermore, an aluminium honeycomb core material has been integrated into the laminate as an internal layer, functioning as a through-thickness reinforcement element. This core configuration induces a beam-like structural effect by spatially separating the outer and inner composite plies, thereby substantially increasing the second moment of inertia and bending stiffness without proportional increases in overall mass. The honeycomb core selected exhibits a baseline density of 4.5 lb/ft³ with 1/8" cell dimensions and 0.0010" foil thickness, with provisions for thickness variation during subsequent optimization analyses (Table 7).[8]

This multi-directional laminate arrangement, combined with the core architecture, enables the structure to resist combined loading scenarios while maintaining structural efficiency and minimizing weight—critical parameters for the proposed application.

PROPERTIES	Units	DURA-CORE II 5052
Density	ton/m^3	7.42E-11
E11 (Young modulus at 0º)	MPa	1.0
E22 (Young modulus at 90º)	MPa	1.0
v12 (Poisson ratio)	-	0.3
G12 (shear modulus)	MPa	1.0
G1Z (out-of-plane shear modulus)	MPa	351.63
G2Z (out-of-plane shear modulus)	MPa	172.37
σ_11 (Tensile strength X_t)	Mpa	-
σ_22 (Tensile strength Y_t)	Mpa	-
Ec_11 (Young modulus at 0º)	MPa	-
Ec_22 (Young modulus at 90º)	MPa	-
σ_11 (Compresive strength X_c)	Mpa	-
σ_22 (Compresive strength Y_c)	Mpa	-

Table 7 DURA-CORE® II 5052 Aluminum Honeycomb mechanical properties [8]

4.4 SIMULATIONS

This section describes the simulation and optimization methodology used for the FEA analysis. The process follows a step-by-step workflow, starting from a basic model definition and load case selection, and progressing through free-size and sizing optimization stages. The simulations aim to minimize the mass of the monocoque while satisfying strength, failure criteria and manufacturing constraints. The final laminate configuration is obtained after all load cases are evaluated and validated through final analyses.

4.4.1 SIMULATION PROCESS

The simulation system used in this project follows a systematic, multi-stage optimization procedure to develop an optimized composite laminate architecture that satisfies structural performance requirements while remaining practical to manufacture. This methodology comprises three distinct optimization phases, each progressively refining the composite design through iterative computational analysis and constraint-based optimization.

The initial phase is the geometry validation stage, which ensures that the model is properly defined by verifying nodal connectivity and element correspondence. Torsional stiffness analysis is used as the primary assessment tool to identify and correct any geometric deficiencies. Following successful validation, the free sizing optimization phase explores different ply thickness configurations to determine optimal fibre orientations for the applied loading conditions. Subsequently, the sizing optimization phase incorporates manufacturing constraints and material specifications to refine the design, ensuring it can be practically manufactured while maintaining structural performance. Finally, constraint verification using the Hill failure criterion confirms that the optimized laminate provides adequate resistance under all prescribed load cases.

This systematic approach ensures that the resulting composite structure achieves optimal structural efficiency, satisfies failure criteria, and remains feasible for the teams to create. The optimization process is shown in Figure 40.

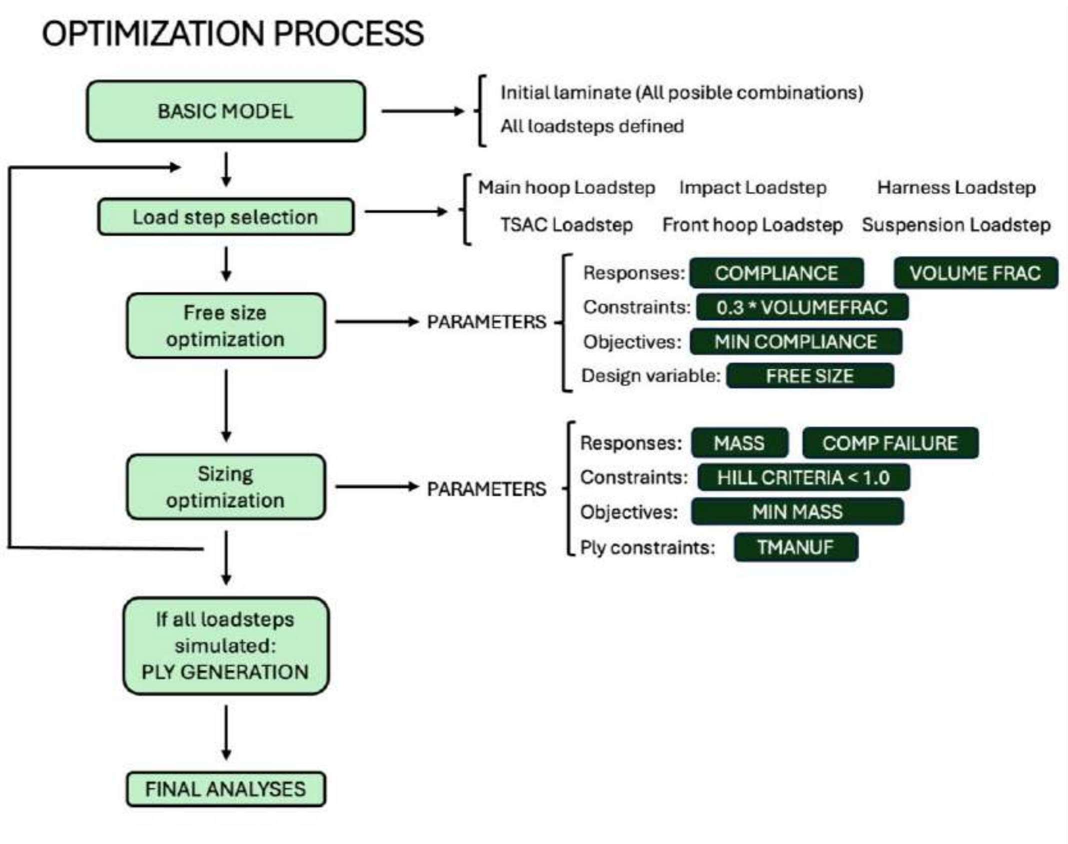

Figure 40 Simulation process schematic

4.4.1.1 Geometry fixing

The initial phase of the optimization methodology employs a preceding analysis stage to identify and rectify any modelling deficiencies, including surface inconsistencies and non-conformities that could compromise the integrity of following simulations by altering the results. For this preliminary validation, the torsional stiffness test was selected as the governing assessment criterion, as it provides an evaluation of the structural connectivity and nodal integrity across the model, putting through a test to critical suspension joints and interface nodes. The iterative refinement procedure required five discrete iterations of model correction and analysis verification to establish proper element connectivity and nodal correspondence throughout the structural mesh. During this iterative phase, the primary source of computational impedance was identified within the one-dimensional (1D) beam elements employed in the suspension system discretization. Through systematic debugging and geometric adjustment, these modelling issues were successfully resolved, thereby enabling the structural model to proceed to subsequent optimization stages with verified geometric and topological integrity.

Each 1D mesh element is discretized through a dual-nodal architecture, where each individual element is defined by two nodal points. An issue emerged with this discretization approach: the nodal coordinates undergo automatic re-initialization whenever any connected elements are removed or modified from the model geometry. This nodal re-definition induces a discontinuity in the mesh topology and, consequently, in the structural system defined by the mesh. Should the finite element analysis proceed under these compromised conditions, the discontinuous nodal configuration results in the disassociation of suspension linkage elements that should otherwise remain kinematically coupled. This topological failure propagates incorrect displacement and force values throughout the model, which are important for simulations like torsional stiffness analyses where structural coupling and load transfer pathways are of importance.

Upon completion of the geometric validation, a baseline torsional stiffness analysis was conducted employing the corrected model geometry and the preliminary laminate configuration described previously. The computational results obtained at this baseline stage yielded a torsional stiffness of 2742.66 Nm/deg and a corresponding total monocoque mass of 56.88 kg (Table 8). These initial analytical metrics establish the reference configuration from which subsequent optimization iterations will be evaluated.

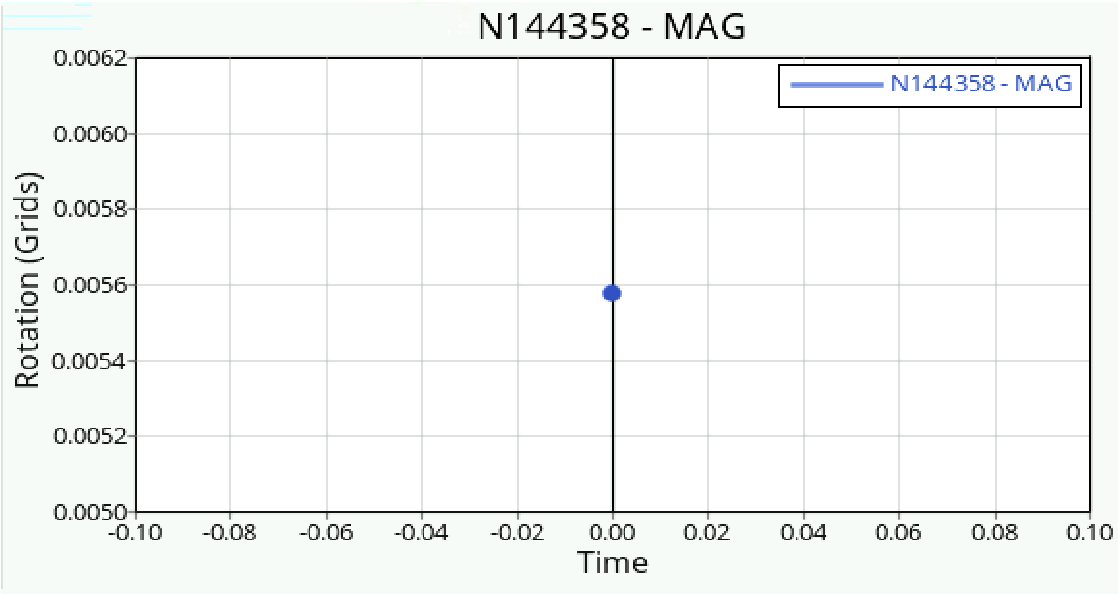

Table 8 Initial torsional stiffness tests results

4.4.1.2 Free sizing

During this optimization stage, the composite ply laminate thicknesses are systematically optimized without additional constraints. Throughout these simulations, the algorithm identifies and evaluates distinct ply stacking sequences and laminate configurations that are contingent upon the applied loading conditions. The computational module utilized for this optimization phase is the dedicated optimization solver, which operates independently from the standard finite element analysis procedures. This specialized module establishes and evaluates alternative design variables and generates corresponding optimization responses that serve as input data for subsequent analysis iterations.

OPTIMIZATION RESPONSES

The optimization responses constitute the quantitative metrics that the computational solver evaluates iteratively during the optimization process to determine the appropriate design modifications. At each iteration cycle, the response quantities provide guidance to the solver regarding which parameters require evaluation and adjustment. These responses establish the linkage between design variables, structural constraints, and the physical finite element model, thereby enabling a comprehensive assessment of model performance. For the free sizing optimization procedure implemented in this study, two primary response metrics are employed: composite compliance and volumetric fraction.

DESIGN VARIABLES

The design variables represent the adjustable parameters that the optimization solver manipulates to satisfy the established objectives and constraints. These quantities constitute the degrees of freedom that the algorithm explores within the solution space. For the present investigation, the design variables have been configured to operate under the free sizing methodology, with modifications applied directly to the laminate stack sequence and individual ply thickness values.

OPTIMIZATION CONSTRAINTS

The optimization constraints define the permissible boundaries and limitations that the design solution must satisfy throughout the iterative solution process. These constraints are imposed directly upon the optimization response metrics. Within the context of the free sizing optimization procedure, the volumetric fraction reduction constraint has been established at 0.3, thereby stipulating a maximum thirty percent reduction of the composite material volume. The underlying objective of this volumetric constraint is to systematically reduce the structural mass of the model while maintaining structural adequacy.

OBJECTIVES

The optimization objective represents the singular performance metric that the solver endeavours to improve while simultaneously satisfying all imposed constraints. For the free sizing optimization methodology, the primary objective is the minimization of structural compliance, which is mathematically defined as the inverse of stiffness. This objective formulation ensures that the resulting design exhibits optimal stiffness performance while respecting the mass reduction constraint. Figure 41 represents the resulting ply shape after a free size optimization.

Figure 41 Free sizing example with suspension loads

4.4.1.3 Sizing

Following the completion of the free sizing optimization phase, the laminate configuration requires further refinement to ensure manufacturability and compliance with the rule's constraints on mechanical properties of the monocoque. The subsequent sizing optimization procedure establishes a revised set of optimization responses, constraints, and objectives specifically formulated to enhance the practical feasibility of the design outcomes.

The optimization responses employed during the sizing phase comprise the composite failure criterion (COMP FAILURE) and the total structural mass (MASS). The primary objective of this optimization stage is the minimization of total mass while maintaining the composite failure coefficient, evaluated through the Hill failure criterion, below a critical threshold of unity. During this refinement process, additional constraints must be imposed upon both the material failure coefficient and the individual ply thickness values, as these parameters are predetermined by the commercial specifications and manufacturing tolerances established by the composite cloth supplier. The implementation of these manufacturer-imposed constraints ensures that the resulting laminate configuration can be practically realized through standard production methodologies.

The optimization results from this sizing phase yield a laminate stacking sequence that exhibits comparable fibre orientation distributions to the free sizing results, yet with individually adjusted ply thicknesses that reflect the discrete thickness increments and material specifications of each individual ply type. This iterative refinement ensures that the final design maintains optimal structural efficiency while remaining compatible with established manufacturing processes and material availability.

4.4.1.4 Sets definition

The computational analysis of each individual load case generates a distinct lamina architecture, wherein each resulting ply configuration exhibits a continuous, non-discrete geometry that is inherently unsuitable for practical manufacturing implementation. Upon completion of all load case evaluations, it becomes necessary to establish discrete ply sets that systematically consolidate and organize the simulation results into a manufacturable composite structure. This consolidation process requires comprehensive examination of each individual ply generated by the optimization algorithm, with particular attention directed toward determining optimal layer positioning and geometric definition.

The raw simulation outputs, as presented in figure 22, exhibit ply geometries that have been individually refined to satisfy the constraint criteria established during the preceding sizing optimization phase. However, these raw computational results maintain continuous, irregular geometries that preclude direct manufacturing implementation. Through systematic analysis and geometric refinement, the continuous ply geometries derived from raw simulation data are transformed into discrete, well-defined shapes that possess practical manufacturability and facilitate subsequent processing and assembly operations, as shown in figure 23. This transition from continuous theoretical geometry to discrete manufacturable geometry ensures that the optimized laminate design can be reliably fabricated using established composite manufacturing methodologies. In Figure 42, the simulation result is displayed and in the next figure, the sophisticated result after the final optimization (Figure 43).

Figure 42 Suspension loads sizing simulation 18 ply

Figure 43 Final suspension plies set

4.4.1.5 Analyses results

Following the completion of the sizing optimization phase and the transformation of all ply geometries into discrete, manufacturable configurations, comprehensive verification of all established design constraints must be conducted. The previously defined load cases serve as the analytical basis for this verification process, employing the Hill failure criterion to demonstrate that the monocoque structure exhibits adequate resistance and structural integrity under the prescribed loading conditions.

A critical consideration in this validation process concerns the structural modelling of insert connection points, wherein mechanical fasteners and component interfaces are discretized using rigid body element (RBE2) formulations. The nodal connectivity between RBE2 elements and the laminate surface generates localized stress concentrations of significant magnitude. These stress singularities introduce computational distortions that can substantially influence the predicted ply quantities necessary to satisfy the Hill failure criterion constraints. While such geometric stress concentrations may artificially elevate the required lamina thickness and ply count in the immediate vicinity of these connection nodes, the overall ply orientation characteristics and fundamental fiber architecture patterns remain consistent throughout the optimization iterations. Therefore, the underlying laminate fiber configuration and ply type selections demonstrate reliable consistency across all simulation scenarios, enabling confident assessment of the optimized composite architecture despite localized computational anomalies associated with rigid element boundary conditions. In the following figures the different rigid elements used as attachments are shown (Figure 44 – 49)

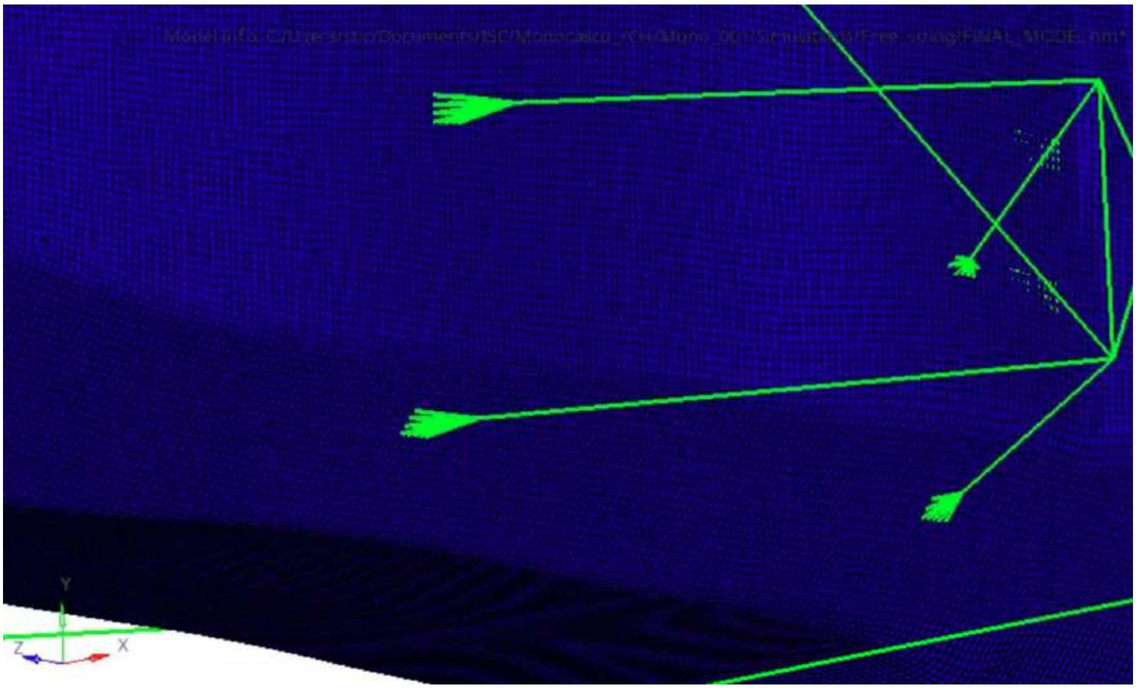

Figure 44 Front suspension RB2 pick up points to monocoque surface elements

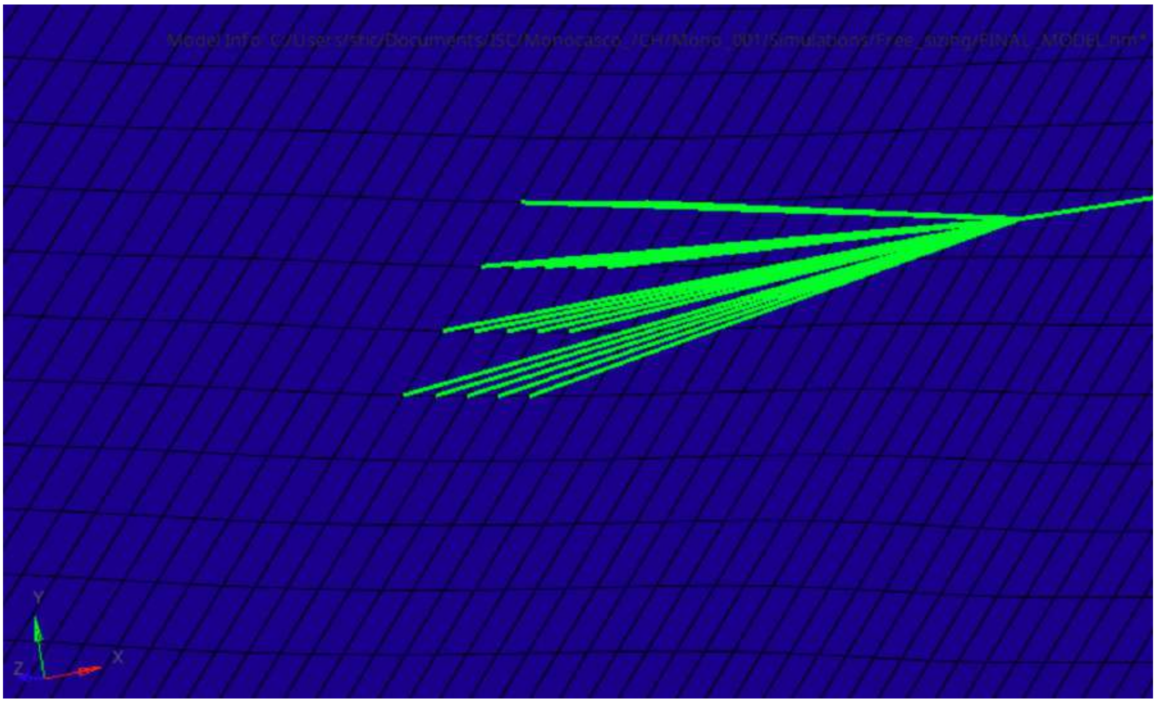

Figure 45 RBE2 suspension pick up point connection detailed

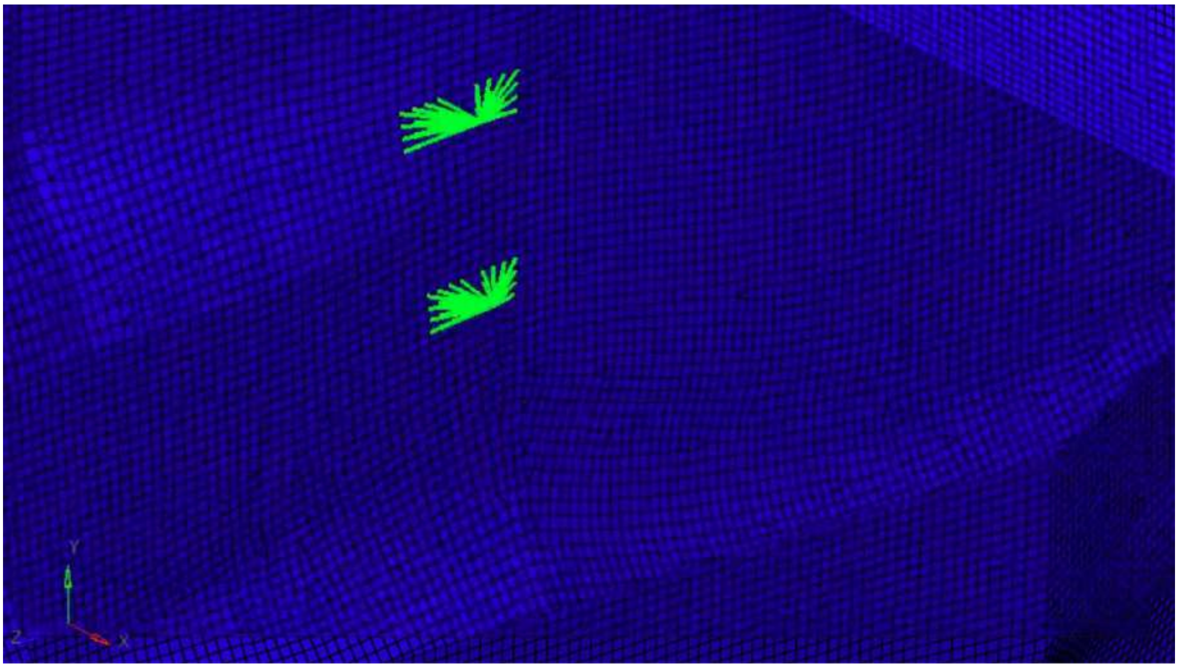

Figure 46 Main Hoop attachments RBE2 elements

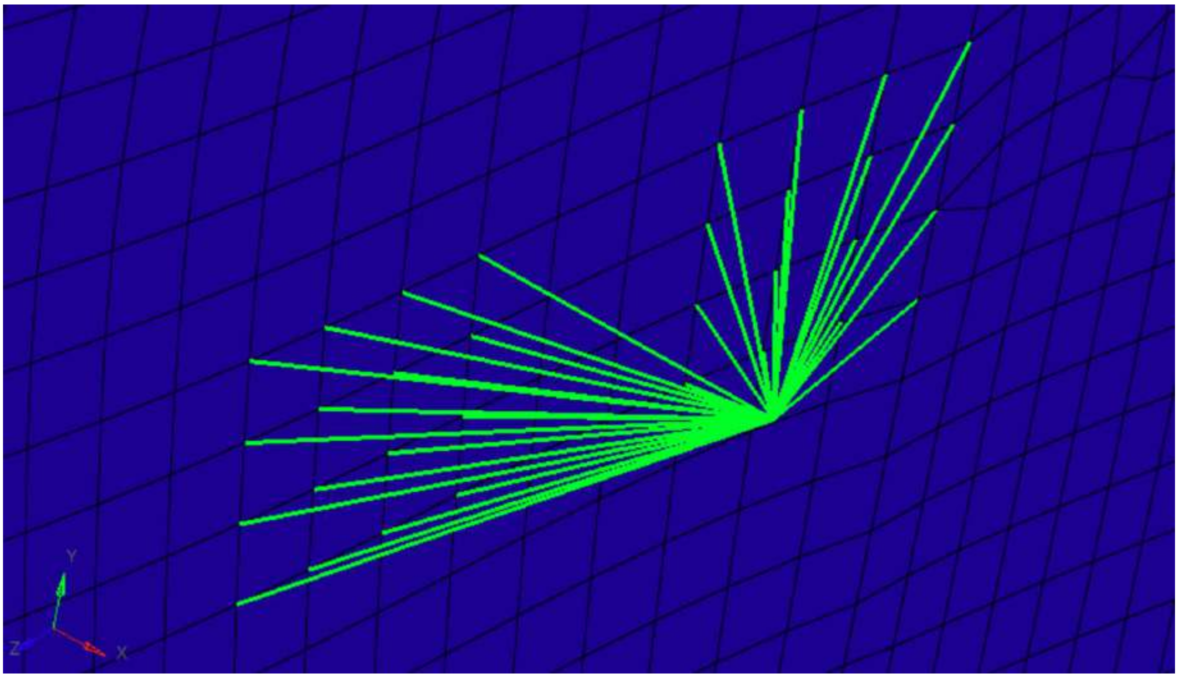

Figure 47 Main Hoop attachments RBE2 element detailed

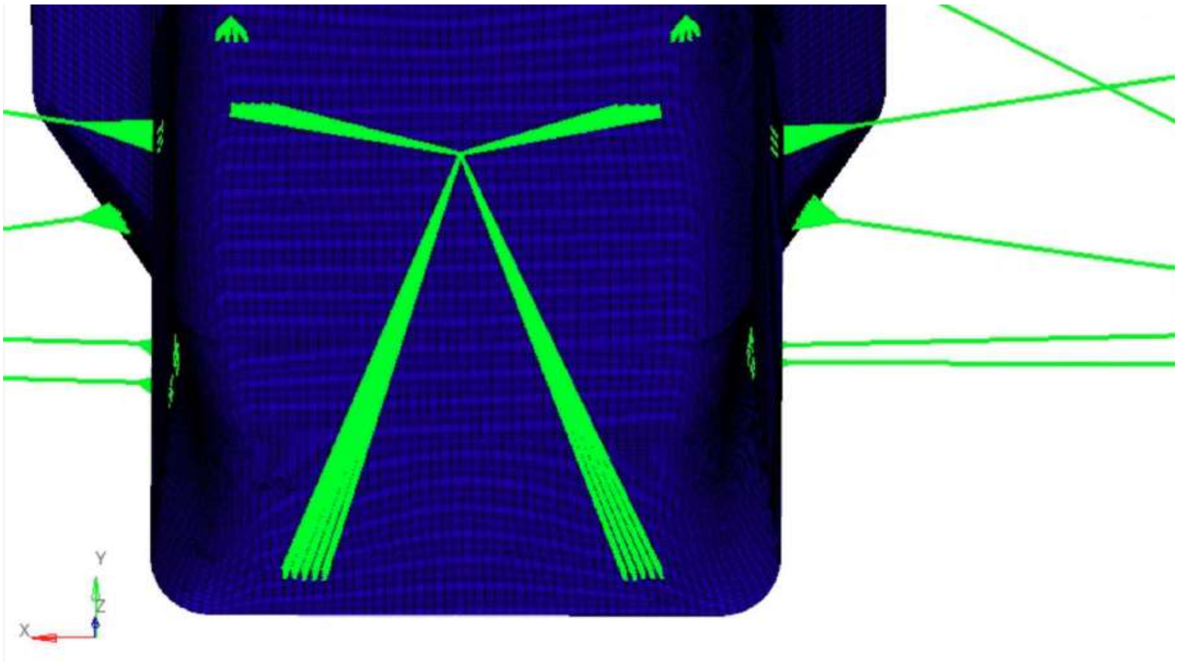

Figure 48 TSAC RBE2 element

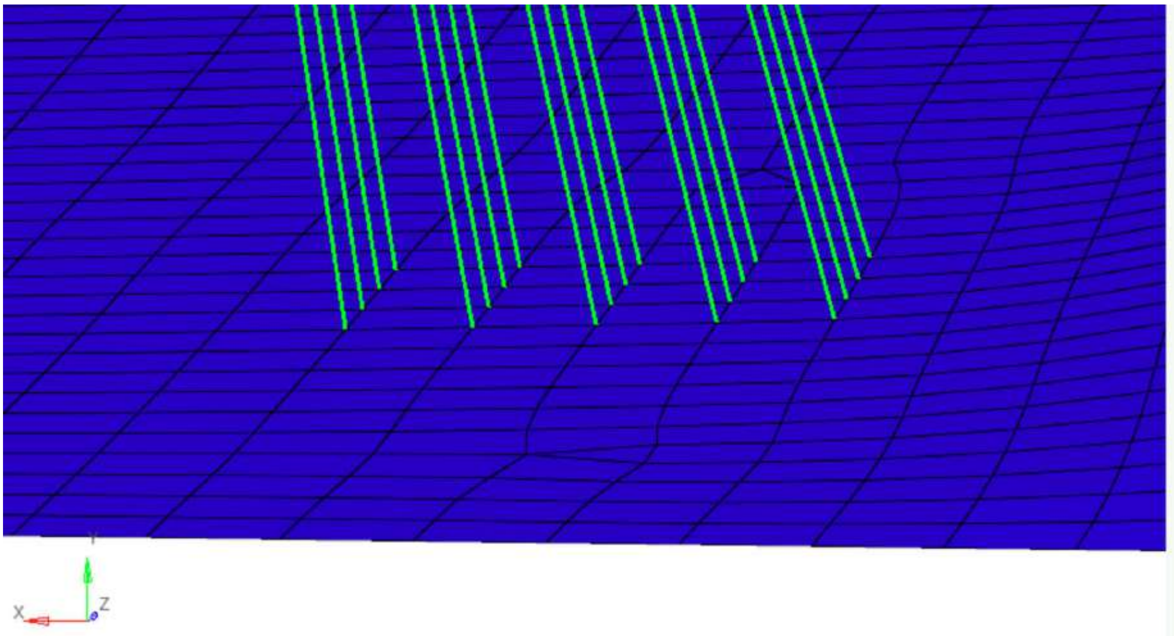

Figure 49 TSAC RBE2 element detailed

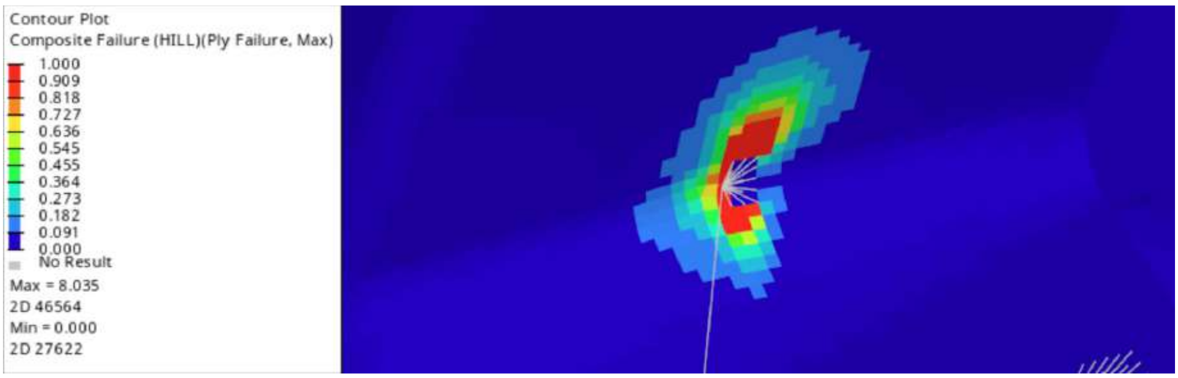

Figure 50 Suspension point transmitting forces through a RBE2 rigid element

4.4.2 HOOP LOADSTEP

The driver's safety is contemplated in the Formula Student Germany rules with the roll over envelope. This envelope is created with the front hoop and the main hoop. These hoops themselves don't affect the simulations as the attachments are the one contemplated in our constraints.

The rule T. 3. 16. 1 [Ref] states that if two parts of the primary structure are bolted together each attachment point between the two parts must be able to carry 30kN in any direction.

The two hoops belong to the primary structure, so each attachment point mush be able to carry these loads. In this case the insert is not being contemplated in the simulations, so the attachment point of the main hoop and front hoop are RBE2 elements positioned in the same spot.

HOOP LOAD CASE		
Load X axis	30000	N
Load Y axis	30000	N
Load Z axis	30000	N

Table 9 Hoop load case

The scope of the following simulations is two verify, following the Hill failure criterium, if the laminate fails under the proposed loads. The objective with this failure criteria is to get the value of the simulation under 1 (Figure 51). With the use of RBE2 elements, as explained before, condition the results on their nearby area. The main hoop bracing is included on the hoop laminate distribution.

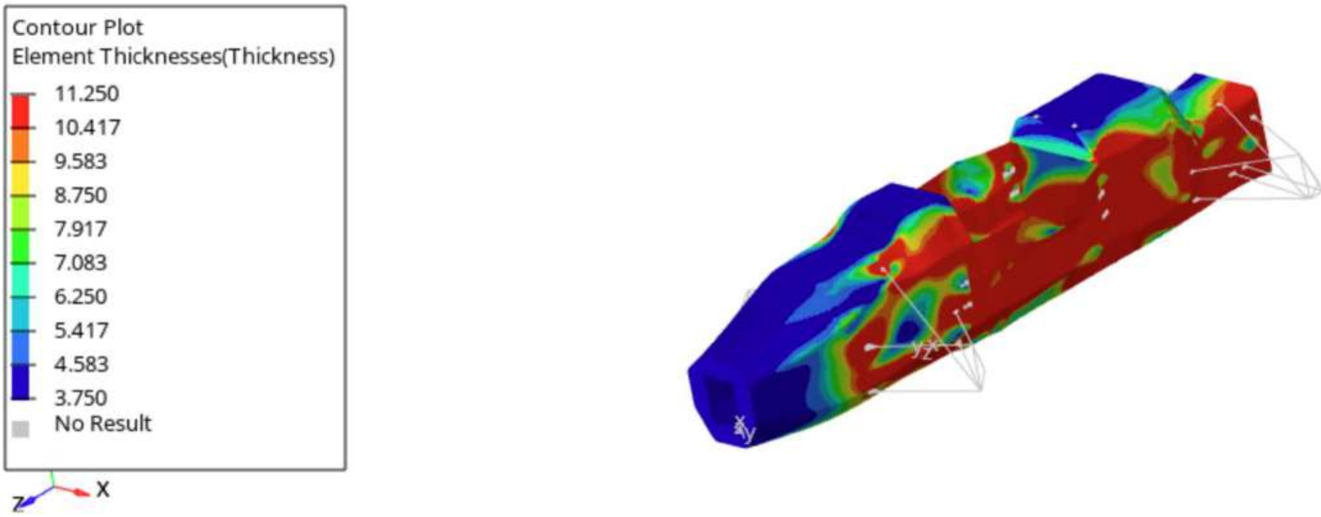

Figure 51 Main hoop loadstep free size optimization

After the free sizing optimization, the TMANUF parameters are stablished, the constraints, responses and objectives are changed. In Figure 52, the parameters stablish the thickness of each element. Furthermore, the laminate is more discrete.

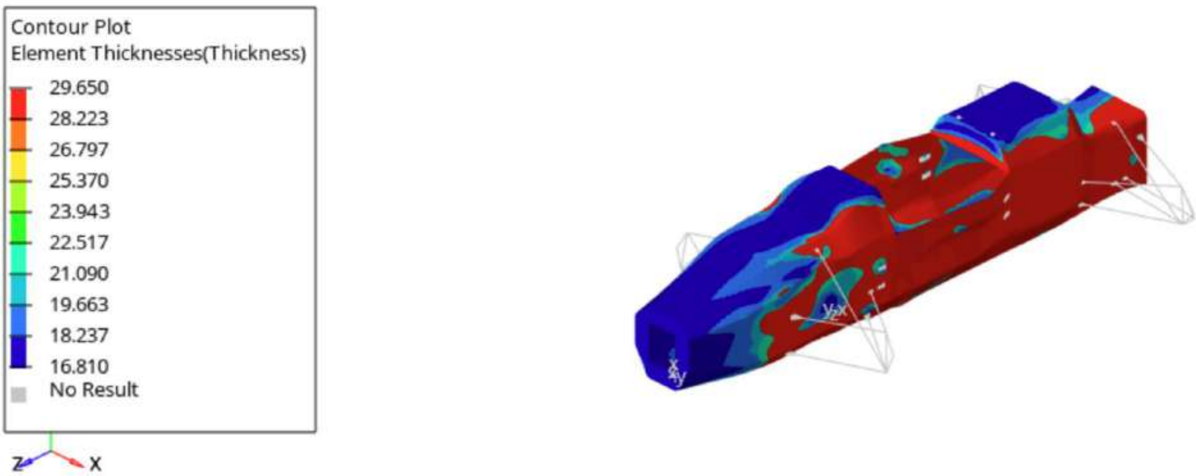

Figure 52 Main hoop loadstep sizing optimization

The result on this simulation creates a new laminate compliant with the manufacturing and stress constraints. Due to the problems mentioned before with the RBE2 elements, the resulting laminate is not representative. For this reason, the plies materials, orientations and forms have been considered but not the number of plies.

4.4.3 TSAC LOAD STEP

The TSAC is one of the critical components of the car. Its objective is to protect and hold in place the tractive system accumulator in all kinds of events. To develop confident simulation, it has taken the reference weight of a battery pack in formula student, so a 38,5 kg accumulator is used. Critical components, as stated in rule T3.3[1], must be able to withstand 40G in the longitudinal and transverse direction, and 20G in the vertical direction. In this case the loadstep that will be used in the simulation is the following (Table 10):

TSAC LOAD CASE		
Load X axis	19031,4	N
Load Y axis	19031,4	N
Load Z axis	9515,7	N

Table10 TSAC loadstep

This loadstep is applied on a RBE2 elements that simulates the TSAC. The simulation results are the following (Figure 53 – 54):

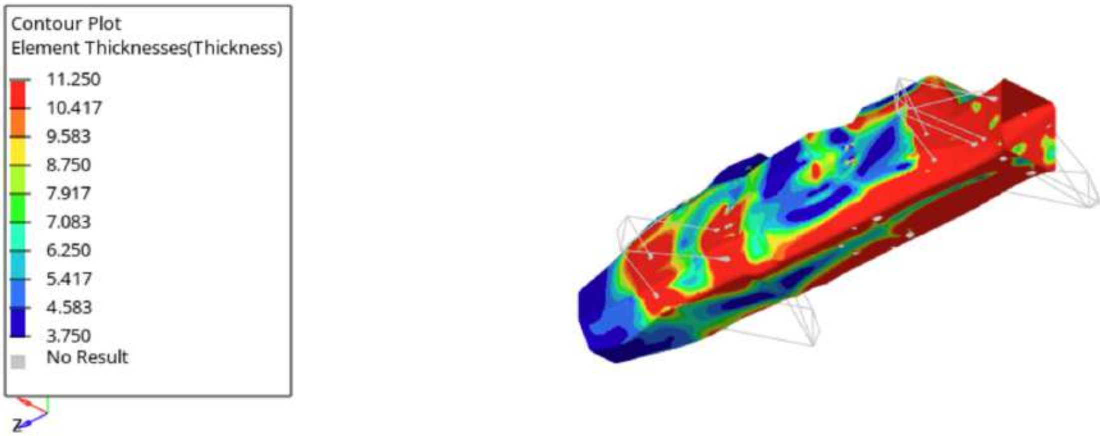

Figure 53 TSAC loadstep free size optimization

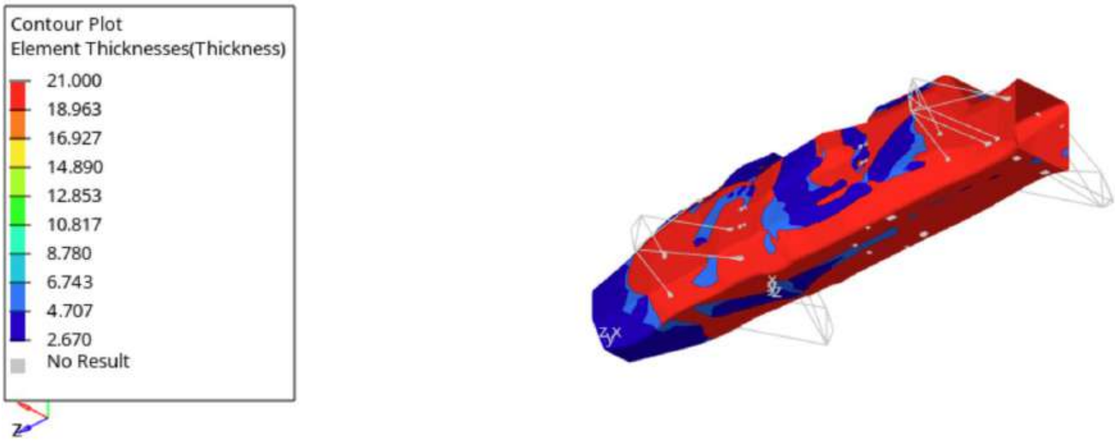

Figure 54 TSAC loadstep Sizing optimization

4.4.4 HARNESS LOADS

The harness is divided into two sections: The shoulder harness placed near the shoulder of the driver and the lap / antisubmarine belts which are placed below the driver and have other load distributions.

The attachment points for shoulder and lap belts must be capable of withstanding a minimum tensile load of 13 kN, while the attachment points for anti-submarine belts (lower anchors) must support a load of at least 6,5kN (Table 11). The attachment points have been modelled as RBE2 elements for both the shoulder and the harness attachment points. The simulation results are shown on Figures 55 to 58.

	Axis	Value	Units
Anti Submarine	y	6500	N
Lap Belts	y	13000	N
shoulder harness	z	13000	N

Table 11 Harness Loadstep

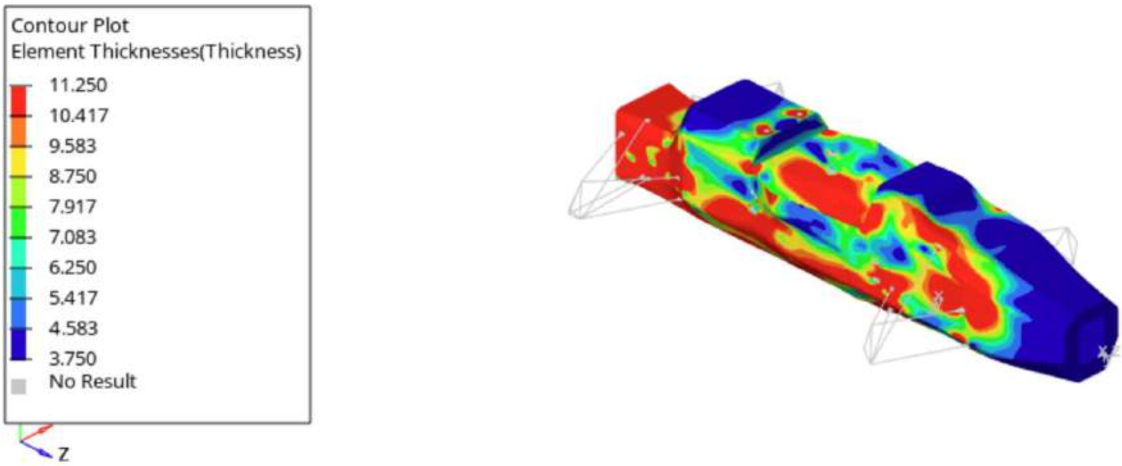

Figure 55 Harness loadstep free size simulation isometric

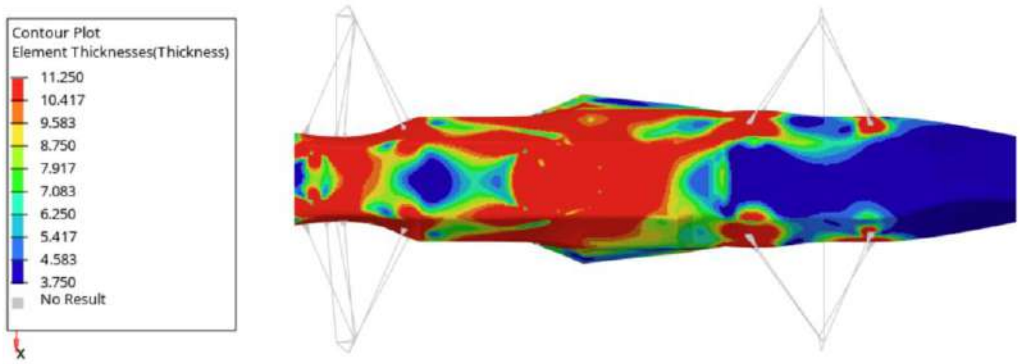

Figure 56 Harness loadstep free size simulation floor

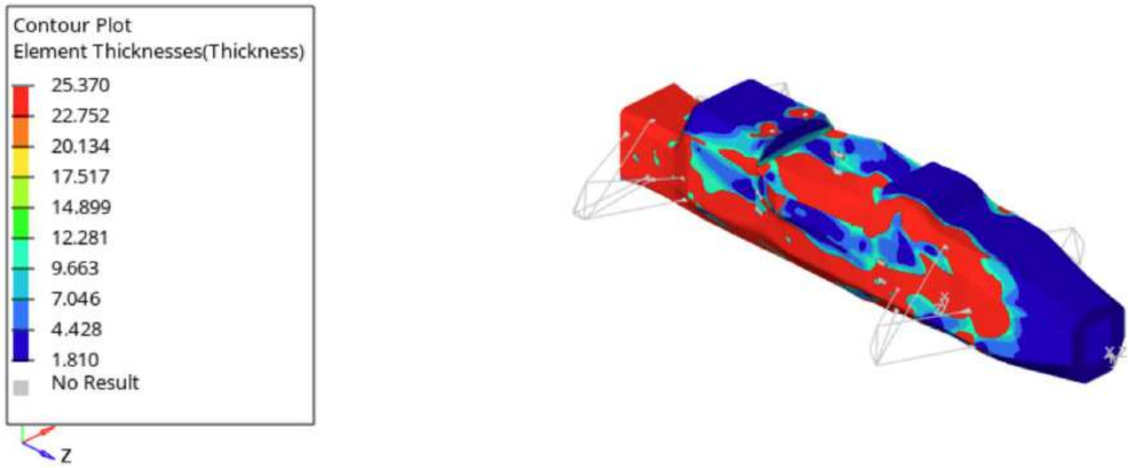

Figure 57 Harness loadstep sizing simulation top

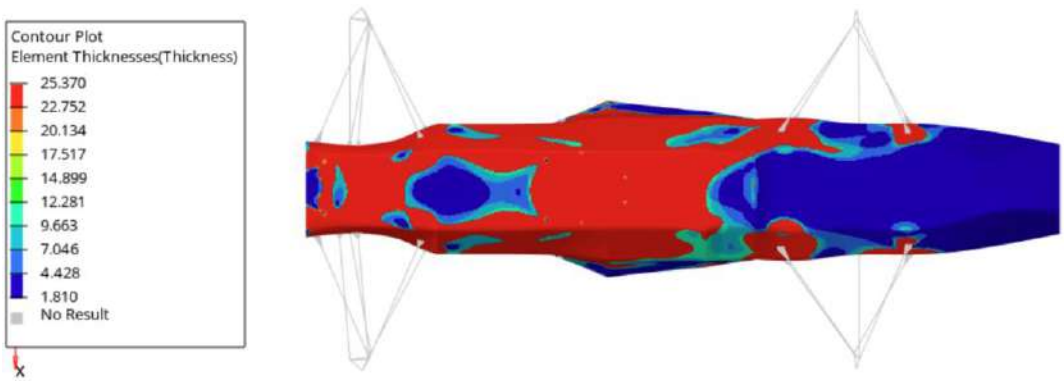

Figure 58 Harness loadstep sizing simulation top

4.4.5 Suspension Loadstep

The suspension loadstep simulates the structural integrity of the monocoque under dynamic loading conditions representative of cornering, acceleration, and braking. This load case simulates the complex multiaxial stress states generated by suspension component loads and inertial forces experienced during high-performance vehicle operation (Table 12). The free size and the sizing optimization reveal the ideal place of each ply (Figure 59 – 60).

Highest operating force Front						
	Up-fore	Up-aft	Low-fore	Low-Aft	Push/Pull	Tie/Toe
Comp	6701	3035	1748	5886	2541	1566
Tens	-165	-2503	-16754	-5733	-961	-2302

Highest operating force Front						
	Up-fore	Up-aft	Low-fore	Low-Aft	Push/Pull	Tie/Toe
Comp	6262	2916	5878	2927	4632	4003
Tens	-435	-2343	-14377	-12776	-811	-1427

Table 12 Suspension loads (N) [9]

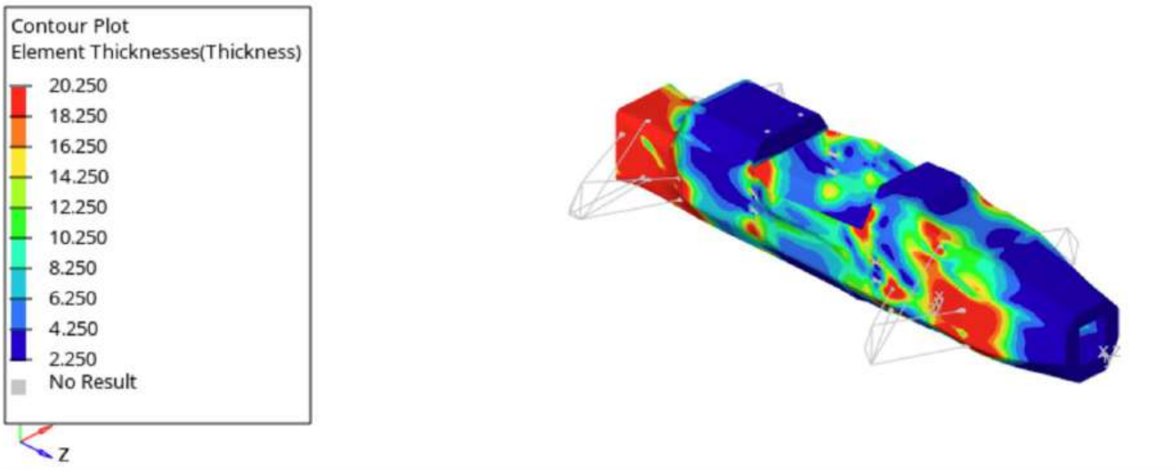

Figure 59 Suspension loadstep free size simulation isometric

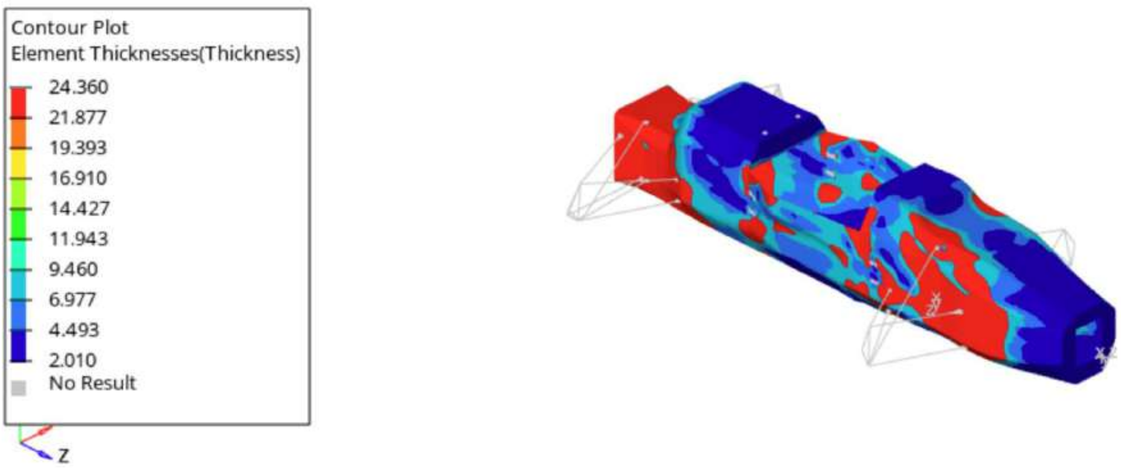

Figure 60 Suspension loadstep sizing optimization

4.5 IMPACT LOADSTEP

The impact loadstep analysis evaluates the structural performance of the monocoque under two critical load scenarios representative of severe crash conditions. The impact load cases are two: a side impact load of 7.5 kN and a front impact load of 20 kN corresponding to an 8g deceleration event on a vehicle with a mass of 250 kg (Table 13). The free size optimization methodology was applied to the composite laminate architecture to identify optimal ply thickness distributions under these impact loading conditions. After the free size optimization, the sizing optimization finishes the process stablishing the laminate thickness with failure constraints (Figure 61 -62).

IMPACT LOAD CASE		
Side impact	7500	N
Front impact (8g 250kg)	20000	N

Table 13 Impact loadstep

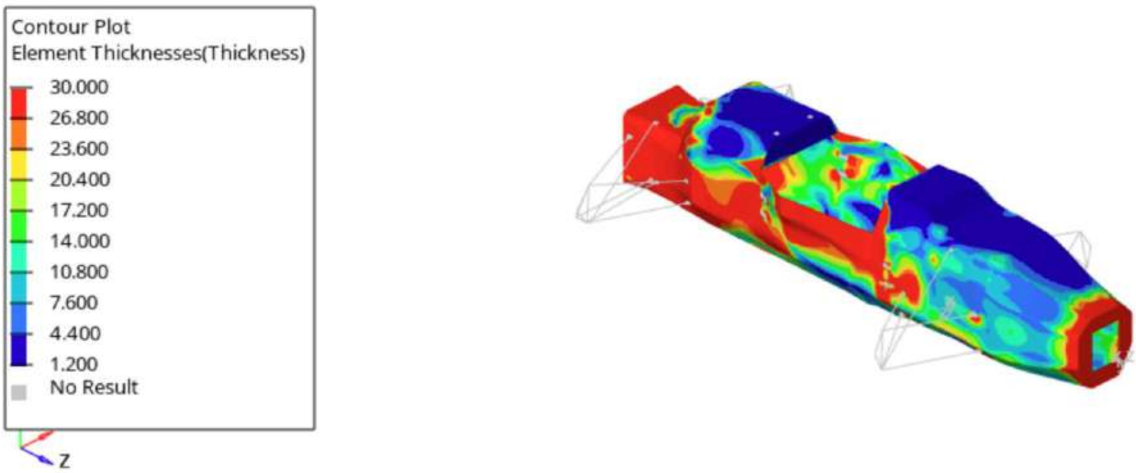

Figure 61 Impact loadstep free size optimization

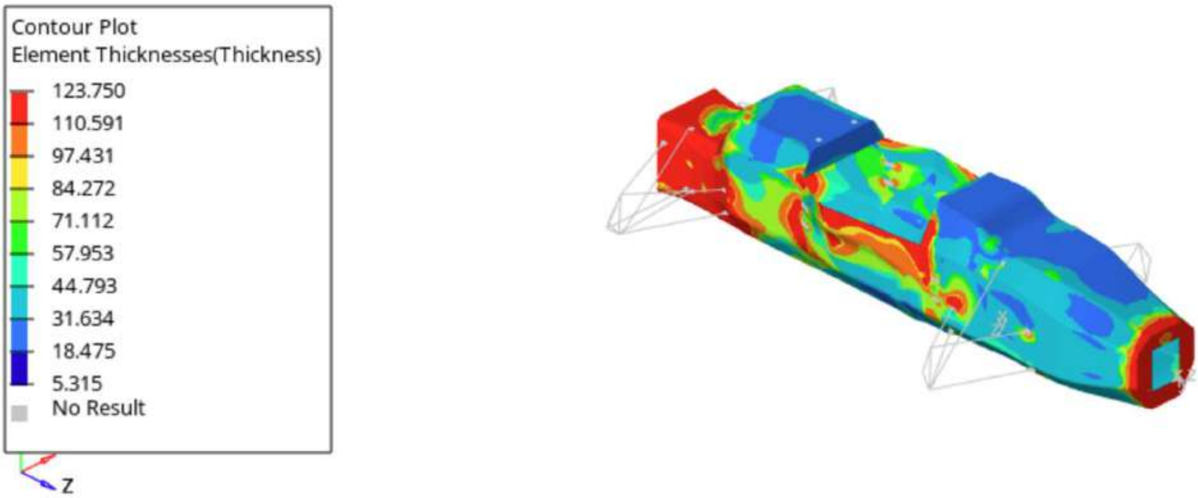

Figure 62 Impact loadstep sizing optimization

Chapter 5. RESULTS AND FINAL DESIGN

5.1 SIMULATION RESULTS

The optimization process shows where to place the optimum ply configuration for each loadstep. The ply results are analysed, and each form of the plies must be changed. For optimal performance, the laminate must be balanced in both ply forms, symmetries and lay up configuration.

At the start, the monocoque weight was 72 kg because of the additional ply thicknesses added for the free size optimization. However, the comparison must be made with ISC last season car, the IFS-07. This formula chassis had a total weight of 38,5 Kg and a torsional stiffness of approximately 2300 Nm/deg (Figure 63).

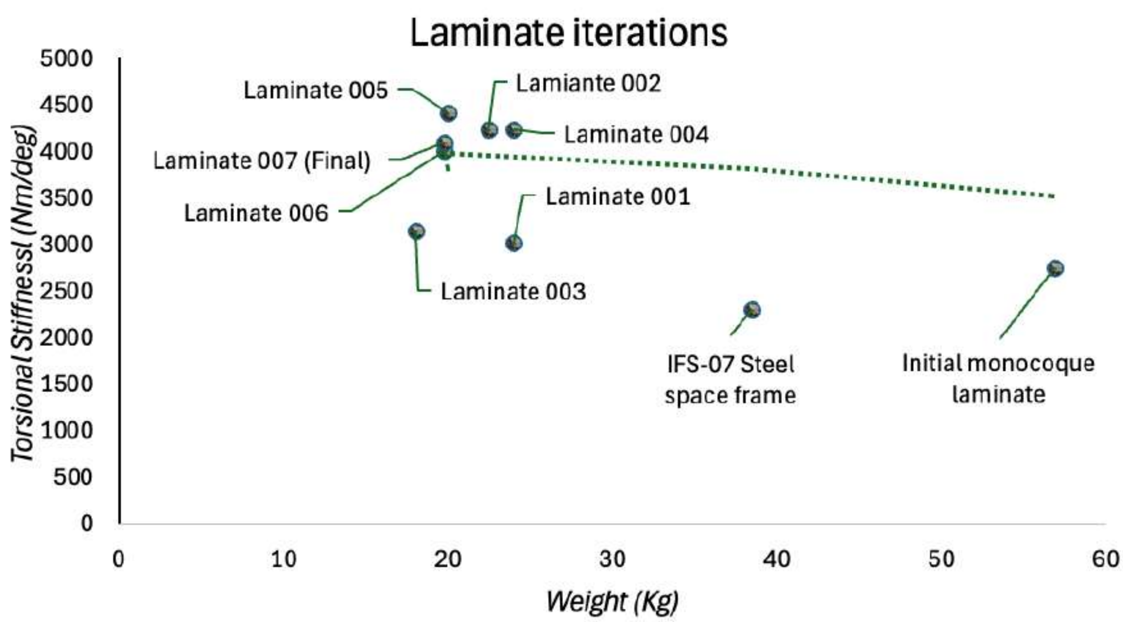

Figure 63 Representation of all laminate iterations

The laminate iterations were done by variating ply orders, honeycomb thickness and different material configurations for each ply. The key was to create an asymmetrical laminate maintaining the 45ºx45º plies on the bottom side of the laminate. This distribution creates great torsional stiffness while keeping the weight down. The identification of the zones is done by cross referencing the thickness diagram over the monocoque with the thickness reference in the characteristics card (Table 13 -14).

FINAL LAMINATE DISTRIBUTION (Zones)		
Zone Number	Thickness (mm)	Chassis part
Zone 2	26.12	Non - structural / body
Zone 6	27.44	Side impact (part) / Main Hoop bracing insert
Zone 5	27.64	TSAC
Zone 8	27.90	Suspension
Zone 9	28.10	Harness
Zone 10	28.30	Impact
Zone 11	28.96	Connection between harness / TSAC / Hoop sets
Zone 12	29.42	Intersections between harness / TSAC / Hoop sets
Zone 14	29.62	Lap belts and antisubmarine belts
Zone 15	29.42	Intersections between harness / TSAC / Hoop sets
Zone 17	29.88	Cockpit reinforcement
Zone 20	31.20	Front Hoop and Main hoop inserts

Table 13 Final Laminate zones distribution

FINAL LAMINATE DISTRIBUTION (Laminates)		
Zone Number	Ply distribution	Number of layers
Zone 2	0/45/H/45/45	4+H
Zone 6	0/45/45/45/H/45/45/45/45	8+H
Zone 5	0/45/0/0/H/45/45/45/45	8+H
Zone 8	0/45/0/0/45/H/45/45/45/45/45	10+H
Zone 9	0/45/45/0/0/H/0/45/45/45/45	10+H
Zone 10	0/45/0/0/0/H/0/45/45/45/45	10+H
Zone 11	0/45/45/45/0/0/H/45/45/45/45/45/45	12+H
Zone 12	/45/0/0/45/0/0/H/45/45/45/45/45/45/4	14+H
Zone 14	0/45/45/0/0/0/0/H/45/45/0/45/45/45/45	14+H
Zone 15	/45/45/0/0/45/45/H/45/45/0/45/45/45/4	14+H
Zone 17	5/0/0/45/45/0/0/H/0/45/45/45/45/45/45	16+H
Zone 20	15/45/0/0/45/45/H/45/45/0/45/45/45/45	20+H

Table 14 Final zones laminates

The results with the optimized laminate surpass the objective (Figure 64 – 65). The total mass of the optimized monocoque is **19,78Kg** and the torsional stiffness is **4083 Nm/deg** (Table 15).

STIFFNESS	4089,0371	NM/deg
MASS	19,78	Kg

Table 15 Final monocoque results

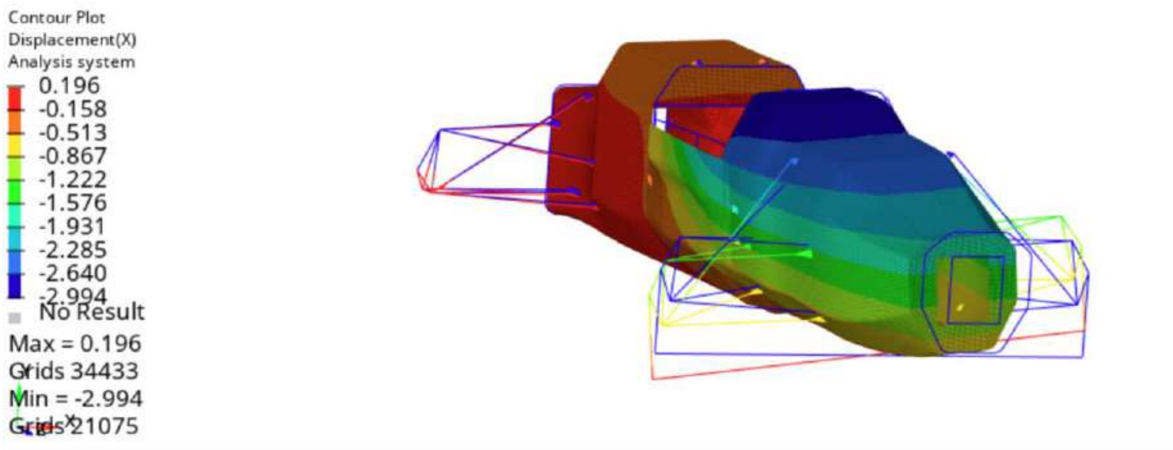

Figure 64 Torsional stiffness results

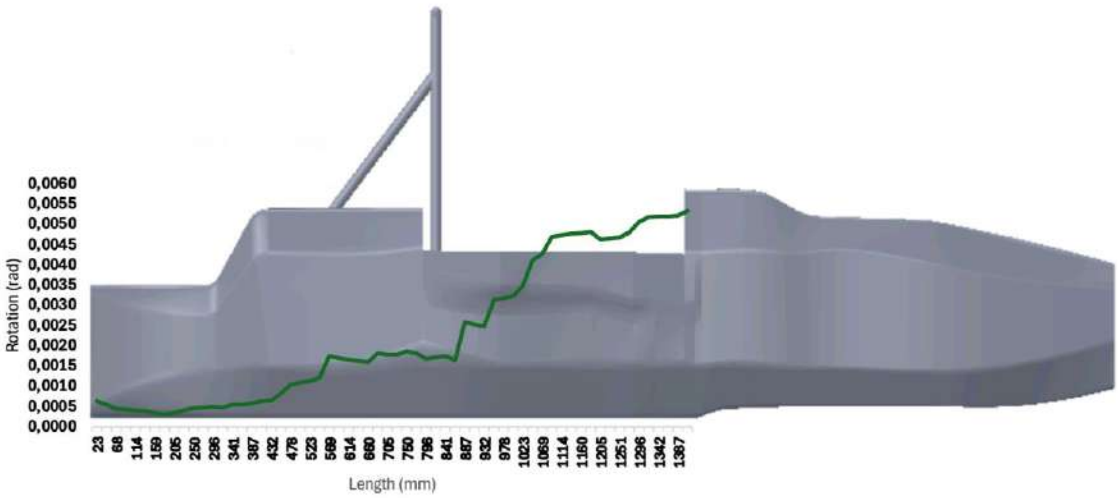

Figure 65 Element rotation across the monocoque

5.1.1 SIMULATION ANALYSES

The final laminate must be tested to show compliance with the rules. Now the objective torsional stiffness and weight goal have been achieved, then we do the initial analyses to ensure that the design is rule complaint. During these analyses, several anomalies turned up as the RBE2 elements pose a problem in this kind of simulation. As mentioned before, this are not considered because the infinite stiffness of these elements creates a zero-compliance point near the insertion elements so this will be ignored.

These simulations are done using the Hill failure criterion. In simple words, to considered that the laminate has not failed the value has to be under 1.

5.1.1.1 Main hoop load step compliance

Application of the main hoop load step case mentioned above. In this case a redesign on the edge of the monocoque connecting the cockpit and the shoulder harness placement. This edge is a stress concentration point, so a fillet on this edge would be essential.

Main hoop load case results are shown in Figures 66 to 71.

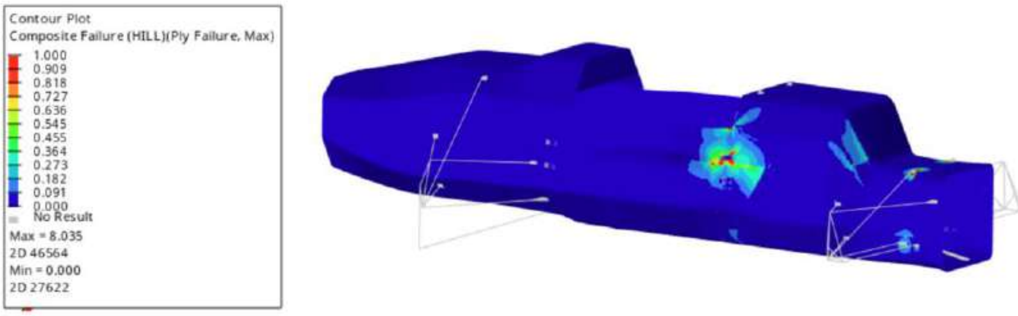

Figure 66 30 kN test in the x direction to the main hoop attachment

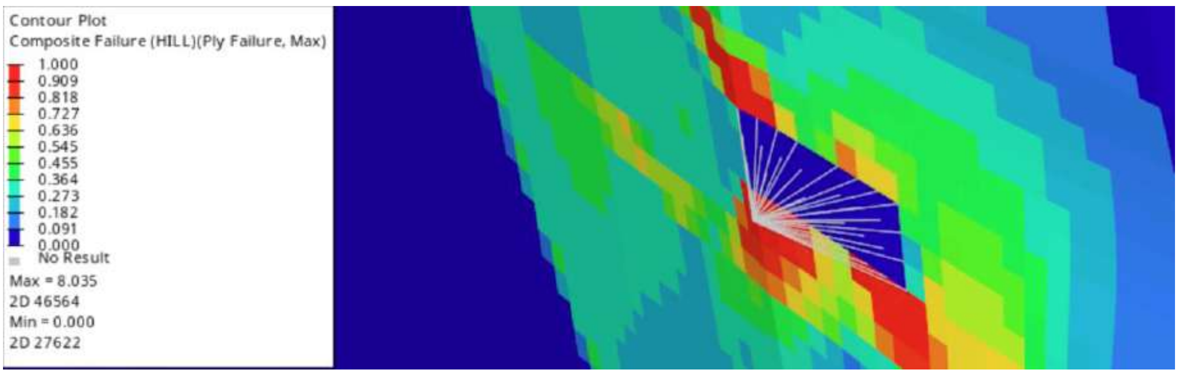

Figure 67 30 kN test in the x direction to the main hoop attachment detailed

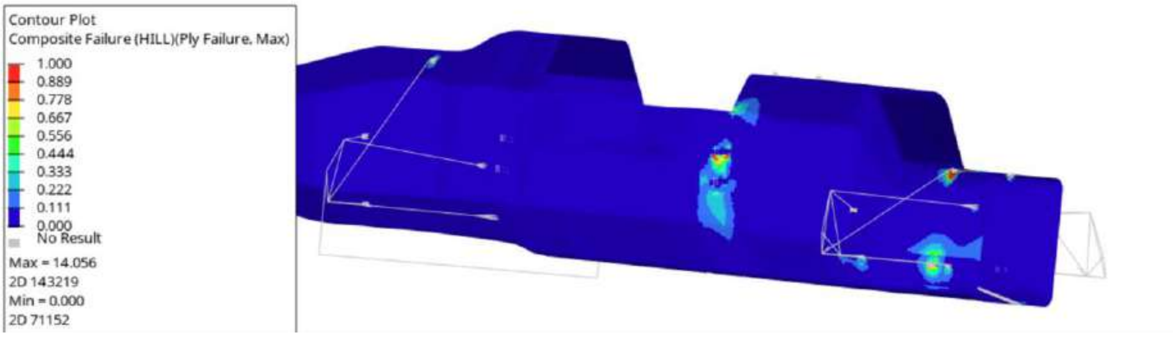

Figure 68 30 kN test in the y direction to the main hoop attachment

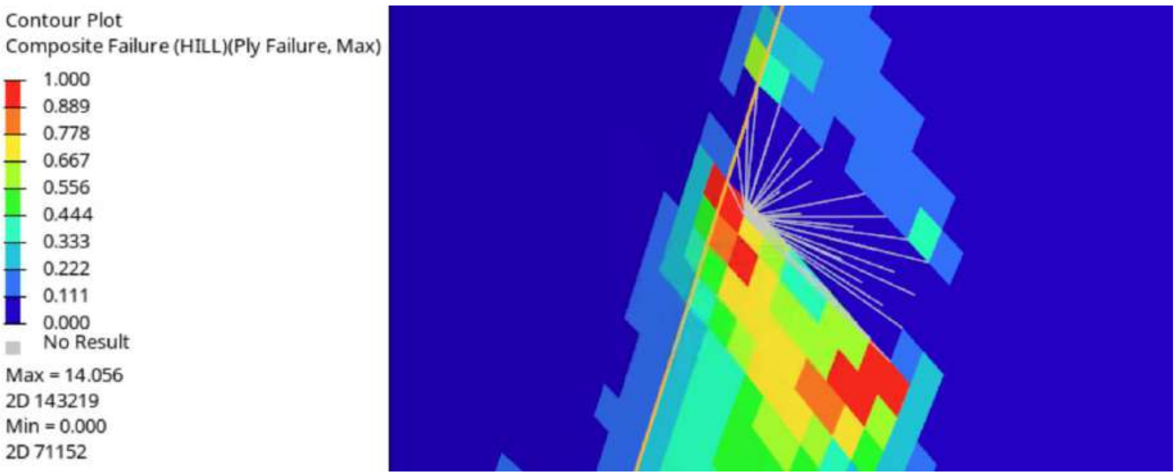

Figure 69 30 kN test in the y direction to the main hoop attachment detailed

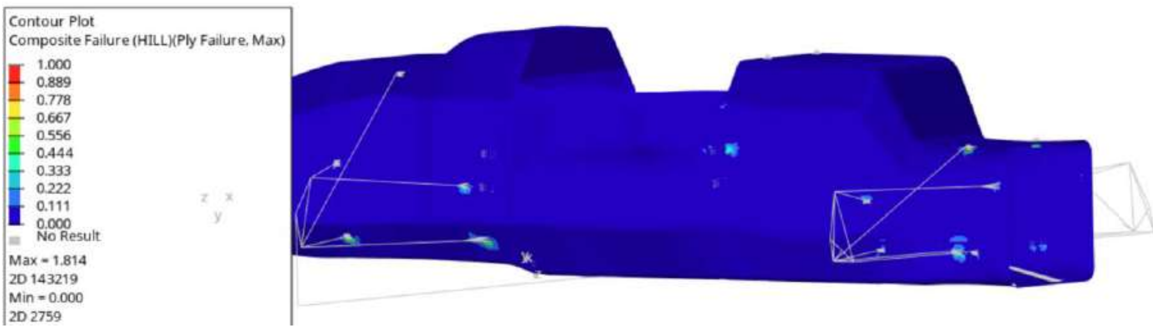

Figure 70 30 kN test in the z direction to the main hoop attachment

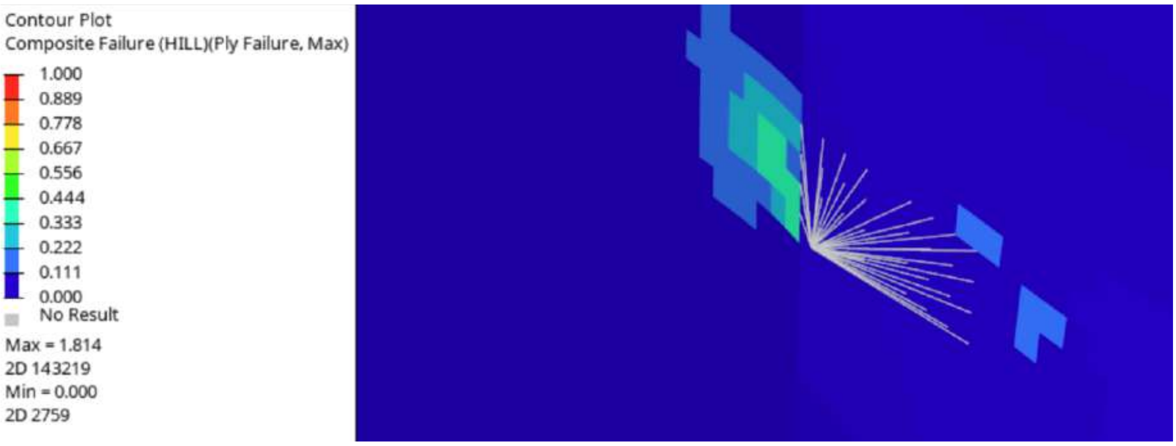

Figure 71 30 kN test in the z direction to the main hoop attachment detailed

5.1.1.2 TSAC load step compliance

Application of the TSAC load step mentioned above. TSAC load case results are shown in Figures 72 to 77.

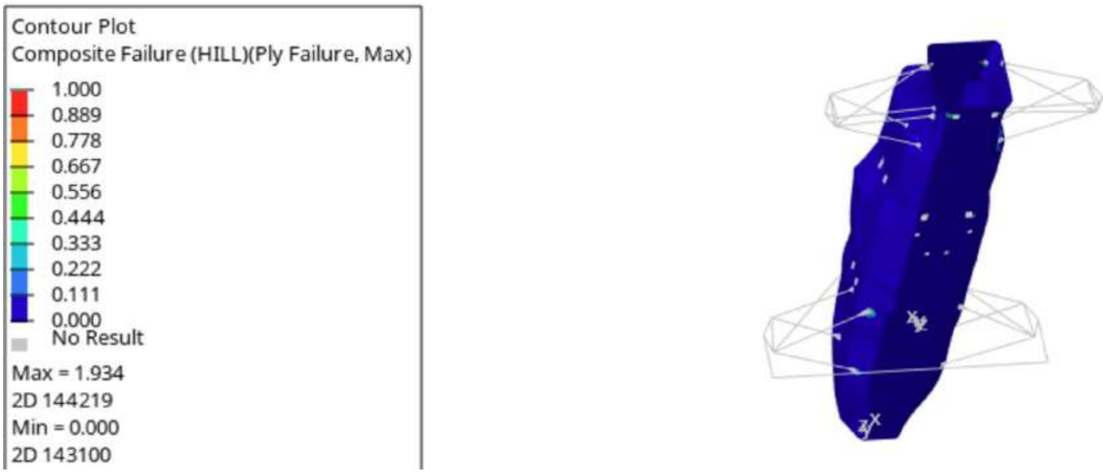

Figure 72 19kN test in the x direction to the TSAC

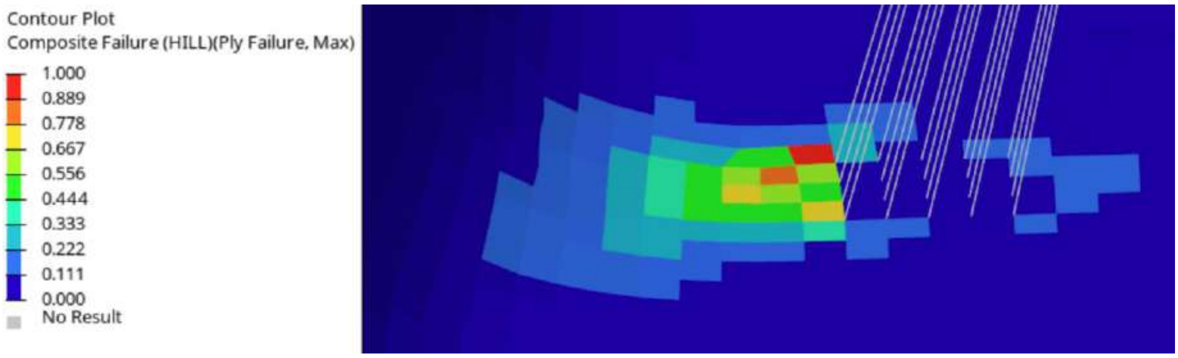

Figure 73 19kN test in the x direction to the TSAC

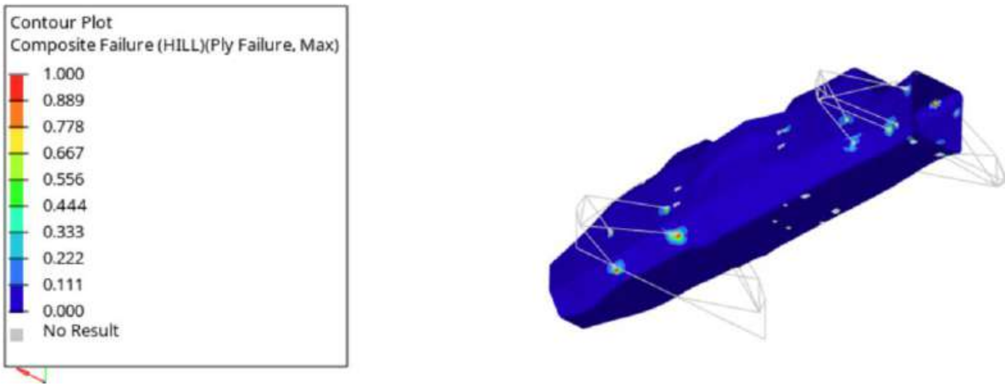

Figure 74 19kN test in the y direction to the TSAC

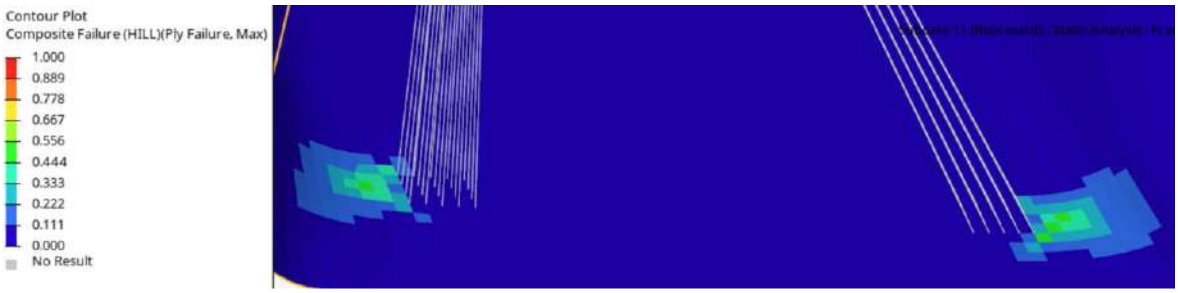

Figure 75 19kN test in the y direction to the TSAC detailed

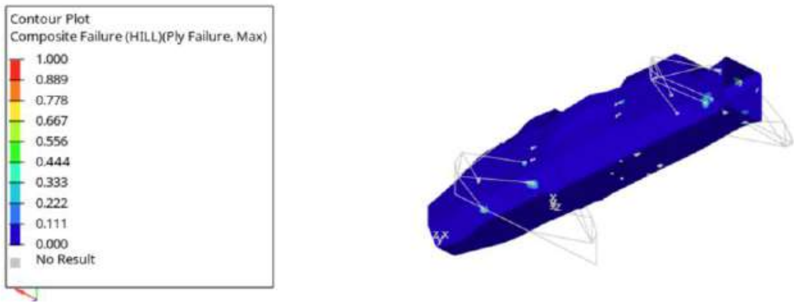

Figure 76 9,5kN test in the z direction to the TSAC

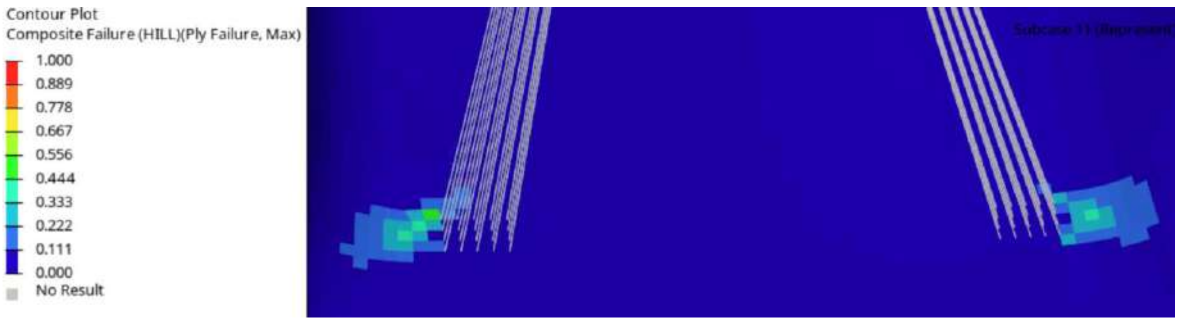

Figure 77 9,5kN test in the z direction to the TSAC detailed

5.1.1.3 Front Impact Load step compliance

A load of 20 kN will be applied (considering a standard formula student vehicle weighing approximately 250 kg subjected to an 8g impact). The results indicate that a major redesign must be implemented on the internal edges of the AIP using fillets. Although this component falls outside the scope of the current project, the AIP could be dimensioned in future development iterations. The front bulkhead support structure successfully sustains the load, which represents the critical design validation point for this analysis.

Impact load case results are shown in Figures 78.

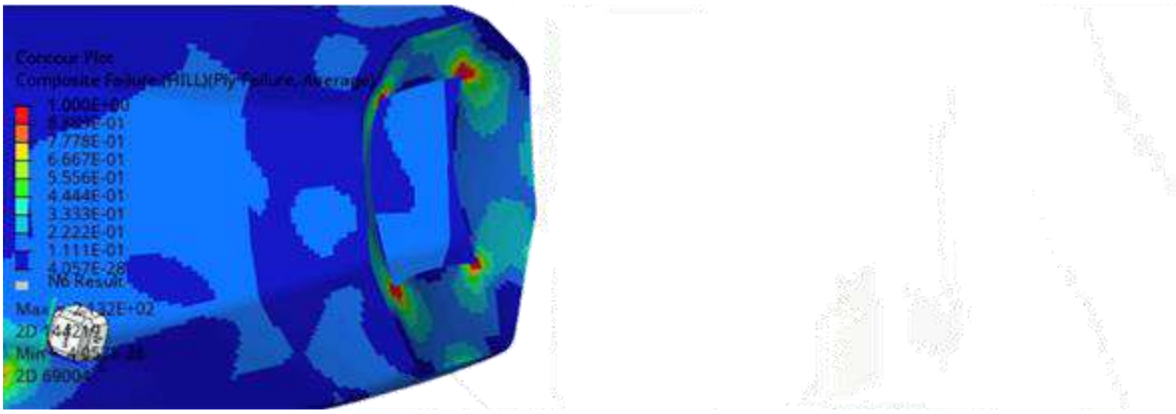

Figure 78 Frontal impact test 250kg at 8G

5.1.1.3.1 Side Impact Load step compliance

According to the T3.15.4[1], the side impact structure must demonstrate perimeter shear strength of 7.5 kN to withstand side impact loading scenarios.. The results demonstrate that the structure successfully resists the applied side impact loading without exceeding the critical failure threshold, thereby confirming compliance. Side impact load case results are shown in Figures 79 and 80.

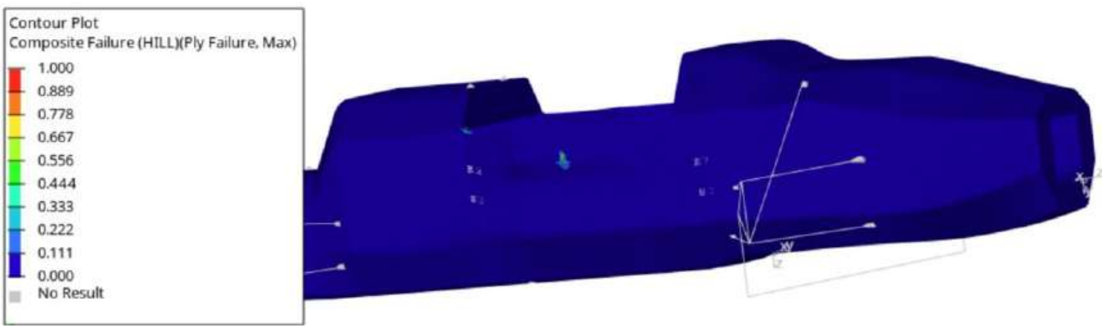

Figure 79 7,5 kN side impact

Figure 80 7,5 kN side impact detailed

5.1.1.4 Harness load step compliance

Application of the Anti-submarine load step mentioned above. Anti-submarine load case results are shown in Figure 81.

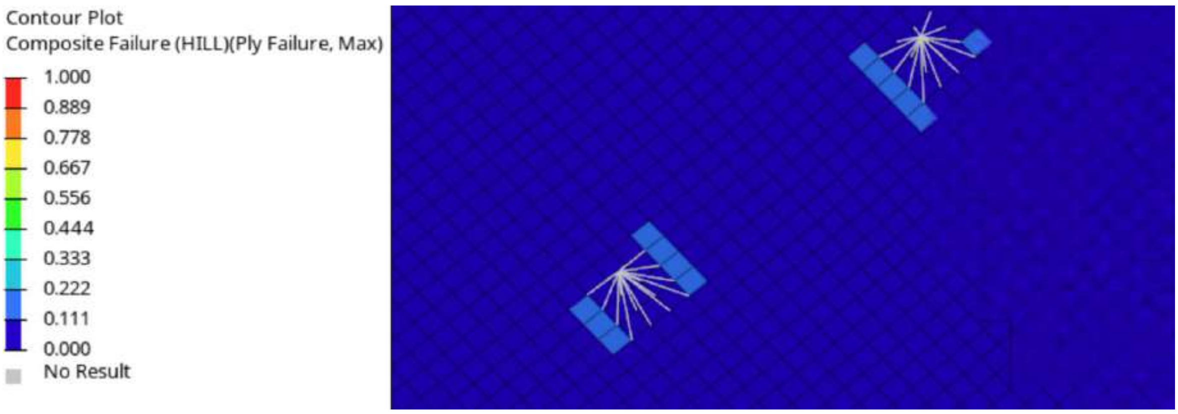

Figure 81 antisubmarine loads

Application of the shoulder and lap belt harness load step mentioned above. Shoulder and lap bet harness load case results are shown in Figures 82 to 84.

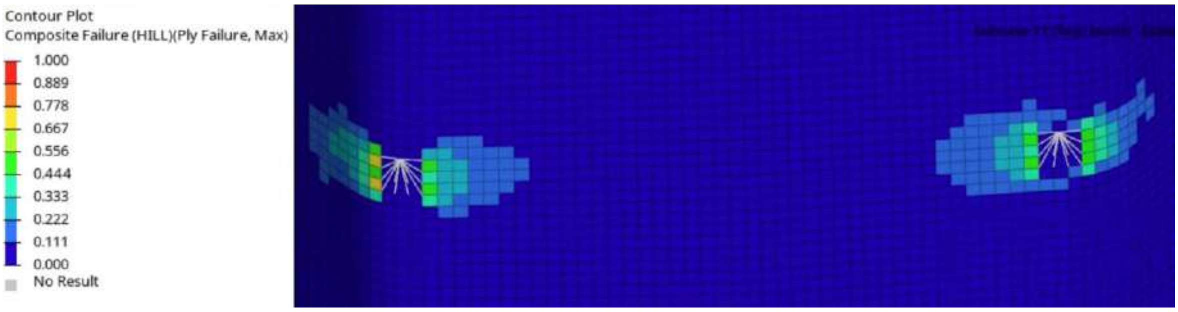

Figure 82 Lap belts compliance test

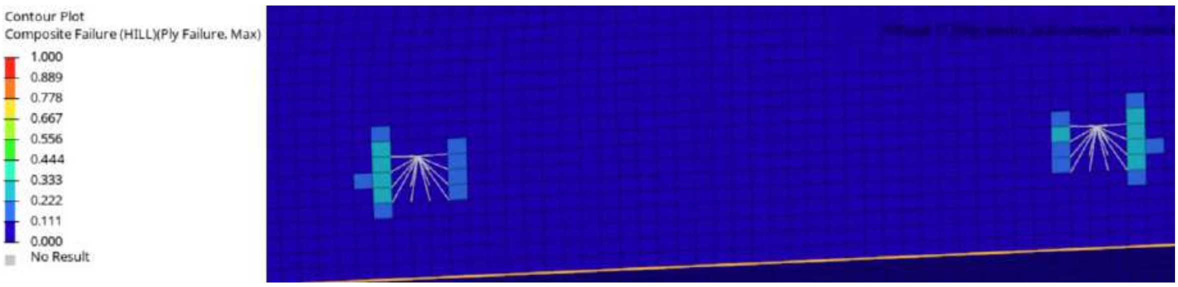

Figure 84 Shoulder harness compliance test

5.2 FINAL PLY DISTRIBUTION

The final laminate groups the results from all the simulations. Each optimization process had a main ply set, which was repeated into multiple plies. In the final model, each set was defined for the purpose of the loads it supports. First, let look at the final shapes of each set that will be represented on their most representative side.

SUSPENSION SET:

The suspension load step created two main set shapes. The first one represented in Figure 85 carries the loads applied on each suspension pick up point. The second shape represented in Figure 86 connects the rear and the front suspension. In Figure 87, the mid evolution from both shapes is displayed. However, these results need to be filtered in: Symmetry and manufacturability, as many of these shapes are impossible to manufacture.

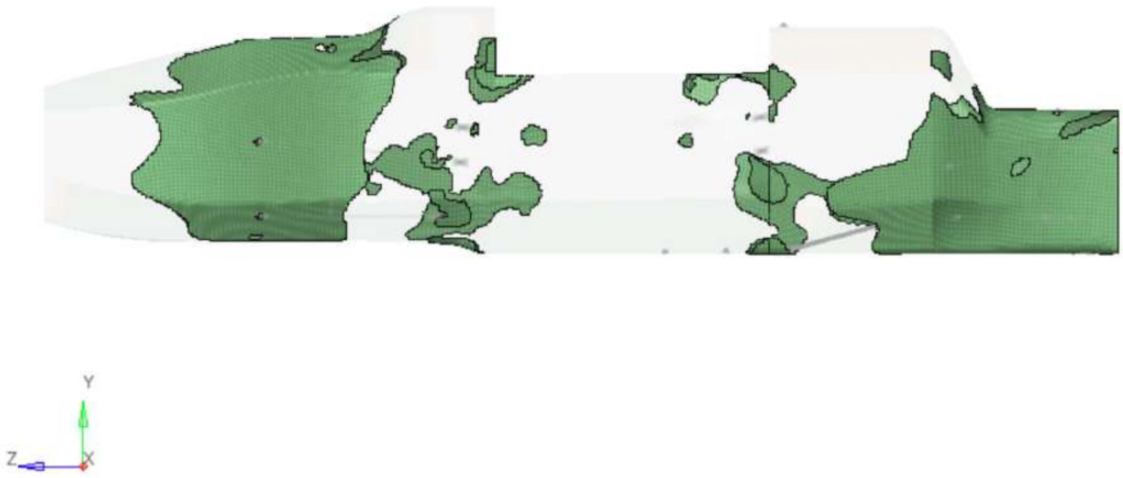

Figure 85 Suspension load step sizing optimization Ply 21 set 9401

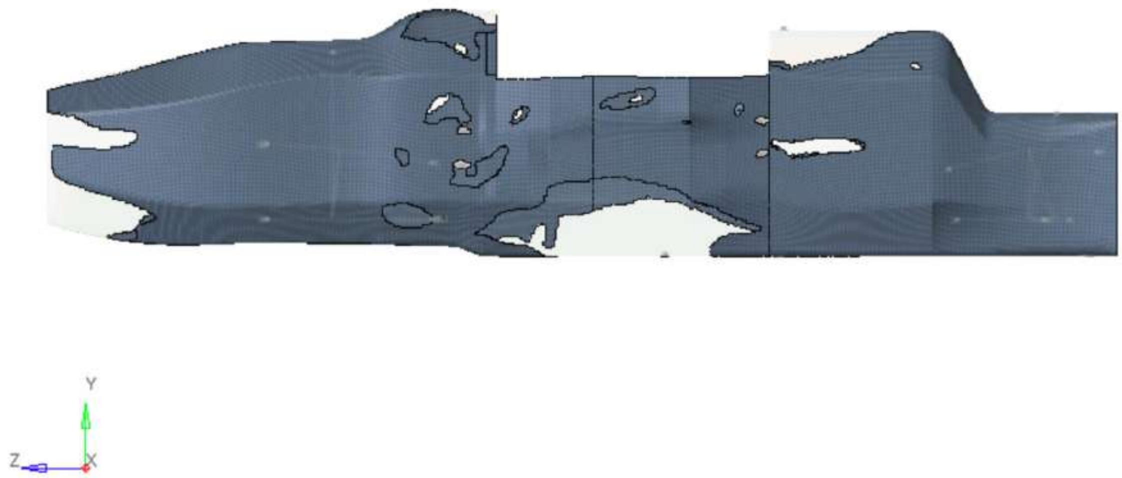

Figure 86 Suspension load step sizing optimization Ply 23 set 9201

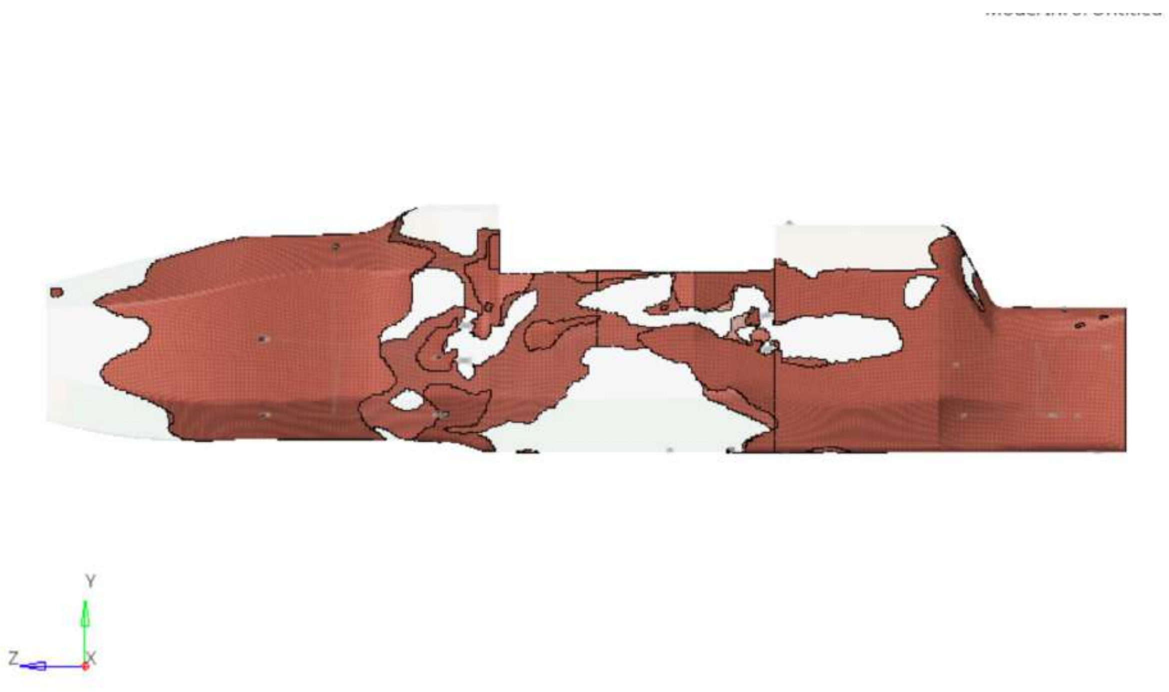

Figure 87 Suspension load step sizing optimization Ply 26 set 9201

The final suspension set groups these three requests from the simulation. These are the results (Figure 88 – 91):

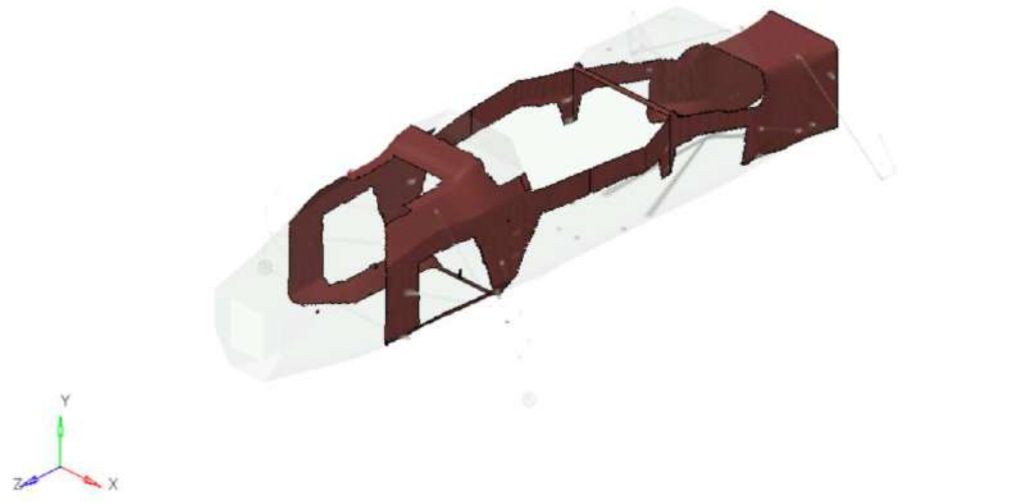

Figure 88 Suspension set isometric view

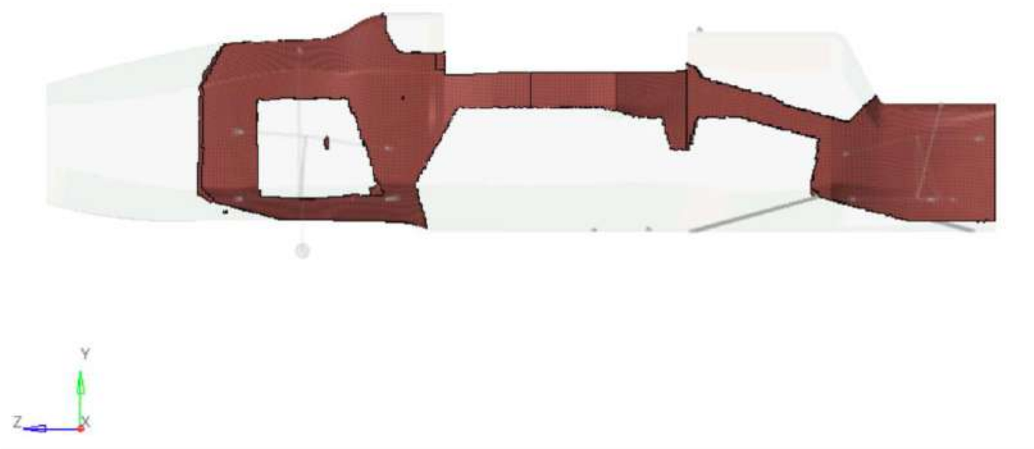

Figure 89 Suspension set side view

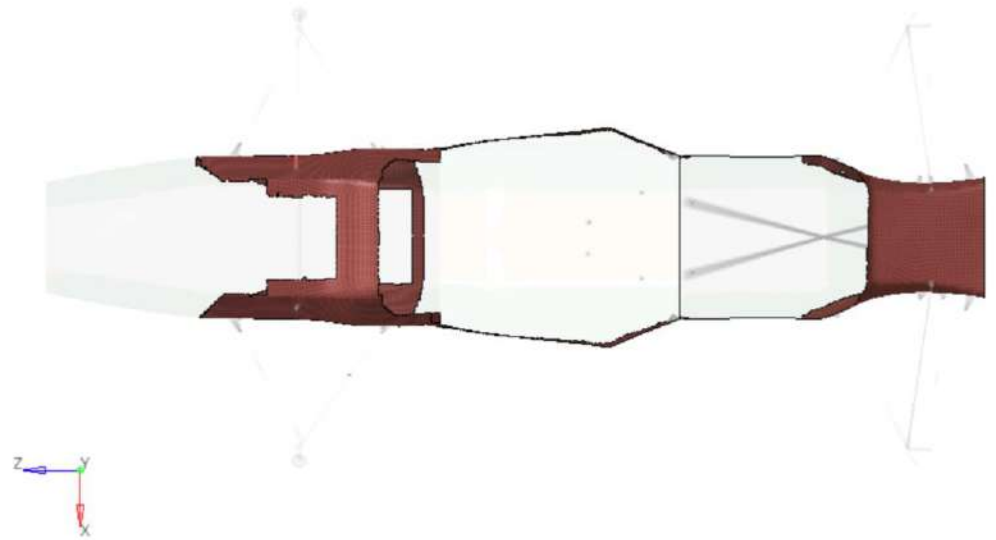

Figure 90 Suspension set top view

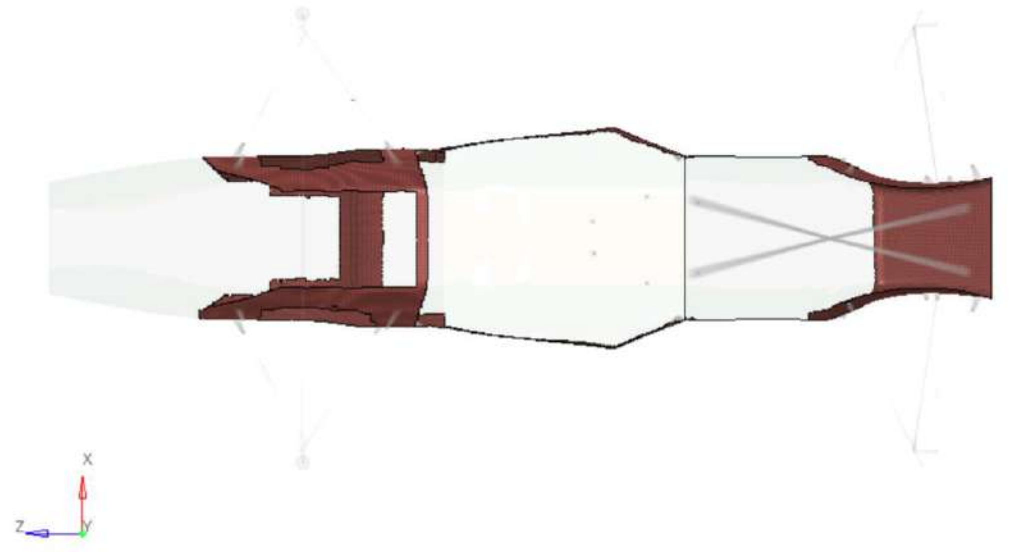

Figure 91 Suspension set floor view

HARNESS SET:

The harness load step sizing optimization is easier to identify. The main supports needed are at shoulder height of the driver because of the shear load of the shoulder harness and the floor of the tub because of the lap and antisubmarine belts. On figure 92, where the material is needed is marked in red. In the side view, the shoulder harness support shows itself also marked in red.

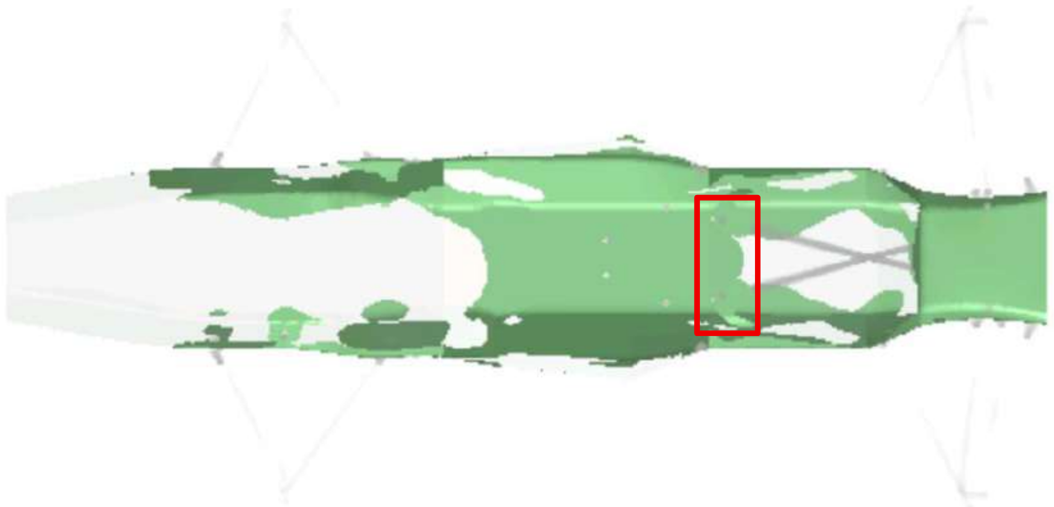

Figure 92 Harness load step sizing optimization Ply37 set 9401(top view)

Figure 93 Harness load step sizing optimization Ply37 set 9401(top and bottom view)

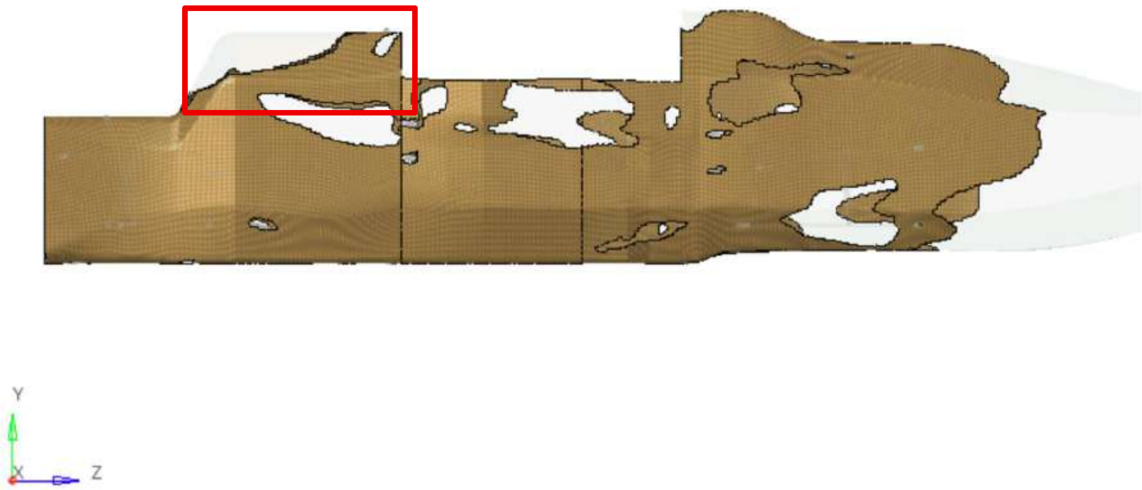

Figure 94 Harness load step sizing optimization Ply37 set 9401(side view)

The result for the harness set is (Figure 95 – 98):

Figure 95 Harness set isometric view

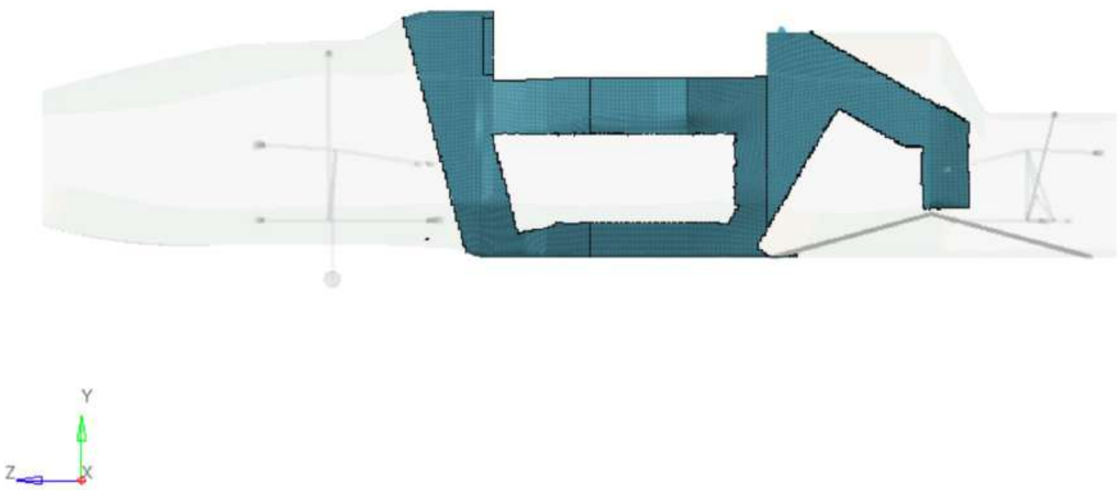

Figure 96 Harness set side view

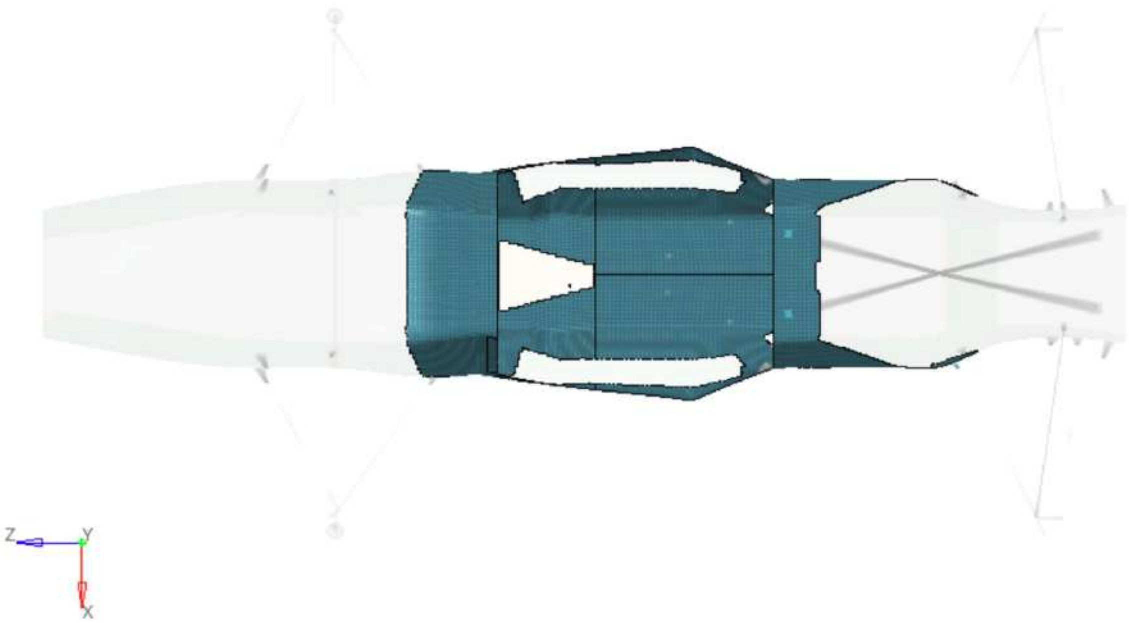

Figure 97 Harness set top view

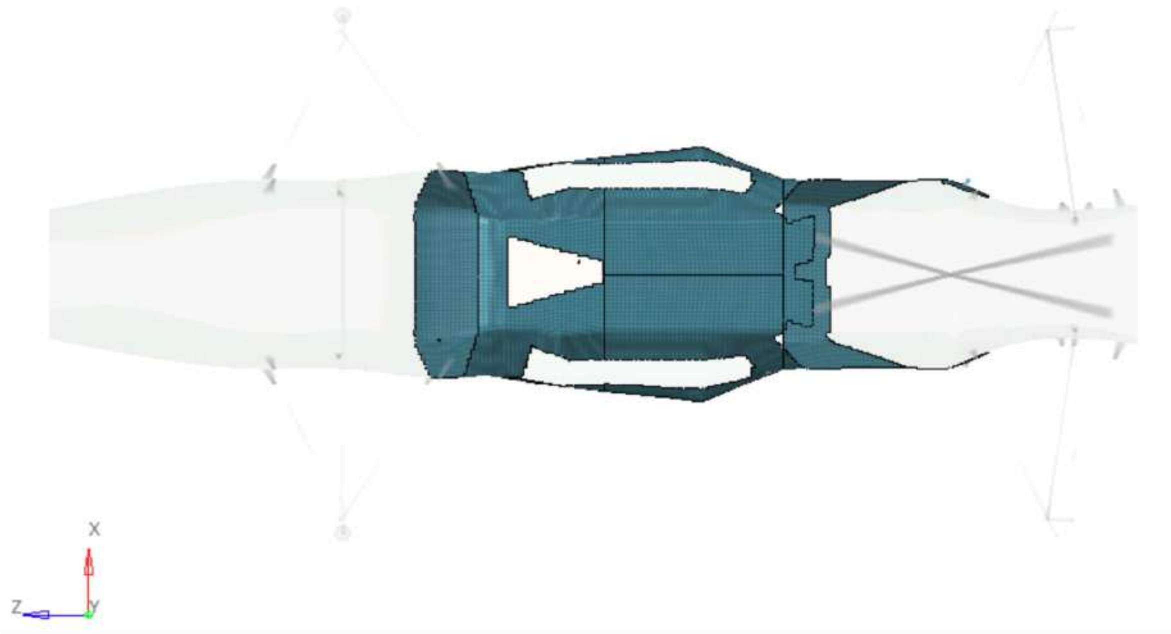

Figure 98 Harness set bottom view

TSAC SET:

The load step for the TSAC sizing optimization presents a different ply distribution requirement. The regions that primarily need reinforcement are near the rear suspension, since the load path concentrates a significant portion of the transmitted forces of the TSAC.

On Figure 99, the reinforcement goes beyond the TSAC RBE2 element, so this will be used as connection with other plies. In Figure 100, the reinforcement gets to the low suspension pick up points, so this will become the reference to create the new set.

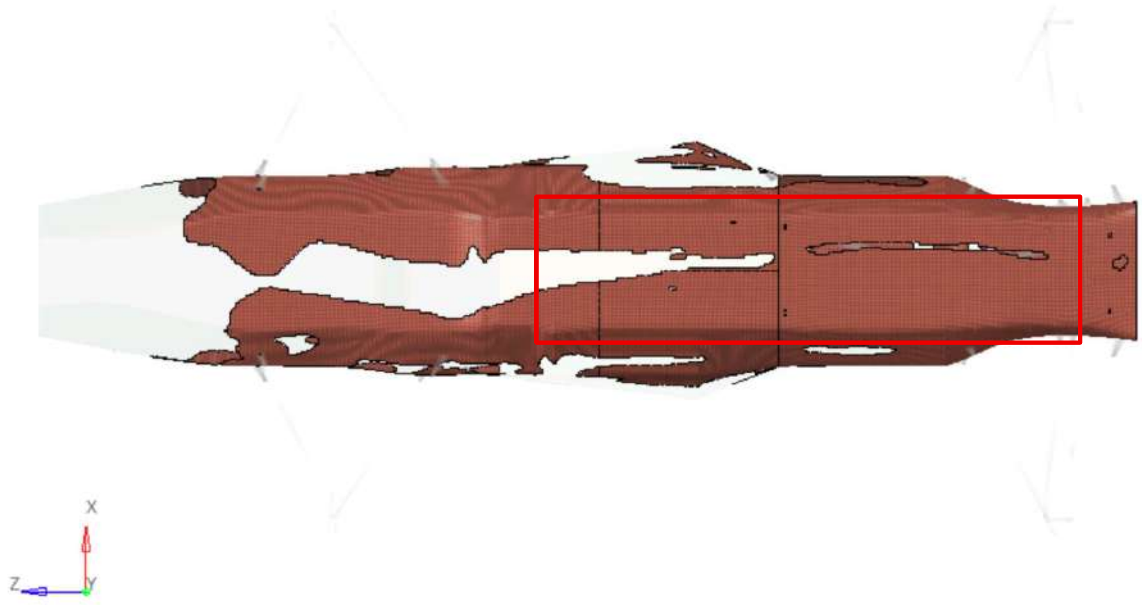

Figure 99 TSAC load step sizing optimization Ply 10 set 8301(Floor view)

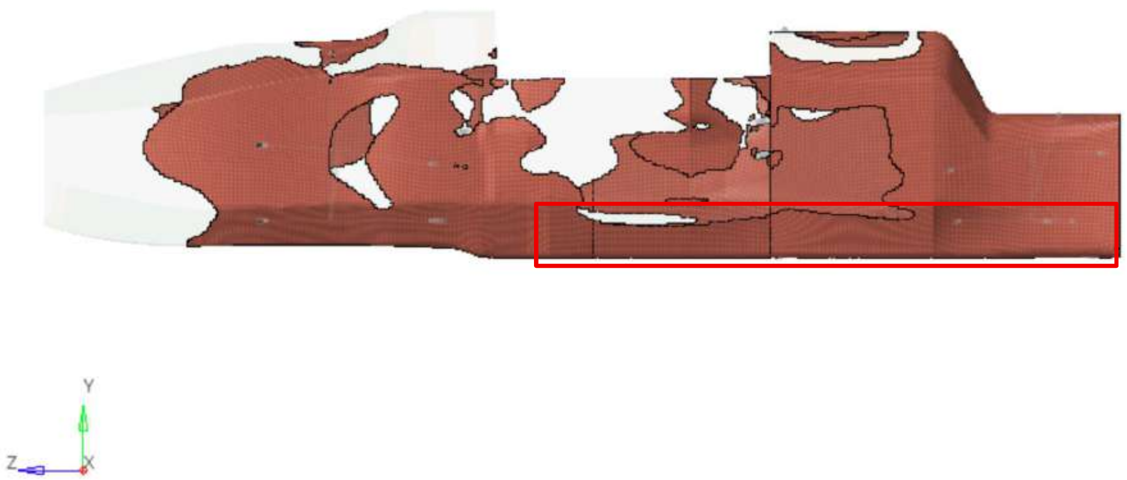

Figure 100 TSAC loadstep sizing optimization Ply 10 set 8301(Side view)

The result of the TSAC set is the following (Figure 101-103):

Figure 101 Harness set isometric view

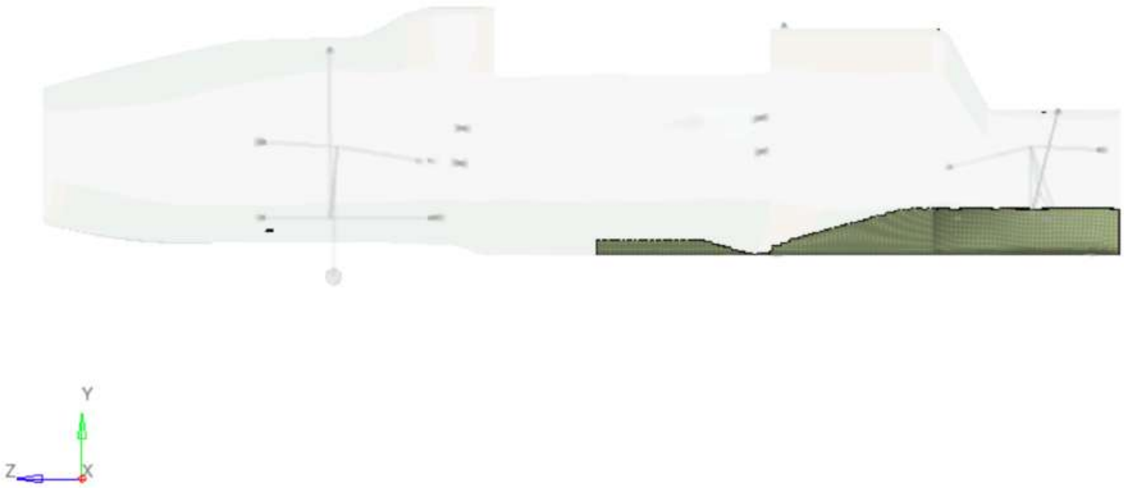

Figure 102 TSAC set side view

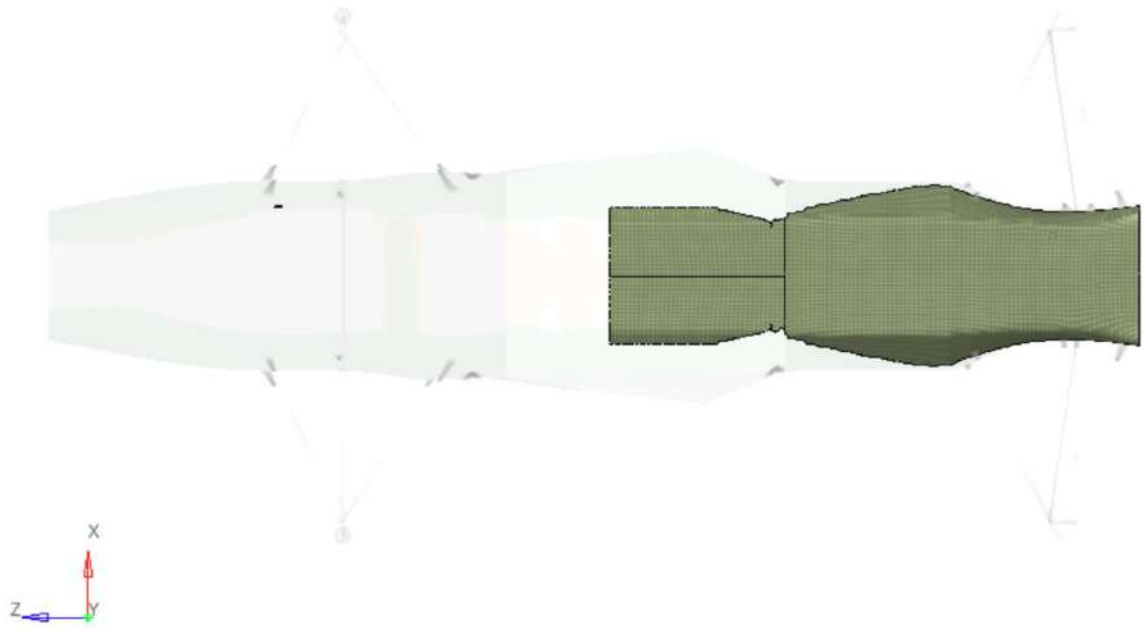

Figure 103 Harness set top view

HOOP SET:

The hoop loadstep is the most demanding of all so not only a separate set has been defined for, but the suspension and harness set have been used to reinforce these parts. The load path concentrates near the attachments (Figure 104).

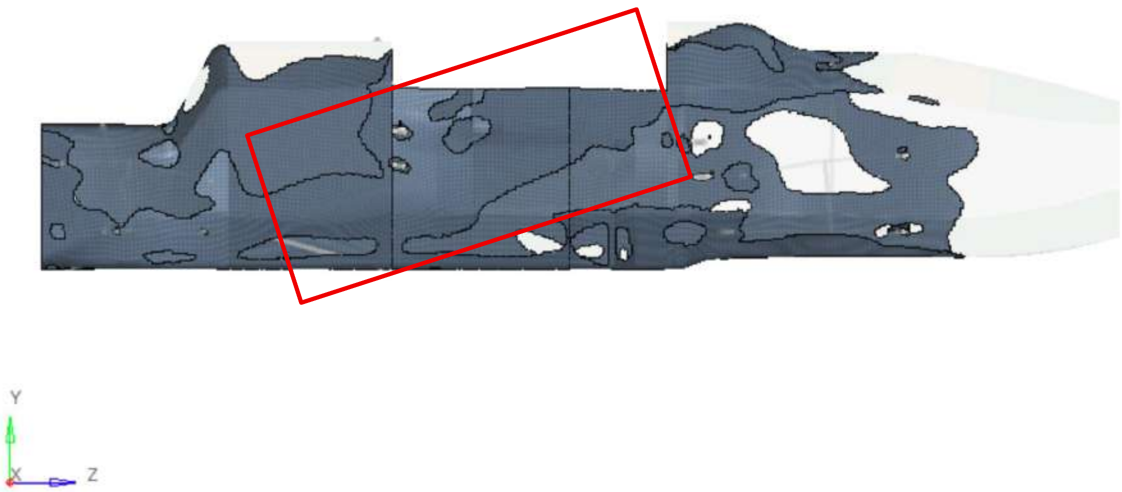

Figure 104 Hoops loadstep sizing optimization Ply 23 set 7417(Side view)

The resulting set for the hoop loadstep (Figure 105 – 107):

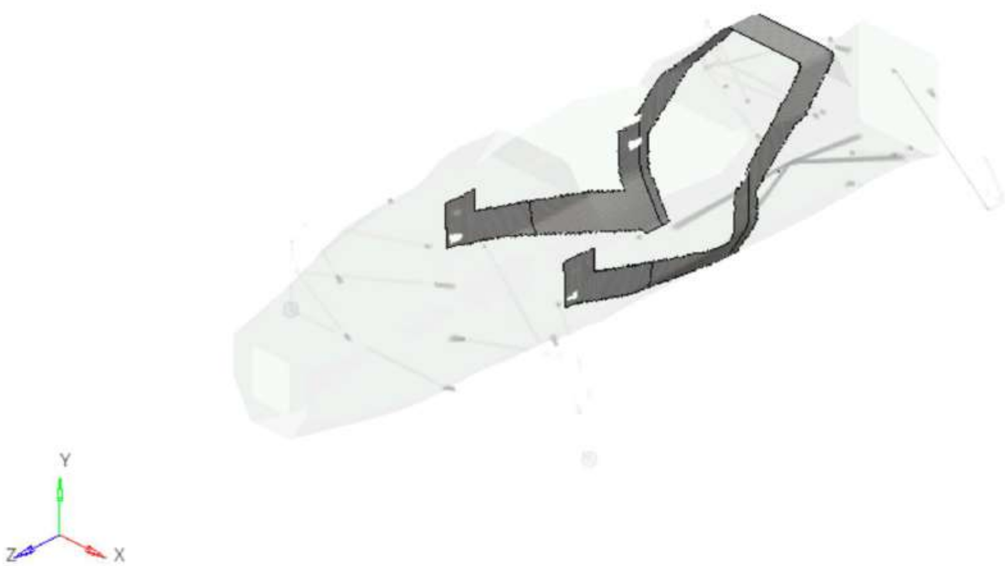

Figure 105 Hoop set isometric view

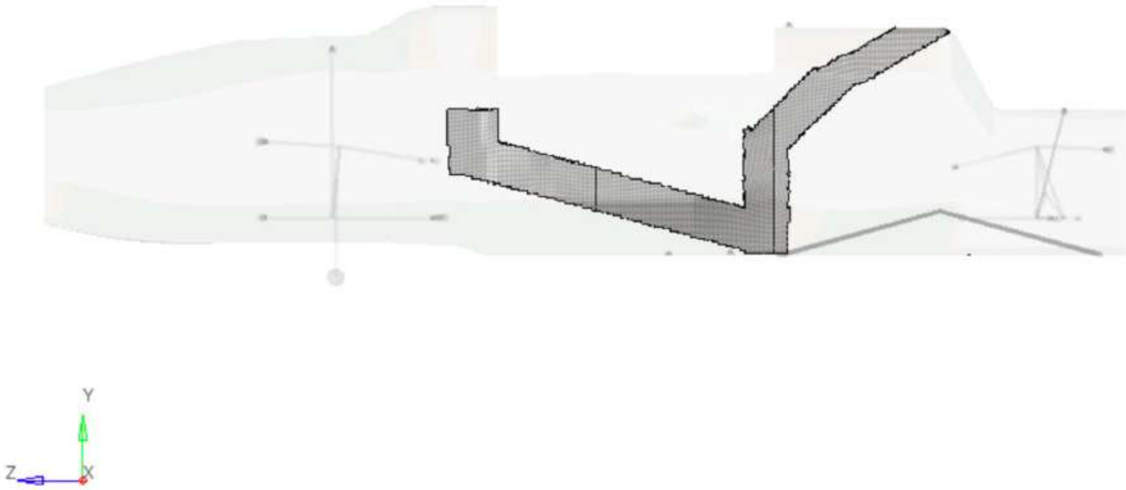

Figure 106 Hoop set top side view

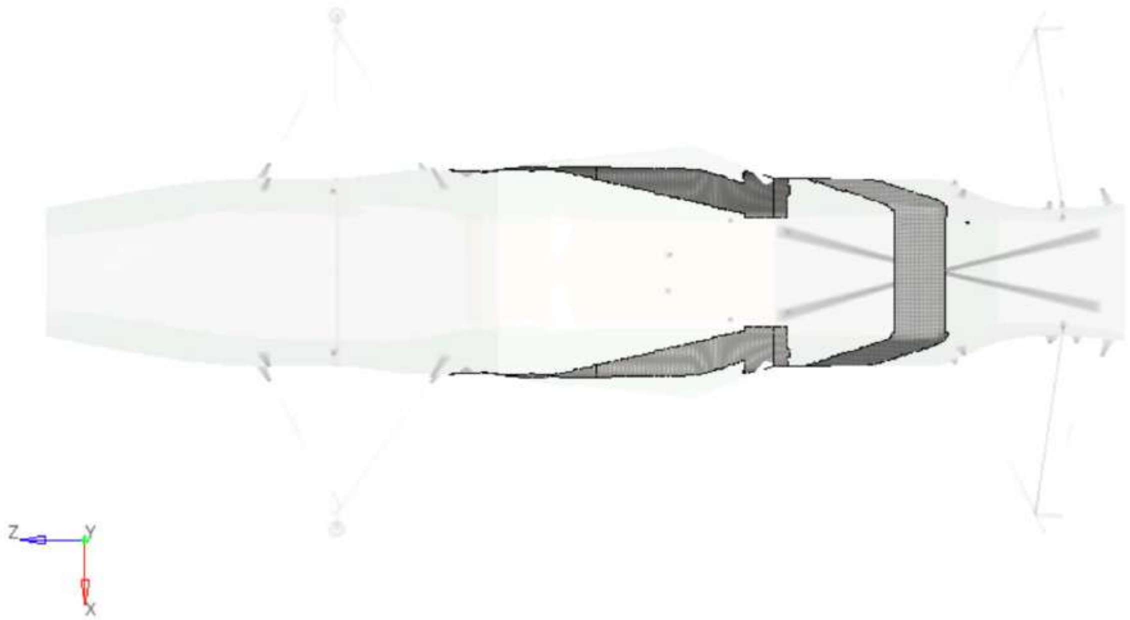

Figure 107 Hoop set top view

IMPACT SET:

The loadstep for the impact sizing optimization differs from all the other sets. This set reinforces the front of the car for frontal impacts and connects the front bulkhead to other sets that support it (Figure 108 - 110).

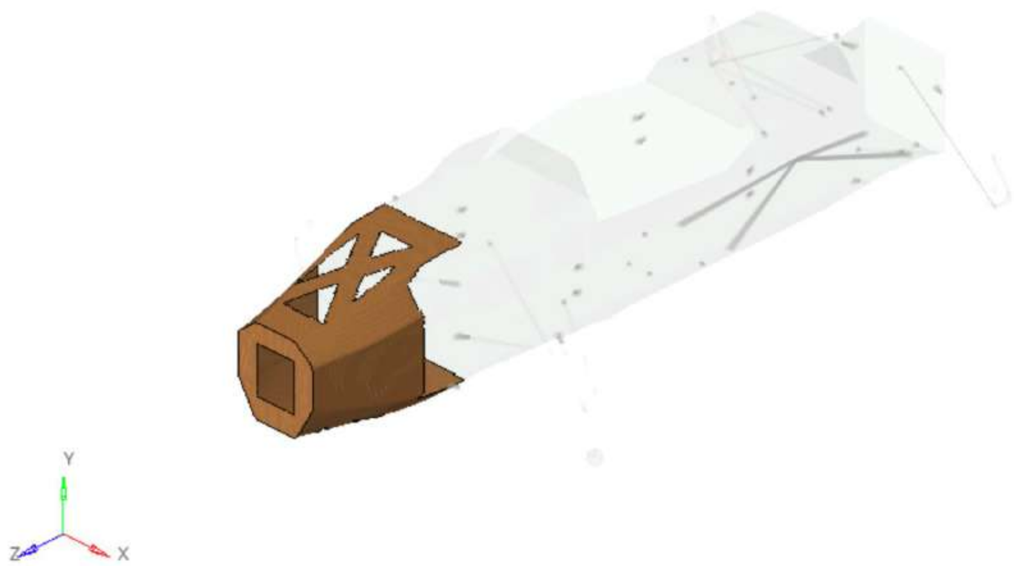

Figure 108 Impact set isometric view

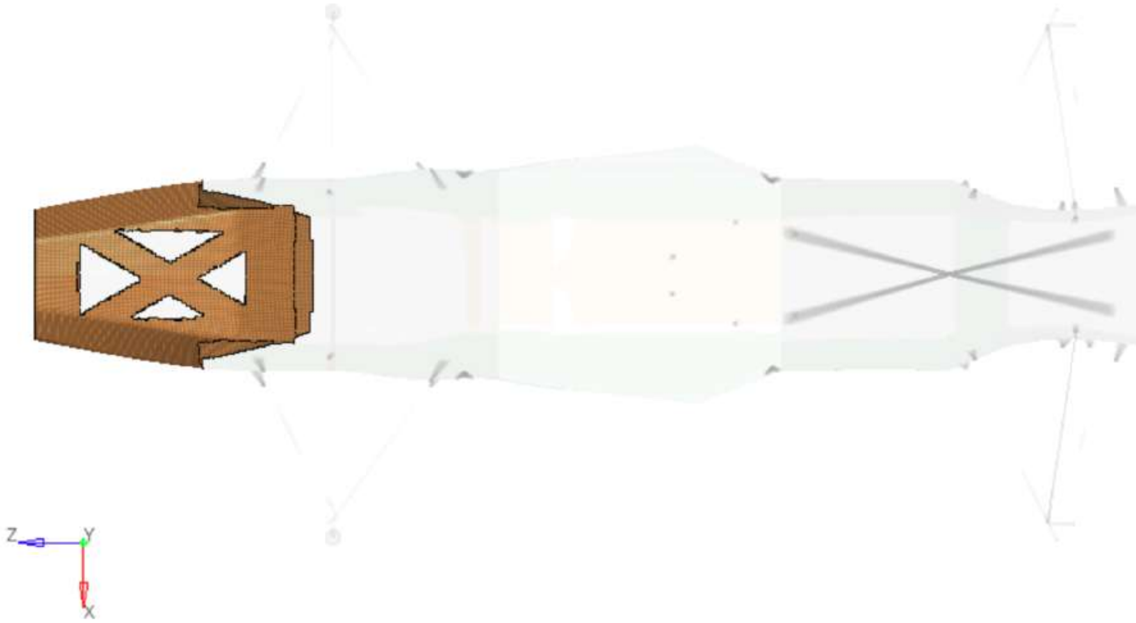

Figure 109 Impact set top isometric view

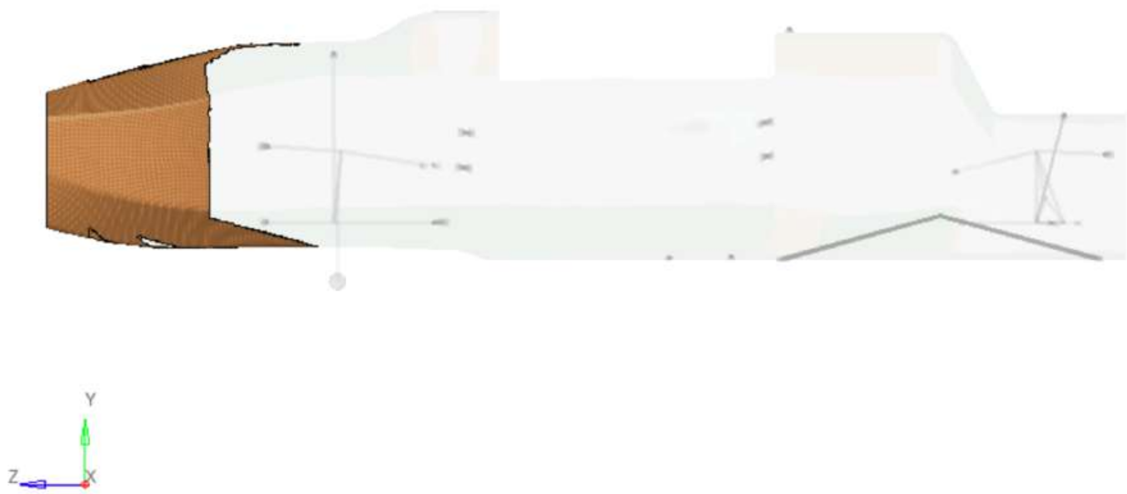

Figure 110 Impact set isometric view

THICKNESS DISTRIBUTION:

The final sets have stablished the desired symmetry in the laminate. However, the thickness and ply distribution is also important for the laminate to behave correctly. For the thicknesses, the ply shapes have been adjusted to have a similar thickness along the monocoque. From Figures 111 to 114 shows the variation with only 6mm in total on the whole laminate.

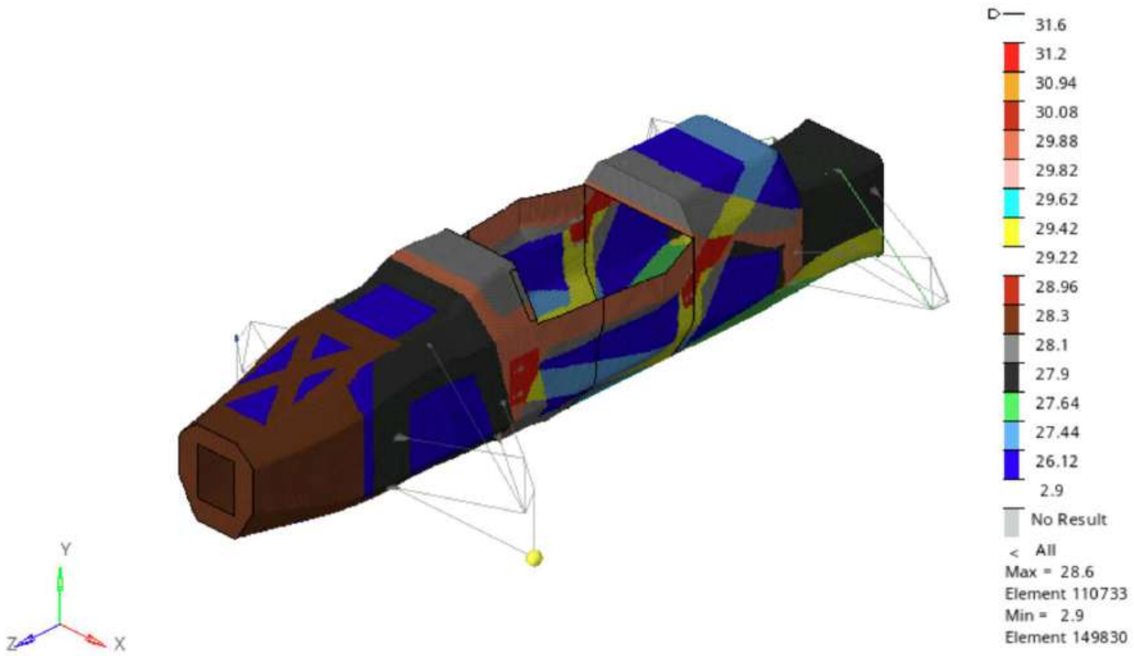

Figure 111 Thickness variation along the whole monocoque isometric view

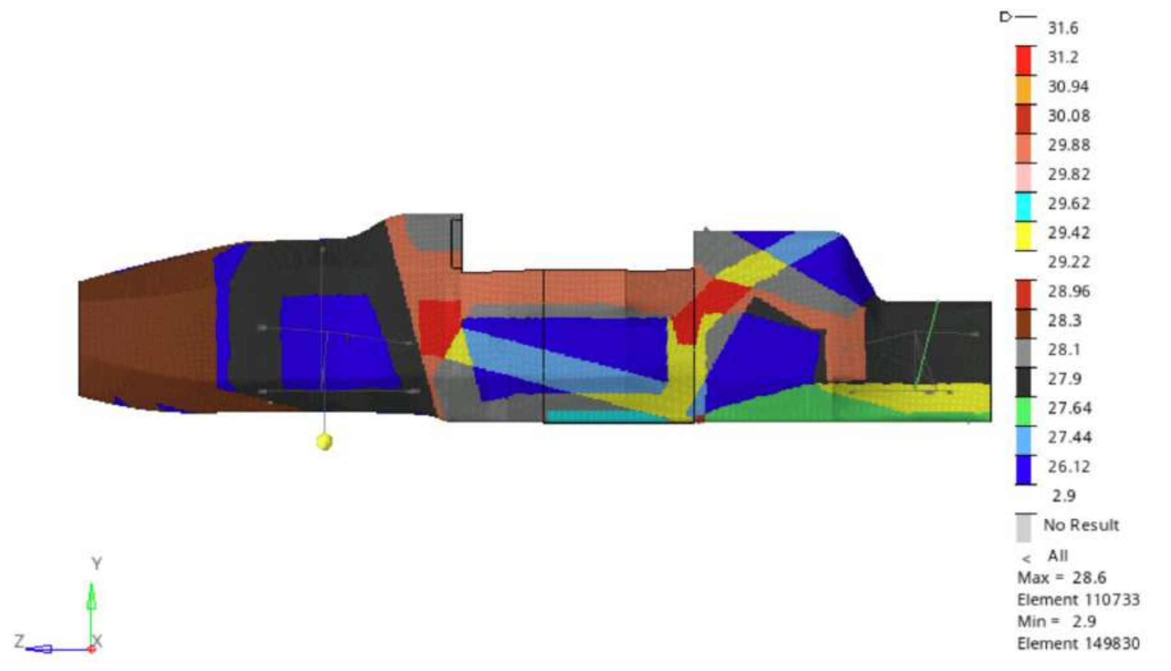

Figure 112 Thickness variation along the whole monocoque side view

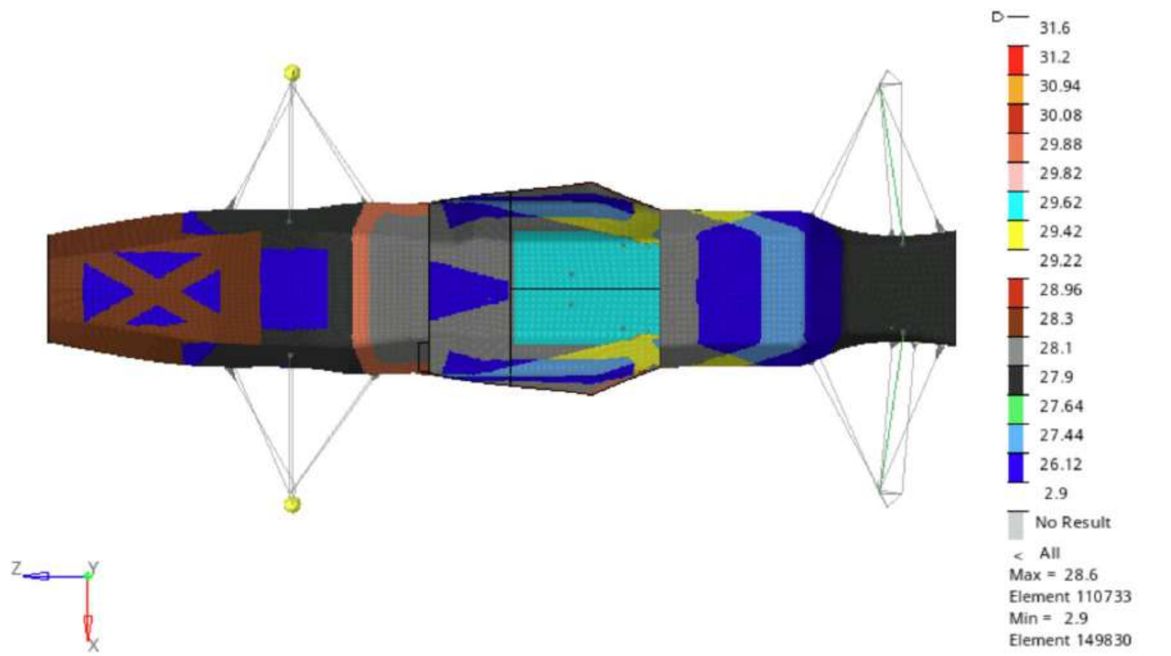

Figure 113 Thickness variation along the whole monocoque top view

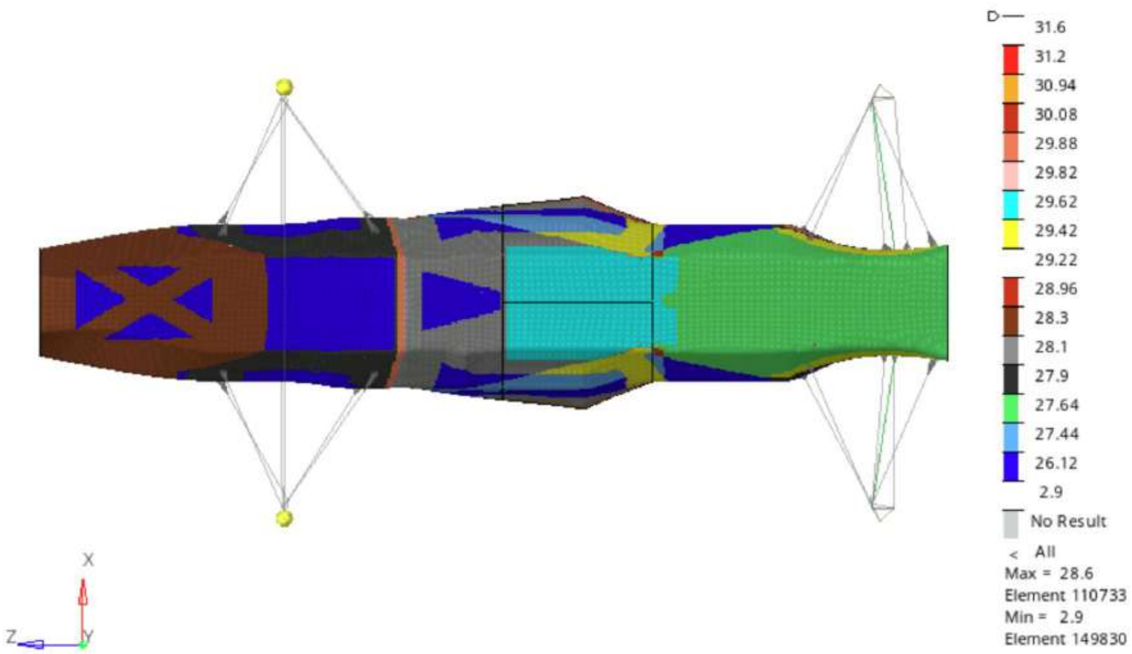

Figure 114 Thickness variation along the whole monocoque bottom view

FINAL LAMINATE CHARACTERISTICS:

The final laminate has a total of 31 plies distributed in 7 different shapes. The laminate is asymmetrical because in all the sizing optimization the solver proposed an asymmetrical lay-up. The laminate has 21 different zones in total with different layup distribution in each one. The engineering data can be found in the APPENDIX 1 section.

The final laminate distribution has a symmetric and balanced form to ensure great mechanical properties (Figure 115 - 118).

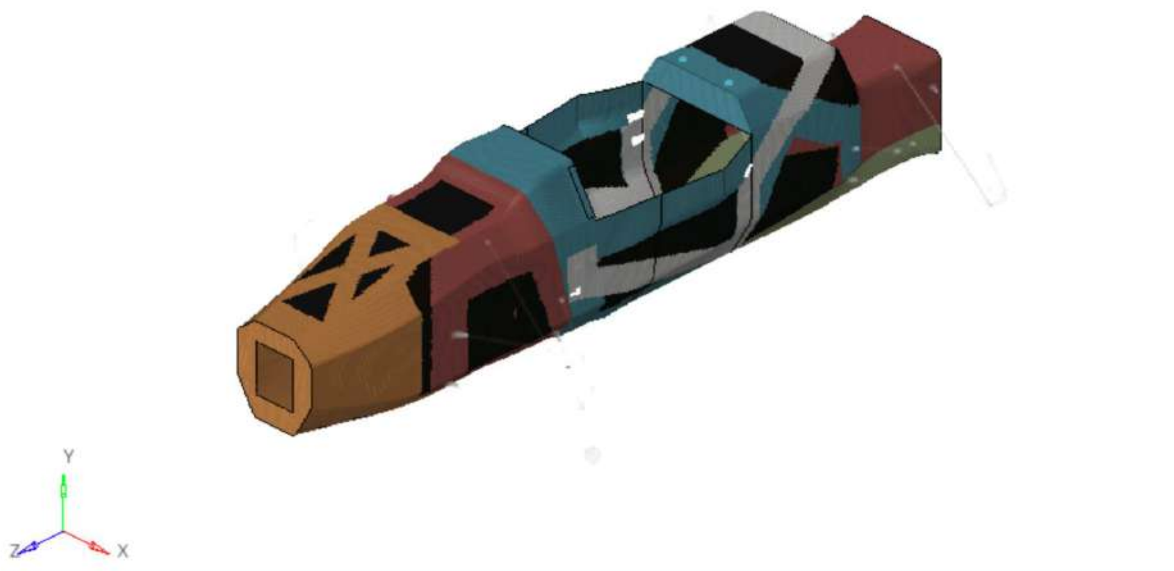

Figure 115 Final laminate distribution isometric view

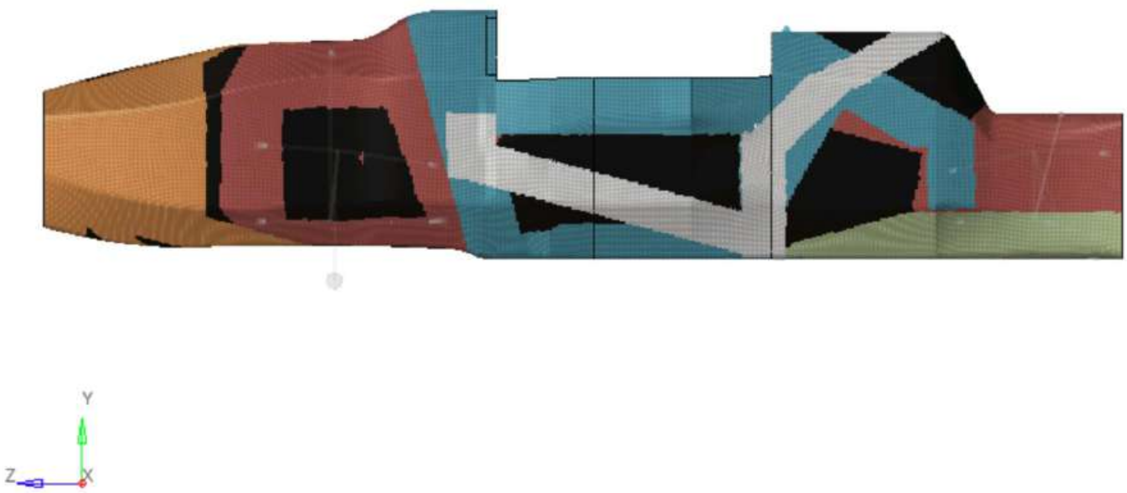

Figure 116 Final laminate distribution side view

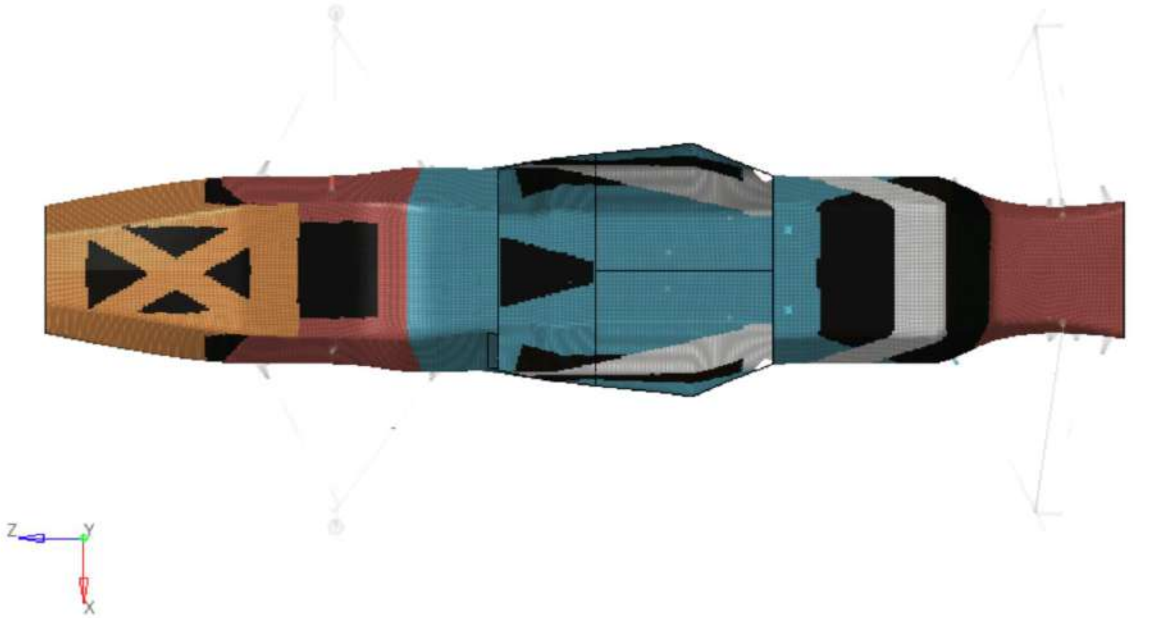

Figure 117 Final laminate distribution top view

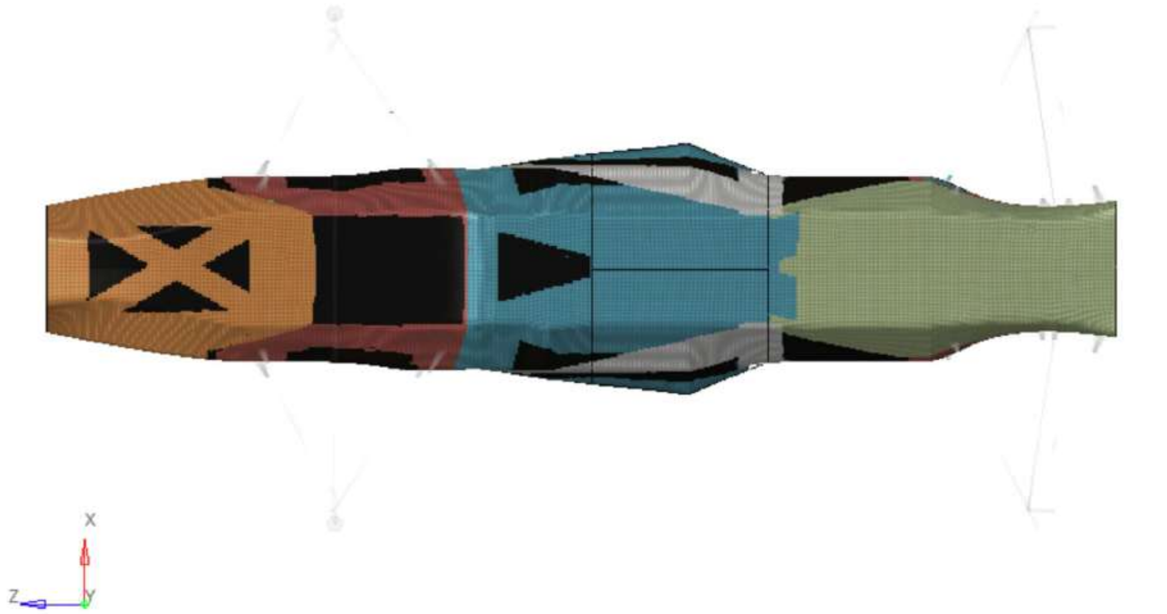

Figure 118 Final laminate distribution bottom view

Chapter 6. CONCLUSIONS

Conclusions of this thesis are shown below:

1. The design and simulation of the monocoque chassis optimized throughout this project demonstrates improvements in ergonomics, dynamic performance and overall weight reduction, while maintaining structural integrity and compliance with the Formula Student 2026 regulations.

2. Altair HW software has proven to be an effective tool for the successful shape thickness and shape optimization of composite structures.

3. This research has expanded the understanding of composite material behaviour under loading conditions and the failure criteria employed during the optimization process.

4. The simulation and optimization methodologies used during this work, represent key technical competencies that could be applied in the future developments of the ISC FS Racing Team.

Chapter 7. ECONOMIC IMPACT

This project does not involve any fabrication process. The materials displayed are used for their mechanical properties as a real approach to the simulations. Taken this into account, for the reproduction of this project only software licenses are needed. In this case, all of them were for student use so many were free of costs thanks to the ISC FS Racing Team.

The software tools required for this project include SolidWorks for 3D modelling, Altair Hypermesh for finite element analysis and composite optimization, and Optimum Kinematics for vehicle dynamics analysis. However, all these software licenses were accessed through the ISC FS Racing Team sponsor agreements, which means there was no direct cost to the project. This is an advantage for Formula Student team members, as commercial licenses for professional software can be very expensive, but for educational purposes they provide free or discounted access to ensure students can learn with industry-standard tools.

The estimated annual costs of these licenses on the commercial market are:

- SolidWorks: €7,000 - €12,000 per year (3D CAD modelling)
- Altair Hypermesh (Altair One - Hyperworks package): €5,000 - €15,000 per year (FEA and composite optimization)
- Optimum Kinematics: €2,000 - €5,000 per year (vehicle dynamics analysis)
- Total, estimated commercial cost: €14,000 - €32,000 per year

(This cost values are an estimate as they depend on each specific deal with the software developer)

In this project, all licenses were accessed at zero cost through student academic use, except the optimum kinematics software that was acquired at 500€ with a special student discount.

Chapter 8. SUSTAINABLE DEVELOPMENT GOALS

This project promotes sustainable development in the automotive sector by creating more sustainable vehicles through weight reduction and material optimization. These improvements increase vehicle range and reduce energy consumption. The project development fosters innovation in the automotive industry, particularly in the university environment and by applying advanced technologies.

This type of project lead to the creation of more sustainable and safe means of transportation, applicable to urban mobility and future projects. The optimization of the laminate and weight reduction leads to rational use of materials. This results in reduced emissions by improving the energy efficiency of electric vehicles. Therefore, this project aligns with the Sustainable Development Goals (SDGs), particularly contributing to SDGs 7, 9, 12, and 13

Figure 118 SDG's followed by the project

Chapter 9. BIBLIOGRAPHY

[1] «Formula Student Rules 2026, Version: 1.1, Rev-15f99a7». Disponible en: https://www.formulastudent.de/fileadmin/user_upload/all/2026/rules/FS-Rules_2026_v1.1.pdf

[2] W. F. Milliken y D. L. Milliken, *Race car vehicle dynamics*. en R, no. 146. Warrendale, PA: Society of Automotive Engineers Internat, 1995.

[3] A. K. Kaw, *Mechanics of composite materials*, 2. ed. en Mechanical engineering series, no. 29. Boca Raton, FL: CRC Taylor & Francis, 2006.

[4] O. Danielsson y A. G. Cocaña, «Influence of Body Stiffness on Vehicle Dynamics Characteristics in Passenger Cars».

[2] «Tema 8 Composites_19_20 DIM- ICAI Ingeniería de Materiales».

[6] G. W. Milton, *The theory of composites*, 1. publ. en Cambridge monographs on applied and computational mathematics, no. 6. Cambridge: Cambridge University Press, 2002.

[8] «PDS-SE84LV-03-0625». Disponible en: https://www.gurit.com/wp-content/uploads/2025/08/PDS-SE84LV-03-0625.pdf

[9] «DURA-CORE II 5052-090922».. Disponible en: https://thegillcorp.com/wp-content/uploads/2023/03/DURA-CORE-II-5052.pdf

[9] «TFM-Hernandez-RosBriales, Antonio (1)».

APPENDIX I LAMINATE ENGINEERING DATA

Final Laminate Zone 2:

Laminate Matrices

[ABD] Matrix

N_x	+4.594E+04	+2.531E+04	+5.805E+02	+1.411E+04	+1.403E+05	+3.573E+03	ε_x^0
N_y	+2.531E+04	+4.534E+04	+5.805E+02	+1.403E+05	+2.188E+04	+3.573E+03	ε_y^0
N_{xy}	+5.805E+02	+5.805E+02	+2.603E+04	+3.573E+03	+3.573E+03	+1.419E+05	γ_{xy}^0
M_x	+1.411E+04	+1.403E+05	+3.573E+03	+7.517E+06	+4.103E+06	+9.403E+04	κ_x
M_y	+1.403E+05	+2.188E+04	+3.573E+03	+4.103E+06	+7.417E+06	+9.403E+04	κ_y
M_{xy}	+3.573E+03	+3.573E+03	+1.419E+05	+9.403E+04	+9.403E+04	+4.219E+06	κ_{xy}

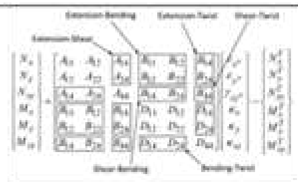

$[ABD]^{-1}$ Matrix

ε_x^0	+3.858E-05	-2.421E-05	-3.077E-07	+1.058E-06	-1.244E-06	+2.307E-09	N_x
ε_y^0	-2.421E-05	+3.892E-05	-3.146E-07	-1.244E-06	+1.031E-06	+2.852E-09	N_y
γ_{xy}^0	-3.077E-07	-3.146E-07	+4.705E-05	+2.313E-09	+2.858E-09	-1.582E-06	N_{xy}
κ_x	+1.058E-06	-1.244E-06	+2.307E-09	+2.338E-07	-1.457E-07	-1.885E-09	M_x
κ_y	-1.244E-06	+1.031E-06	+2.852E-09	-1.457E-07	+2.359E-07	-1.928E-09	M_y
κ_{xy}	+2.313E-09	+2.858E-09	-1.582E-06	-1.885E-09	-1.928E-09	+2.903E-07	M_{xy}

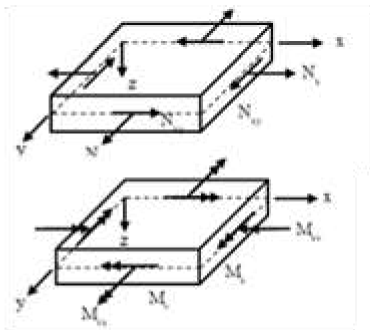

Engineering constants

	E_x	E_y	E_z	G_{xy}	G_{xz}	G_{yz}
In-plane	+9.923E+02	+9.836E+02		+8.136E+02		
Bending	+2.880E+03	+2.854E+03		+2.320E+03		
Zero-Curvature	+1.218E+03	+1.202E+03		+9.961E+02		

	ν_{xy}	ν_{yx}	ν_{xz}	ν_{zx}	ν_{yz}	ν_{zy}
In-plane	+0.627	+0.622				
Bending	+0.623	+0.617				
Zero-Curvature	+0.558	+0.551				

Homogenized Matrices

Thickness Normalized Homogenized Membrane Matrix

N_x	+1.759E+03	+9.690E+02	+2.222E+01	ε_x^0
N_y	+9.690E+02	+1.736E+03	+2.222E+01	ε_y^0
N_{xy}	+2.222E+01	+2.222E+01	+9.965E+02	γ_{xy}^0

Thickness Normalized Homogenized Bending Matrix

M_x	+4.137E+01	+4.113E+02	+1.047E+01	κ_x
M_y	+4.113E+02	+6.414E+01	+1.047E+01	κ_y
M_{xy}	+1.047E+01	+1.047E+01	+4.158E+02	κ_{xy}

Thickness Normalized Homogenized Coupling Matrix

N_x	+5.062E+03	+2.763E+03	+6.332E+01	κ_x
N_y	+2.763E+03	+4.994E+03	+6.332E+01	κ_y
N_{xy}	+6.332E+01	+6.332E+01	+2.841E+03	κ_{xy}

Final Laminate zone 5:

Laminate Matrices

[ABD] Matrix

N_x	+1.423E+05	+5.107E+04	+1.141E+03	-4.417E+05	+4.227E+05	+1.093E+04	ε_x^o
N_y	+5.107E+04	+1.032E+05	+1.141E+03	+4.227E+05	+5.968E+04	+1.093E+04	ε_y^o
N_{xy}	+1.141E+03	+1.141E+03	+5.270E+04	+1.093E+04	+1.093E+04	+4.263E+05	γ_{xy}^o
M_x	-4.417E+05	+4.227E+05	+1.093E+04	+2.442E+07	+8.801E+06	+1.965E+05	κ_x
M_y	+4.227E+05	+5.968E+04	+1.093E+04	+8.801E+06	+1.798E+07	+1.965E+05	κ_y
M_{xy}	+1.093E+04	+1.093E+04	+4.263E+05	+1.965E+05	+1.965E+05	+9.082E+06	κ_{xy}

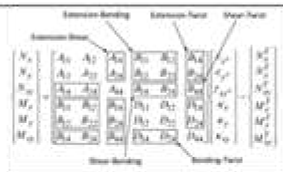

$[ABD]^{-1}$ Matrix

ε_x^o	+1.416E-05	-9.261E-06	-9.539E-08	+6.379E-07	-6.143E-07	-1.927E-09	N_x
ε_y^o	-9.261E-06	+1.655E-05	-1.321E-07	-6.225E-07	+4.675E-07	+7.819E-10	N_y
γ_{xy}^o	-9.539E-08	-1.321E-07	+3.059E-05	-1.816E-09	+6.706E-10	-1.435E-06	N_{xy}
κ_x	+6.379E-07	-6.143E-07	-1.927E-09	+8.248E-08	-5.330E-08	-5.649E-10	M_x
κ_y	-6.225E-07	+4.675E-07	+7.819E-10	-5.330E-08	+9.460E-08	-7.487E-10	M_y
κ_{xy}	-1.816E-09	+6.706E-10	-1.435E-06	-5.649E-10	-7.487E-10	+1.775E-07	M_{xy}

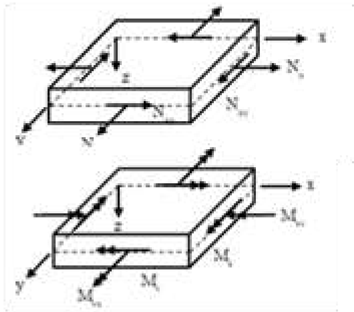

Engineering constants

	E_x	E_y	E_z	G_{xy}	G_{xz}	G_{yz}
In-plane	+2.555E+03	+2.186E+03		+1.183E+03		
Bending	+6.890E+03	+6.007E+03		+3.202E+03		
Zero-Curvature	+4.233E+03	+3.071E+03		+1.906E+03		

	ν_{xy}	ν_{yx}	ν_{xz}	ν_{zx}	ν_{yz}	ν_{zy}
In-plane	+0.654	+0.560				
Bending	+0.646	+0.563				
Zero-Curvature	+0.495	+0.359				

Homogenized Matrices

Thickness Normalized Homogenized Membrane Matrix

N_x	+5.147E+03	+1.848E+03	+4.130E+01	ε_x^o
N_y	+1.848E+03	+3.734E+03	+4.130E+01	ε_y^o
N_{xy}	+4.130E+01	+4.130E+01	+1.907E+03	γ_{xy}^o

Thickness Normalized Homogenized Bending Matrix

M_x	-1.156E+03	+1.107E+03	+2.860E+01	κ_x
M_y	+1.107E+03	+1.562E+02	+2.860E+01	κ_y
M_{xy}	+2.860E+01	+2.860E+01	+1.116E+03	κ_{xy}

Thickness Normalized Homogenized Coupling Matrix

N_x	+1.388E+04	+5.001E+03	+1.117E+02	κ_x
N_y	+5.001E+03	+1.022E+04	+1.117E+02	κ_y
N_{xy}	+1.117E+02	+1.117E+02	+5.161E+03	κ_{xy}

Final laminate Zone 6:

Laminate Matrices

[ABD] Matrix

N_x	+9.319E+04	+6.164E+04	+1.441E+03	+1.027E+04	+1.439E+05	+3.672E+03	ε_x^o
N_y	+6.164E+04	+9.259E+04	+1.441E+03	+1.439E+05	+1.843E+04	+3.672E+03	ε_y^o
N_{xy}	+1.441E+03	+1.441E+03	+6.318E+04	+3.672E+03	+3.672E+03	+1.455E+05	γ_{xy}^o
M_x	+1.027E+04	+1.439E+05	+3.672E+03	+1.609E+07	+1.052E+07	+2.458E+05	κ_x
M_y	+1.439E+05	+1.843E+04	+3.672E+03	+1.052E+07	+1.598E+07	+2.458E+05	κ_y
M_{xy}	+3.672E+03	+3.672E+03	+1.455E+05	+2.458E+05	+2.458E+05	+1.078E+07	κ_{xy}

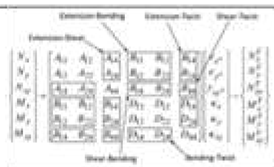

$[ABD]^{-1}$ Matrix

ε_x^o	+2.093E-05	-1.447E-05	-1.467E-07	+4.010E-07	-4.358E-07	+5.726E-10	N_x
ε_y^o	-1.447E-05	+2.103E-05	-1.490E-07	-4.358E-07	+3.930E-07	+7.514E-10	N_y
γ_{xy}^o	-1.467E-07	-1.490E-07	+1.634E-05	+5.729E-10	+7.518E-10	-2.204E-07	N_{xy}
κ_x	+4.010E-07	-4.358E-07	+5.726E-10	+1.191E-07	-8.149E-08	-8.525E-10	M_x
κ_y	-4.358E-07	+3.930E-07	+7.514E-10	-8.149E-08	+1.197E-07	-8.666E-10	M_y
κ_{xy}	+5.729E-10	+7.518E-10	-2.204E-07	-8.525E-10	-8.666E-10	+9.573E-08	M_{xy}

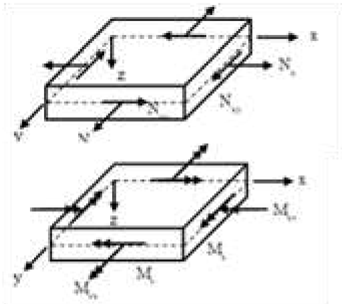

Engineering constants

	E_x	E_y	E_z	G_{xy}	G_{xz}	G_{yz}
In-plane	+1.741E+03	+1.733E+03		+2.230E+03		
Bending	+4.878E+03	+4.852E+03		+6.067E+03		
Zero-Curvature	+1.901E+03	+1.888E+03		+2.302E+03		

	ν_{xy}	ν_{yx}	ν_{xz}	ν_{zx}	ν_{yz}	ν_{zy}
In-plane	+0.691	+0.688				
Bending	+0.684	+0.681				
Zero-Curvature	+0.666	+0.661				

Homogenized Matrices

Thickness Normalized Homogenized Membrane Matrix

N_x	+3.396E+03	+2.246E+03	+5.253E+01	ε_x^o
N_y	+2.246E+03	+3.374E+03	+5.253E+01	ε_y^o
N_{xy}	+5.253E+01	+5.253E+01	+2.303E+03	γ_{xy}^o

Thickness Normalized Homogenized Bending Matrix

M_x	+2.727E+01	+3.823E+02	+9.753E+00	κ_x
M_y	+3.823E+02	+4.896E+01	+9.753E+00	κ_y
M_{xy}	+9.753E+00	+9.753E+00	+3.865E+02	κ_{xy}

Thickness Normalized Homogenized Coupling Matrix

N_x	+9.346E+03	+6.111E+03	+1.428E+02	κ_x
N_y	+6.111E+03	+9.282E+03	+1.428E+02	κ_y
N_{xy}	+1.428E+02	+1.428E+02	+6.264E+03	κ_{xy}

Final laminate Zone 8:

Laminate Matrices

[ABD] Matrix

N_x	+1.465E+05	+6.303E+04	+1.441E+03	-2.980E+05	+4.322E+05	+1.095E+04	ε_x^0
N_y	+6.303E+04	+1.080E+05	+1.441E+03	+4.322E+05	+2.091E+05	+1.095E+04	ε_y^0
N_{xy}	+1.441E+03	+1.441E+03	+6.483E+04	+1.095E+04	+1.095E+04	+4.374E+05	γ_{xy}^0
M_x	-2.980E+05	+4.322E+05	+1.095E+04	+2.561E+07	+1.087E+07	+2.482E+05	κ_x
M_y	+4.322E+05	+2.091E+05	+1.095E+04	+1.087E+07	+1.894E+07	+2.482E+05	κ_y
M_{xy}	+1.095E+04	+1.095E+04	+4.374E+05	+2.482E+05	+2.482E+05	+1.118E+07	κ_{xy}

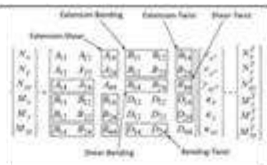

$[ABD]^{-1}$ Matrix

ε_x^0	+1.306E-05	-8.700E-06	-9.296E-08	+5.084E-07	-4.937E-07	-9.556E-10	N_x
ε_y^0	-8.700E-06	+1.573E-05	-1.445E-07	-4.988E-07	+3.112E-07	+2.930E-09	N_y
γ_{xy}^0	-9.296E-08	-1.445E-07	+2.096E-05	-8.635E-10	+2.839E-09	-8.195E-07	N_{xy}
κ_x	+5.084E-07	-4.937E-07	-9.556E-10	+7.399E-08	-4.856E-08	-5.399E-10	M_x
κ_y	-4.988E-07	+3.112E-07	+2.930E-09	-4.856E-08	+8.851E-08	-8.190E-10	M_y
κ_{xy}	-8.635E-10	+2.839E-09	-8.195E-07	-5.399E-10	-8.190E-10	+1.215E-07	M_{xy}

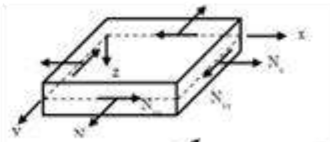

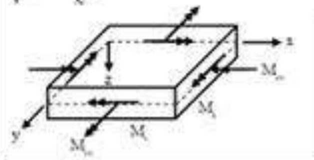

Engineering constants

	E_x	E_y	E_z	G_{xy}	G_{xz}	G_{yz}
In-plane	+2.745E+03	+2.278E+03		+1.710E+03		
Bending	+7.468E+03	+6.243E+03		+4.548E+03		
Zero-Curvature	+3.933E+03	+2.898E+03		+2.323E+03		

	ν_{xy}	ν_{yx}	ν_{xz}	ν_{zx}	ν_{yz}	ν_{zy}
In-plane	+0.666	+0.553				
Bending	+0.656	+0.549				
Zero-Curvature	+0.584	+0.430				

Homogenized Matrices

Thickness Normalized Homogenized Membrane Matrix

N_x	+5.252E+03	+2.259E+03	+5.167E+01	ε_x^0
N_y	+2.259E+03	+3.870E+03	+5.167E+01	ε_y^0
N_{xy}	+5.167E+01	+5.167E+01	+2.323E+03	γ_{xy}^0

Thickness Normalized Homogenized Bending Matrix

M_x	-7.657E+02	+1.111E+03	+2.812E+01	κ_x
M_y	+1.111E+03	+5.371E+02	+2.812E+01	κ_y
M_{xy}	+2.812E+01	+2.812E+01	+1.124E+03	κ_{xy}

Thickness Normalized Homogenized Coupling Matrix

N_x	+1.415E+04	+6.008E+03	+1.372E+02	κ_x
N_y	+6.008E+03	+1.047E+04	+1.372E+02	κ_y
N_{xy}	+1.372E+02	+1.372E+02	+6.180E+03	κ_{xy}

Final laminate Zone 9:

Laminate Matrices

[ABD] Matrix

N_x	+1.898E+05	+5.798E+04	+1.291E+03	-6.852E+04	+3.527E+05	+9.098E+03	ε_x^o
N_y	+5.798E+04	+1.134E+05	+1.291E+03	+3.527E+05	-1.468E+04	+9.098E+03	ε_y^o
N_{xy}	+1.291E+03	+1.291E+03	+5.987E+04	+9.098E+03	+9.098E+03	+3.558E+05	γ_{xy}^o
M_x	-6.852E+04	+3.527E+05	+9.098E+03	+3.272E+07	+1.034E+07	+2.307E+05	κ_x
M_y	+3.527E+05	-1.468E+04	+9.098E+03	+1.034E+07	+2.011E+07	+2.307E+05	κ_y
M_{xy}	+9.098E+03	+9.098E+03	+3.558E+05	+2.307E+05	+2.307E+05	+1.067E+07	κ_{xy}

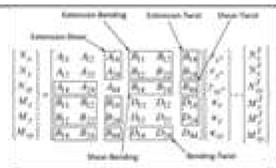

$[ABD]^{-1}$ Matrix

ε_x^o	+6.827E-06	-3.865E-06	-5.899E-08	+1.130E-07	-1.806E-07	+9.033E-10	N_x
ε_y^o	-3.865E-06	+1.139E-05	-1.546E-07	-1.849E-07	+1.712E-07	-9.690E-10	N_y
γ_{xy}^o	-5.899E-08	-1.546E-07	+2.084E-05	+9.751E-10	-1.034E-09	-6.950E-07	N_{xy}
κ_x	+1.130E-07	-1.806E-07	+9.033E-10	+3.995E-08	-2.264E-08	-3.455E-10	M_x
κ_y	-1.849E-07	+1.712E-07	-9.690E-10	-2.264E-08	+6.466E-08	-8.663E-10	M_y
κ_{xy}	+9.751E-10	-1.034E-09	-6.950E-07	-3.455E-10	-8.663E-10	+1.170E-07	M_{xy}

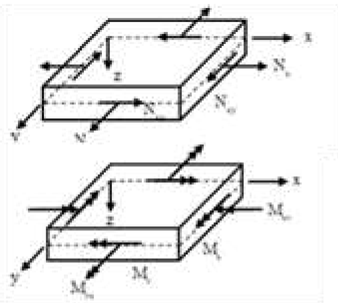

Engineering constants

	E_x	E_y	E_z	G_{xy}	G_{xz}	G_{yz}
In-plane	+5.213E+03	+3.123E+03		+1.708E+03		
Bending	+1.354E+04	+8.364E+03		+4.624E+03		
Zero-Curvature	+5.699E+03	+3.404E+03		+2.130E+03		

	ν_{xy}	ν_{yx}	ν_{xz}	ν_{zx}	ν_{yz}	ν_{zy}
In-plane	+0.566	+0.339				
Bending	+0.567	+0.350				
Zero-Curvature	+0.511	+0.305				

Homogenized Matrices

Thickness Normalized Homogenized Membrane Matrix

N_x	+6.754E+03	+2.063E+03	+4.596E+01	ε_x^o
N_y	+2.063E+03	+4.035E+03	+4.596E+01	ε_y^o
N_{xy}	+4.596E+01	+4.596E+01	+2.131E+03	γ_{xy}^o

Thickness Normalized Homogenized Bending Matrix

M_x	-1.736E+02	+8.933E+02	+2.305E+01	κ_x
M_y	+8.933E+02	-3.719E+01	+2.305E+01	κ_y
M_{xy}	+2.305E+01	+2.305E+01	+9.013E+02	κ_{xy}

Thickness Normalized Homogenized Coupling Matrix

N_x	+1.770E+04	+5.590E+03	+1.248E+02	κ_x
N_y	+5.590E+03	+1.088E+04	+1.248E+02	κ_y
N_{xy}	+1.248E+02	+1.248E+02	+5.769E+03	κ_{xy}

Final laminate Zone 10:

Laminate Matrices

[ABD] Matrix

N_x	+2.078E+05	+5.316E+04	+1.141E+03	-1.312E+06	+4.071E+05	+1.120E+04	ε_x^0
N_y	+5.316E+04	+1.303E+05	+1.141E+03	+4.071E+05	-2.702E+05	+1.120E+04	ε_y^0
N_{xy}	+1.141E+03	+1.141E+03	+5.517E+04	+1.120E+04	+1.120E+04	+4.061E+05	γ_{xy}^0
M_x	-1.312E+06	+4.071E+05	+1.120E+04	+3.695E+07	+9.580E+06	+2.065E+05	κ_x
M_y	+4.071E+05	-2.702E+05	+1.120E+04	+9.580E+06	+2.294E+07	+2.065E+05	κ_y
M_{xy}	+1.120E+04	+1.120E+04	+4.061E+05	+2.065E+05	+2.065E+05	+9.935E+06	κ_{xy}

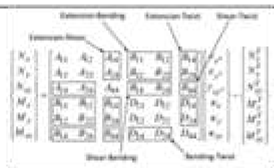

$[ABD]^{-1}$ Matrix

ε_x^0	+1.278E-05	-8.740E-06	-7.767E-08	+7.128E-07	-6.274E-07	-3.155E-09	N_x
ε_y^0	-8.740E-06	+1.439E-05	-9.746E-08	-6.202E-07	+5.837E-07	-1.628E-09	N_y
γ_{xy}^0	-7.767E-08	-9.746E-08	+2.593E-05	-3.223E-09	-1.549E-09	-1.059E-06	N_{xy}
κ_x	+7.128E-07	-6.274E-07	-3.155E-09	+7.221E-08	-5.011E-08	-4.320E-10	M_x
κ_y	-6.202E-07	+5.837E-07	-1.628E-09	-5.011E-08	+8.255E-08	-5.617E-10	M_y
κ_{xy}	-3.223E-09	-1.549E-09	-1.059E-06	-4.320E-10	-5.617E-10	+1.440E-07	M_{xy}

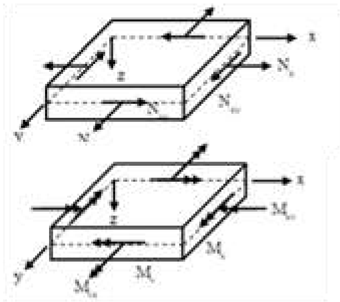

Engineering constants

	E_x	E_y	E_z	G_{xy}	G_{xz}	G_{yz}
In-plane	+2.765E+03	+2.456E+03		+1.363E+03		
Bending	+7.332E+03	+6.414E+03		+3.677E+03		
Zero-Curvature	+6.577E+03	+4.124E+03		+1.949E+03		

	ν_{xy}	ν_{yx}	ν_{xz}	ν_{zx}	ν_{yz}	ν_{zy}
In-plane	+0.684	+0.607				
Bending	+0.694	+0.607				
Zero-Curvature	+0.408	+0.256				

Homogenized Matrices

Thickness Normalized Homogenized Membrane Matrix

N_x	+7.344E+03	+1.878E+03	+4.033E+01	ε_x^0
N_y	+1.878E+03	+4.605E+03	+4.033E+01	ε_y^0
N_{xy}	+4.033E+01	+4.033E+01	+1.950E+03	γ_{xy}^0

Thickness Normalized Homogenized Bending Matrix

M_x	-3.277E+03	+1.017E+03	+2.798E+01	κ_x
M_y	+1.017E+03	-6.747E+02	+2.798E+01	κ_y
M_{xy}	+2.798E+01	+2.798E+01	+1.014E+03	κ_{xy}

Thickness Normalized Homogenized Coupling Matrix

N_x	+1.956E+04	+5.072E+03	+1.093E+02	κ_x
N_y	+5.072E+03	+1.214E+04	+1.093E+02	κ_y
N_{xy}	+1.093E+02	+1.093E+02	+5.260E+03	κ_{xy}

Final laminate Zone 11:

Laminate Matrices

[ABD] Matrix

N_x	+1.895E+05	+8.740E+04	+2.002E+03	-4.456E+05	+4.263E+05	+1.103E+04	ε_x^o
N_y	+8.740E+04	+1.505E+05	+2.002E+03	+4.263E+05	+5.624E+04	+1.103E+04	ε_y^o
N_{xy}	+2.002E+03	+2.002E+03	+8.986E+04	+1.103E+04	+1.103E+04	+4.299E+05	γ_{xy}^o
M_x	-4.456E+05	+4.263E+05	+1.103E+04	+3.399E+07	+1.597E+07	+3.662E+05	κ_x
M_y	+4.263E+05	+5.624E+04	+1.103E+04	+1.597E+07	+2.754E+07	+3.662E+05	κ_y
M_{xy}	+1.103E+04	+1.103E+04	+4.299E+05	+3.662E+05	+3.662E+05	+1.642E+07	κ_{xy}

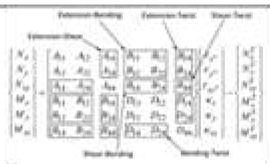

$[ABD]^{-1}$ Matrix

ε_x^o	+1.026E-05	-6.947E-06	-7.268E-08	+3.982E-07	-3.756E-07	-8.270E-10	N_x
ε_y^o	-6.947E-06	+1.165E-05	-1.010E-07	-3.801E-07	+3.043E-07	+1.182E-09	N_y
γ_{xy}^o	-7.268E-08	-1.010E-07	+1.273E-05	-7.395E-10	+1.094E-09	-3.331E-07	N_{xy}
κ_x	+3.982E-07	-3.756E-07	-8.270E-10	+5.767E-08	-3.883E-08	-4.128E-10	M_x
κ_y	-3.801E-07	+3.043E-07	+1.182E-09	-3.883E-08	+6.404E-08	-5.428E-10	M_y
κ_{xy}	-7.395E-10	+1.094E-09	-3.331E-07	-4.128E-10	-5.428E-10	+6.964E-08	M_{xy}

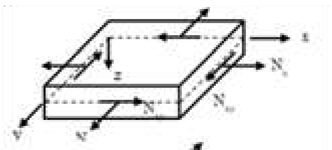

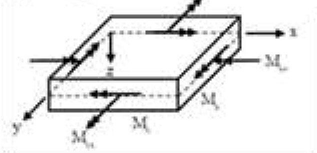

Engineering constants

	E_x	E_y	E_z	G_{xy}	G_{xz}	G_{yz}
In-plane	+3.365E+03	+2.965E+03		+2.713E+03		
Bending	+8.568E+03	+7.715E+03		+7.094E+03		
Zero-Curvature	+4.791E+03	+3.804E+03		+3.102E+03		

	ν_{xy}	ν_{yx}	ν_{xz}	ν_{zx}	ν_{yz}	ν_{zy}
In-plane	+0.677	+0.597				
Bending	+0.673	+0.606				
Zero-Curvature	+0.581	+0.461				

Homogenized Matrices

Thickness Normalized Homogenized Membrane Matrix

N_x	+6.544E+03	+3.018E+03	+6.914E+01	ε_x^o
N_y	+3.018E+03	+5.196E+03	+6.914E+01	ε_y^o
N_{xy}	+6.914E+01	+6.914E+01	+3.103E+03	γ_{xy}^o

Thickness Normalized Homogenized Bending Matrix

M_x	-1.063E+03	+1.017E+03	+2.629E+01	κ_x
M_y	+1.017E+03	+1.341E+02	+2.629E+01	κ_y
M_{xy}	+2.629E+01	+2.629E+01	+1.025E+03	κ_{xy}

Thickness Normalized Homogenized Coupling Matrix

N_x	+1.679E+04	+7.892E+03	+1.809E+02	κ_x
N_y	+7.892E+03	+1.361E+04	+1.809E+02	κ_y
N_{xy}	+1.809E+02	+1.809E+02	+8.113E+03	κ_{xy}

Final Laminate Zone 12:

Laminate Matrices

[ABD] Matrix

N_x	+2.429E+05	+8.879E+04	+2.002E+03	-7.903E+05	+7.264E+05	+1.861E+04	ε_x^o
N_y	+8.879E+04	+1.659E+05	+2.002E+03	+7.264E+05	+2.470E+05	+1.861E+04	ε_y^o
N_{xy}	+2.002E+03	+2.002E+03	+9.150E+04	+1.861E+04	+1.861E+04	+7.336E+05	γ_{xy}^o
M_x	-7.903E+05	+7.264E+05	+1.861E+04	+4.481E+07	+1.625E+07	+3.659E+05	κ_x
M_y	+7.264E+05	+2.470E+05	+1.861E+04	+1.625E+07	+3.082E+07	+3.659E+05	κ_y
M_{xy}	+1.861E+04	+1.861E+04	+7.336E+05	+3.659E+05	+3.659E+05	+1.675E+07	κ_{xy}

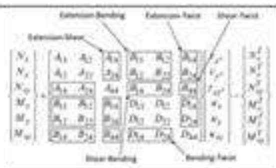

$[ABD]^{-1}$ Matrix

ε_x^o	+8.343E-06	-5.536E-06	-5.692E-08	+3.612E-07	-3.427E-07	-1.030E-09	N_x
ε_y^o	-5.536E-06	+1.017E-05	-8.756E-08	-3.465E-07	+2.318E-07	+1.196E-09	N_y
γ_{xy}^o	-5.692E-08	-8.756E-08	+1.685E-05	-9.721E-10	+1.139E-09	-7.376E-07	N_{xy}
κ_x	+3.612E-07	-3.427E-07	-1.030E-09	+4.499E-08	-2.946E-08	-3.131E-10	M_x
κ_y	-3.465E-07	+2.318E-07	+1.196E-09	-2.946E-08	+5.420E-08	-4.672E-10	M_y
κ_{xy}	-9.721E-10	+1.139E-09	-7.376E-07	-3.131E-10	-4.672E-10	+9.202E-08	M_{xy}

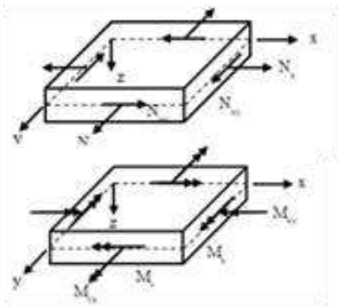

Engineering constants

	E_x	E_y	E_z	G_{xy}	G_{xz}	G_{yz}
In-plane	+4.074E+03	+3.344E+03		+2.018E+03		
Bending	+1.048E+04	+8.694E+03		+5.121E+03		
Zero-Curvature	+6.639E+03	+4.534E+03		+3.109E+03		

	ν_{xy}	ν_{yx}	ν_{xz}	ν_{zx}	ν_{yz}	ν_{zy}
In-plane	+0.664	+0.545				
Bending	+0.655	+0.543				
Zero-Curvature	+0.535	+0.365				

Homogenized Matrices

Thickness Normalized Homogenized Membrane Matrix

N_x	+8.255E+03	+3.018E+03	+6.806E+01	ε_x^o
N_y	+3.018E+03	+5.638E+03	+6.806E+01	ε_y^o
N_{xy}	+6.806E+01	+6.806E+01	+3.110E+03	γ_{xy}^o

Thickness Normalized Homogenized Bending Matrix

M_x	-1.826E+03	+1.678E+03	+4.301E+01	κ_x
M_y	+1.678E+03	+5.707E+02	+4.301E+01	κ_y
M_{xy}	+4.301E+01	+4.301E+01	+1.695E+03	κ_{xy}

Thickness Normalized Homogenized Coupling Matrix

N_x	+2.112E+04	+7.659E+03	+1.724E+02	κ_x
N_y	+7.659E+03	+1.452E+04	+1.724E+02	κ_y
N_{xy}	+1.724E+02	+1.724E+02	+7.894E+03	κ_{xy}

Final Laminate Zone 13:

Laminate Matrices

[ABD] Matrix

N_x	+1.938E+05	+9.936E+04	+2.302E+03	-3.262E+05	+4.433E+05	+1.124E+04	ε_x^o
N_y	+9.936E+04	+1.552E+05	+2.302E+03	+4.433E+05	+2.063E+05	+1.124E+04	ε_y^o
N_{xy}	+2.302E+03	+2.302E+03	+1.020E+05	+1.124E+04	+1.124E+04	+4.485E+05	γ_{xy}^o
M_x	-3.262E+05	+4.433E+05	+1.124E+04	+3.602E+07	+1.798E+07	+4.156E+05	κ_x
M_y	+4.433E+05	+2.063E+05	+1.124E+04	+1.798E+07	+2.866E+07	+4.156E+05	κ_y
M_{xy}	+1.124E+04	+1.124E+04	+4.485E+05	+4.156E+05	+4.156E+05	+1.846E+07	κ_{xy}

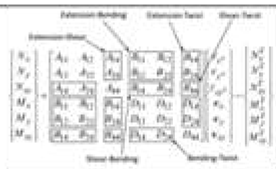

$[ABD]^{-1}$ Matrix

ε_x^o	+9.984E-06	-6.920E-06	-6.849E-08	+3.317E-07	-3.126E-07	-6.303E-10	N_x
ε_y^o	-6.920E-06	+1.148E-05	-1.003E-07	-3.146E-07	+2.218E-07	+1.753E-09	N_y
γ_{xy}^o	-6.849E-08	-1.003E-07	+1.098E-05	-5.893E-10	+1.712E-09	-2.668E-07	N_{xy}
κ_x	+3.317E-07	-3.126E-07	-6.303E-10	+5.251E-08	-3.580E-08	-3.724E-10	M_x
κ_y	-3.146E-07	+2.218E-07	+1.753E-09	-3.580E-08	+6.060E-08	-5.447E-10	M_y
κ_{xy}	-5.893E-10	+1.712E-09	-2.668E-07	-3.724E-10	-5.447E-10	+6.068E-08	M_{xy}

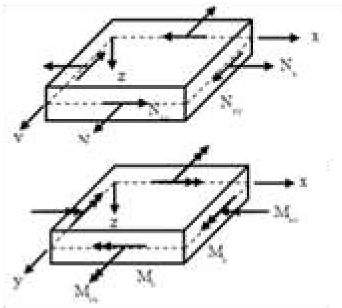

Engineering constants

	E_x	E_y	E_z	G_{xy}	G_{xz}	G_{yz}
In-plane	+3.428E+03	+2.982E+03		+3.116E+03		
Bending	+9.159E+03	+7.937E+03		+7.926E+03		
Zero-Curvature	+4.455E+03	+3.569E+03		+3.489E+03		

	ν_{xy}	ν_{yx}	ν_{xz}	ν_{zx}	ν_{yz}	ν_{zy}
In-plane	+0.693	+0.603				
Bending	+0.682	+0.591				
Zero-Curvature	+0.640	+0.513				

Homogenized Matrices

Thickness Normalized Homogenized Membrane Matrix

N_x	+6.631E+03	+3.400E+03	+7.880E+01	ε_x°
N_y	+3.400E+03	+5.313E+03	+7.880E+01	ε_y°
N_{xy}	+7.880E+01	+7.880E+01	+3.490E+03	γ_{xy}°

Thickness Normalized Homogenized Bending Matrix

M_x	-7.641E+02	+1.038E+03	+2.634E+01	κ_x
M_y	+1.038E+03	+4.833E+02	+2.634E+01	κ_y
M_{xy}	+2.634E+01	+2.634E+01	+1.051E+03	κ_{xy}

Thickness Normalized Homogenized Coupling Matrix

N_x	+1.732E+04	+8.647E+03	+1.999E+02	κ_x
N_y	+8.647E+03	+1.378E+04	+1.999E+02	κ_y
N_{xy}	+1.999E+02	+1.999E+02	+8.878E+03	κ_{xy}

Final laminate Zone 14:

Laminate Matrices

[ABD] Matrix

N_x	+2.861E+05	+8.374E+04	+1.852E+03	-5.368E+05	+6.445E+05	+1.671E+04	ε_x°
N_y	+8.374E+04	+1.713E+05	+1.852E+03	+6.445E+05	+1.535E+04	+1.671E+04	ε_y°
N_{xy}	+1.852E+03	+1.852E+03	+8.654E+04	+1.671E+04	+1.671E+04	+6.497E+05	γ_{xy}°
M_x	-5.368E+05	+6.445E+05	+1.671E+04	+5.269E+07	+1.568E+07	+3.472E+05	κ_x
M_y	+6.445E+05	+1.535E+04	+1.671E+04	+1.568E+07	+3.212E+07	+3.472E+05	κ_y
M_{xy}	+1.671E+04	+1.671E+04	+6.497E+05	+3.472E+05	+3.472E+05	+1.621E+07	κ_{xy}

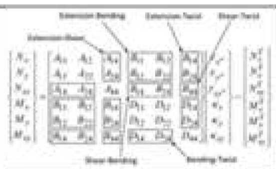

[ABD]$^{-1}$ Matrix

ε_x°	+4.978E-06	-2.929E-06	-3.871E-08	+1.356E-07	-1.647E-07	+6.255E-11	N_x
ε_y°	-2.929E-06	+7.888E-06	-9.553E-08	-1.669E-07	+1.366E-07	-6.321E-10	N_y
γ_{xy}°	-3.871E-08	-9.553E-08	+1.653E-05	+9.489E-11	-6.609E-10	-6.627E-07	N_{xy}
κ_x	+1.356E-07	-1.647E-07	+6.255E-11	+2.713E-08	-1.589E-08	-2.124E-10	M_x
κ_y	-1.669E-07	+1.366E-07	-6.321E-10	-1.589E-08	+4.213E-08	-5.069E-10	M_y
κ_{xy}	+9.489E-11	-6.609E-10	-6.627E-07	-2.124E-10	-5.069E-10	+8.829E-08	M_{xy}

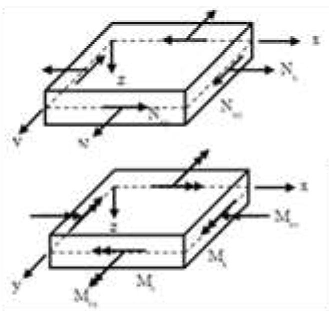

Engineering constants

	E_x	E_y	E_z	G_{xy}	G_{xz}	G_{yz}
In-plane	+6.782E+03	+4.280E+03		+2.042E+03		
Bending	+1.702E+04	+1.096E+04		+5.230E+03		
Zero-Curvature	+8.277E+03	+4.954E+03		+2.921E+03		

	ν_{xy}	ν_{yx}	ν_{xz}	ν_{zx}	ν_{yz}	ν_{zy}
In-plane	+0.588	+0.371				
Bending	+0.586	+0.377				
Zero-Curvature	+0.489	+0.293				

Homogenized Matrices

Thickness Normalized Homogenized Membrane Matrix

N_ξ	+9.660E+03	+2.827E+03	+6.254E+01	ε_ξ°
N_η	+2.827E+03	+5.782E+03	+6.254E+01	ε_η°
$N_{\xi\eta}$	+6.254E+01	+6.254E+01	+2.922E+03	$\gamma_{\xi\eta}^\circ$

Thickness Normalized Homogenized Bending Matrix

M_ξ	-1.224E+03	+1.469E+03	+3.809E+01	K_ξ
M_η	+1.469E+03	+3.500E+01	+3.809E+01	K_η
$M_{\xi\eta}$	+3.809E+01	+3.809E+01	+1.481E+03	$K_{\xi\eta}$

Thickness Normalized Homogenized Coupling Matrix

N_ξ	+2.433E+04	+7.242E+03	+1.603E+02	K_ξ
N_η	+7.242E+03	+1.483E+04	+1.603E+02	K_η
$N_{\xi\eta}$	+1.603E+02	+1.603E+02	+7.483E+03	$K_{\xi\eta}$

Final laminate Zone 15:

Laminate Matrices

[ABD] Matrix

N_ξ	+2.370E+05	+9.431E+04	+2.152E+03	-7.955E+04	+3.631E+05	+9.383E+03	ε_ξ°
N_η	+9.431E+04	+1.606E+05	+2.152E+03	+3.631E+05	-2.458E+04	+9.383E+03	ε_η°
$N_{\xi\eta}$	+2.152E+03	+2.152E+03	+9.702E+04	+9.383E+03	+9.383E+03	+3.663E+05	$\gamma_{\xi\eta}^\circ$
M_ξ	-7.955E+04	+3.631E+05	+9.383E+03	+4.387E+07	+1.737E+07	+3.958E+05	K_ξ
M_η	+3.631E+05	-2.458E+04	+9.383E+03	+1.737E+07	+2.993E+07	+3.958E+05	K_η
$M_{\xi\eta}$	+9.383E+03	+9.383E+03	+3.663E+05	+3.958E+05	+3.958E+05	+1.787E+07	$K_{\xi\eta}$

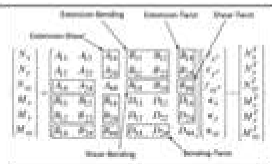

$[ABD]^{-1}$ Matrix

ε_ξ°	+5.920E-06	-3.703E-06	-4.804E-08	+9.219E-08	-1.283E-07	+6.213E-10	N_ξ
ε_η°	-3.703E-06	+8.712E-06	-1.096E-07	-1.291E-07	+1.270E-07	-3.363E-10	N_η
$\gamma_{\xi\eta}^\circ$	-4.804E-08	-1.096E-07	+1.117E-05	+6.356E-10	-3.499E-10	-2.290E-07	$N_{\xi\eta}$
K_ξ	+9.219E-08	-1.283E-07	+6.213E-10	+3.182E-08	-1.968E-08	-2.627E-10	M_ξ
K_η	-1.291E-07	+1.270E-07	-3.363E-10	-1.968E-08	+4.649E-08	-5.862E-10	M_η
$K_{\xi\eta}$	+6.356E-10	-3.499E-10	-2.290E-07	-2.627E-10	-5.862E-10	+6.069E-08	$M_{\xi\eta}$

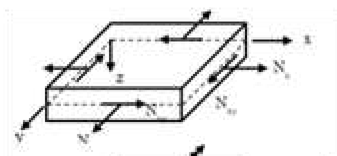

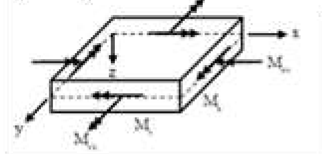

Engineering constants

	E_ξ	E_η	E_z	$G_{\xi\eta}$	$G_{\xi z}$	$G_{\eta z}$
In-plane	+5.742E+03	+3.902E+03		+3.042E+03		
Bending	+1.481E+04	+1.014E+04		+7.765E+03		
Zero-Curvature	+6.175E+03	+4.184E+03		+3.297E+03		

	$\nu_{\xi\eta}$	$\nu_{\eta\xi}$	$\nu_{\xi z}$	$\nu_{z\xi}$	$\nu_{\eta z}$	$\nu_{z\eta}$
In-plane	+0.625	+0.425				
Bending	+0.618	+0.423				
Zero-Curvature	+0.587	+0.398				

Homogenized Matrices

Thickness Normalized Homogenized Membrane Matrix

N_x	+8.057E+03	+3.206E+03	+7.316E+01	ε_x^o
N_y	+3.206E+03	+5.460E+03	+7.316E+01	ε_y^o
N_{xy}	+7.316E+01	+7.316E+01	+3.298E+03	γ_{xy}^o

Thickness Normalized Homogenized Bending Matrix

M_x	-1.838E+02	+8.391E+02	+2.168E+01	κ_x
M_y	+8.391E+02	-5.679E+01	+2.168E+01	κ_y
M_{xy}	+2.168E+01	+2.168E+01	+8.464E+02	κ_{xy}

Thickness Normalized Homogenized Coupling Matrix

N_x	+2.067E+04	+8.183E+03	+1.865E+02	κ_x
N_y	+8.183E+03	+1.411E+04	+1.865E+02	κ_y
N_{xy}	+1.865E+02	+1.865E+02	+8.419E+03	κ_{xy}

Final Laminate Zone 16:

Laminate Matrices

[ABD] Matrix

N_x	+3.042E+05	+7.892E+04	+1.702E+03	-1.822E+06	+7.102E+05	+1.911E+04	ε_x^o
N_y	+7.892E+04	+1.882E+05	+1.702E+03	+7.102E+05	-2.369E+05	+1.911E+04	ε_y^o
N_{xy}	+1.702E+03	+1.702E+03	+8.185E+04	+1.911E+04	+1.911E+04	+7.112E+05	γ_{xy}^o
M_x	-1.822E+06	+7.102E+05	+1.911E+04	+5.706E+07	+1.502E+07	+3.248E+05	κ_x
M_y	+7.102E+05	-2.369E+05	+1.911E+04	+1.502E+07	+3.531E+07	+3.248E+05	κ_y
M_{xy}	+1.911E+04	+1.911E+04	+7.112E+05	+3.248E+05	+3.248E+05	+1.556E+07	κ_{xy}

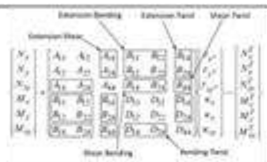

$[ABD]^{-1}$ Matrix

ε_x^o	+8.260E-06	-5.598E-06	-4.879E-08	+4.359E-07	-3.890E-07	-2.019E-09	N_x
ε_y^o	-5.598E-06	+9.554E-06	-6.247E-08	-3.876E-07	+3.415E-07	-1.043E-09	N_y
γ_{xy}^o	-4.879E-08	-6.247E-08	+2.027E-05	-2.028E-09	-1.029E-09	-9.259E-07	N_{xy}
κ_x	+4.359E-07	-3.890E-07	-2.019E-09	+4.421E-08	-3.016E-08	-2.598E-10	M_x
κ_y	-3.876E-07	+3.415E-07	-1.043E-09	-3.016E-08	+5.126E-08	-3.349E-10	M_y
κ_{xy}	-2.028E-09	-1.029E-09	-9.259E-07	-2.598E-10	-3.349E-10	+1.066E-07	M_{xy}

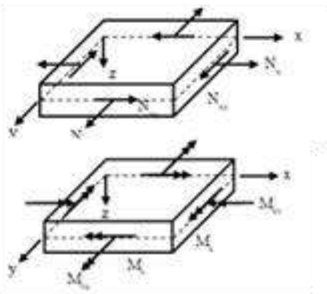

Engineering constants

	E_x	E_y	E_z	G_{xy}	G_{xz}	G_{yz}
In-plane	+4.060E+03	+3.510E+03		+1.655E+03		
Bending	+1.024E+04	+8.828E+03		+4.246E+03		
Zero-Curvature	+9.090E+03	+5.624E+03		+2.744E+03		

	v_{xy}	v_{yx}	v_{xz}	v_{zx}	v_{yz}	v_{zy}
In-plane	+0.678	+0.586				
Bending	+0.682	+0.588				
Zero-Curvature	+0.419	+0.259				

Homogenized Matrices

Thickness Normalized Homogenized Membrane Matrix

N_x	+1.020E+04	+2.647E+03	+5.709E+01	ε_x^o
N_y	+2.647E+03	+6.311E+03	+5.709E+01	ε_y^o
N_{xy}	+5.709E+01	+5.709E+01	+2.745E+03	γ_{xy}^o

Thickness Normalized Homogenized Bending Matrix

M_x	-4.099E+03	+1.597E+03	+4.299E+01	K_x
M_y	+1.597E+03	-5.328E+02	+4.299E+01	K_y
M_{xy}	+4.299E+01	+4.299E+01	+1.600E+03	K_{xy}

Thickness Normalized Homogenized Coupling Matrix

N_x	+2.582E+04	+6.795E+03	+1.470E+02	K_x
N_y	+6.795E+03	+1.598E+04	+1.470E+02	K_y
N_{xy}	+1.470E+02	+1.470E+02	+7.044E+03	K_{xy}

Final laminate Zone 17:

Laminate Matrices

[ABD] Matrix

N_x	+2.904E+05	+9.570E+04	+2.152E+03	-4.317E+05	+6.601E+05	+1.688E+04	ε_x^o
N_y	+9.570E+04	+1.760E+05	+2.152E+03	+6.601E+05	+1.741E+05	+1.688E+04	ε_y^o
N_{xy}	+2.152E+03	+2.152E+03	+9.867E+04	+1.688E+04	+1.688E+04	+6.670E+05	γ_{xy}^o
M_x	-4.317E+05	+6.601E+05	+1.688E+04	+5.363E+07	+1.806E+07	+4.065E+05	κ_x
M_y	+6.601E+05	+1.741E+05	+1.688E+04	+1.806E+07	+3.340E+07	+4.065E+05	κ_y
M_{xy}	+1.688E+04	+1.688E+04	+6.670E+05	+4.065E+05	+4.065E+05	+1.862E+07	κ_{xy}

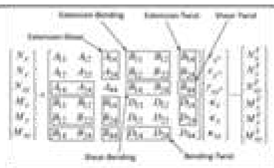

$[ABD]^{-1}$ Matrix

ε_x^o	+4.985E-06	-3.042E-06	-3.948E-08	+1.289E-07	-1.524E-07	+1.645E-10	N_x
ε_y^o	-3.042E-06	+7.817E-06	-9.719E-08	-1.556E-07	+1.036E-07	+2.874E-10	N_y
γ_{xy}^o	-3.948E-08	-9.719E-08	+1.338E-05	+2.181E-10	+2.365E-10	-4.790E-07	N_{xy}
κ_x	+1.289E-07	-1.524E-07	+1.645E-10	+2.713E-08	-1.641E-08	-2.177E-10	M_x
κ_y	-1.556E-07	+1.036E-07	+2.874E-10	-1.641E-08	+4.129E-08	-5.075E-10	M_y
κ_{xy}	+2.181E-10	+2.365E-10	-4.790E-07	-2.177E-10	-5.075E-10	+7.088E-08	M_{xy}

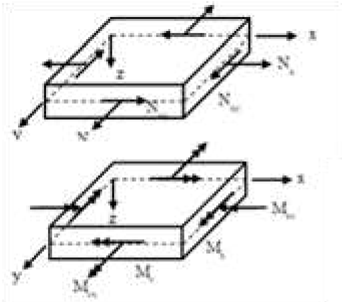

Engineering constants

	E_x	E_y	E_z	G_{xy}	G_{xz}	G_{yz}
In-plane	+6.713E+03	+4.282E+03		+2.502E+03		
Bending	+1.658E+04	+1.089E+04		+6.346E+03		
Zero-Curvature	+7.976E+03	+4.835E+03		+3.301E+03		

	ν_{xy}	ν_{yx}	ν_{xz}	ν_{zx}	ν_{yz}	ν_{zy}
In-plane	+0.610	+0.389				
Bending	+0.605	+0.397				
Zero-Curvature	+0.544	+0.329				

Homogenized Matrices

Thickness Normalized Homogenized Membrane Matrix

N_x	+9.718E+03	+3.203E+03	+7.204E+01	ε_x^o
N_y	+3.203E+03	+5.892E+03	+7.204E+01	ε_y^o
N_{xy}	+7.204E+01	+7.204E+01	+3.302E+03	γ_{xy}^o

Thickness Normalized Homogenized Bending Matrix

M_x	-9.672E+02	+1.479E+03	+3.782E+01	κ_x
M_y	+1.479E+03	+3.900E+02	+3.782E+01	κ_y
M_{xy}	+3.782E+01	+3.782E+01	+1.494E+03	κ_{xy}

Thickness Normalized Homogenized Coupling Matrix

N_x	+2.412E+04	+8.125E+03	+1.828E+02	κ_x
N_y	+8.125E+03	+1.502E+04	+1.828E+02	κ_y
N_{xy}	+1.828E+02	+1.828E+02	+8.376E+03	κ_{xy}

Final laminate Zone 18:

Laminate Matrices

[ABD] Matrix

N_x	+3.084E+05	+9.088E+04	+2.002E+03	-1.681E+06	+7.178E+05	+1.908E+04	ε_x^o
N_y	+9.088E+04	+1.930E+05	+2.002E+03	+7.178E+05	-8.324E+04	+1.908E+04	ε_y^o
N_{xy}	+2.002E+03	+2.002E+03	+9.397E+04	+1.908E+04	+1.908E+04	+7.204E+05	γ_{xy}^o
M_x	-1.681E+06	+7.178E+05	+1.908E+04	+5.865E+07	+1.739E+07	+3.839E+05	κ_x
M_y	+7.178E+05	-8.324E+04	+1.908E+04	+1.739E+07	+3.651E+07	+3.839E+05	κ_y
M_{xy}	+1.908E+04	+1.908E+04	+7.204E+05	+3.839E+05	+3.839E+05	+1.798E+07	κ_{xy}

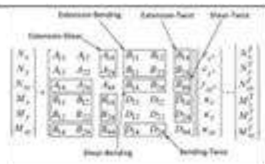

$[ABD]^{-1}$ Matrix

ε_x^o	+7.714E-06	-5.228E-06	-4.953E-08	+3.886E-07	-3.487E-07	-1.505E-09	N_x
ε_y^o	-5.228E-06	+9.058E-06	-6.955E-08	-3.463E-07	+2.885E-07	-4.231E-11	N_y
γ_{xy}^o	-4.953E-08	-6.955E-08	+1.536E-05	-1.535E-09	-9.641E-12	-6.153E-07	N_{xy}
κ_x	+3.886E-07	-3.487E-07	-1.505E-09	+4.068E-08	-2.781E-08	-2.583E-10	M_x
κ_y	-3.463E-07	+2.885E-07	-4.231E-11	-2.781E-08	+4.816E-08	-3.703E-10	M_y
κ_{xy}	-1.535E-09	-9.641E-12	-6.153E-07	-2.583E-10	-3.703E-10	+9.028E-08	M_{xy}

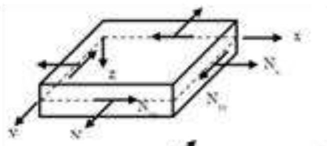

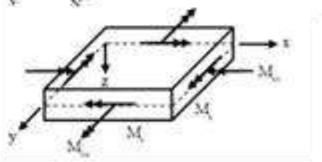

Engineering constants

	E_x	E_y	E_z	G_{xy}	G_{xz}	G_{yz}
In-plane	+4.310E+03	+3.670E+03		+2.164E+03		
Bending	+1.084E+04	+9.155E+03		+5.492E+03		
Zero-Curvature	+8.830E+03	+5.524E+03		+3.123E+03		

	ν_{xy}	ν_{yx}	ν_{xz}	ν_{zx}	ν_{yz}	ν_{zy}
In-plane	+0.678	+0.577				
Bending	+0.684	+0.577				
Zero-Curvature	+0.471	+0.295				

Homogenized Matrices

Thickness Normalized Homogenized Membrane Matrix

N_x	+1.025E+04	+3.021E+03	+6.657E+01	ε_x^o
N_y	+3.021E+03	+6.415E+03	+6.657E+01	ε_y^o
N_{xy}	+6.657E+01	+6.657E+01	+3.124E+03	γ_{xy}^o

Thickness Normalized Homogenized Bending Matrix

M_x	-3.717E+03	+1.587E+03	+4.217E+01	κ_x
M_y	+1.587E+03	-1.840E+02	+4.217E+01	κ_y
M_{xy}	+4.217E+01	+4.217E+01	+1.592E+03	κ_{xy}

Thickness Normalized Homogenized Coupling Matrix

N_x	+2.586E+04	+7.670E+03	+1.693E+02	κ_x
N_y	+7.670E+03	+1.610E+04	+1.693E+02	κ_y
N_{xy}	+1.693E+02	+1.693E+02	+7.928E+03	κ_{xy}

Final Laminate Zone 19:

Laminate Matrices

[ABD] Matrix

N_x	+3.334E+05	+1.201E+05	+2.713E+03	-5.479E+05	+6.550E+05	+1.699E+04	ε_x^0
N_y	+1.201E+05	+2.185E+05	+2.713E+03	+6.550E+05	+5.461E+03	+1.699E+04	ε_y^0
N_{xy}	+2.713E+03	+2.713E+03	+1.237E+05	+1.699E+04	+1.699E+04	+6.602E+05	γ_{xy}^0
M_x	-5.479E+05	+6.550E+05	+1.699E+04	+6.498E+07	+2.350E+07	+5.309E+05	κ_x
M_y	+6.550E+05	+5.461E+03	+1.699E+04	+2.350E+07	+4.301E+07	+5.309E+05	κ_y
M_{xy}	+1.699E+04	+1.699E+04	+6.602E+05	+5.309E+05	+5.309E+05	+2.421E+07	κ_{xy}

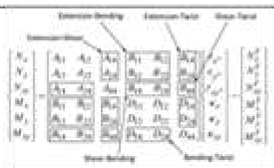

$[ABD]^{-1}$ Matrix

ε_x^0	+4.431E-06	-2.765E-06	-3.506E-08	+1.116E-07	-1.281E-07	+1.493E-10	N_x
ε_y^0	-2.765E-06	+6.481E-06	-7.868E-08	-1.291E-07	+1.119E-07	-8.479E-11	N_y
γ_{xy}^0	-3.506E-08	-7.868E-08	+9.463E-06	+1.673E-10	-1.021E-10	-2.580E-07	N_{xy}
κ_x	+1.116E-07	-1.281E-07	+1.493E-10	+2.273E-08	-1.410E-08	-1.815E-10	M_x
κ_y	-1.291E-07	+1.119E-07	-8.479E-11	-1.410E-08	+3.290E-08	-3.980E-10	M_y
κ_{xy}	+1.673E-10	-1.021E-10	-2.580E-07	-1.815E-10	-3.980E-10	+4.835E-08	M_{xy}

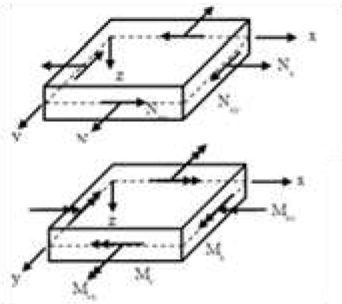

Engineering constants

	E_x	E_y	E_z	G_{xy}	G_{xz}	G_{yz}
In-plane	+7.294E+03	+4.987E+03		+3.415E+03		
Bending	+1.782E+04	+1.231E+04		+8.379E+03		
Zero-Curvature	+8.642E+03	+5.664E+03		+3.997E+03		

	ν_{xy}	ν_{yx}	ν_{xz}	ν_{zx}	ν_{yz}	ν_{zy}
In-plane	+0.624	+0.427				
Bending	+0.620	+0.429				
Zero-Curvature	+0.549	+0.360				

Homogenized Matrices

Thickness Normalized Homogenized Membrane Matrix

N_x	+1.077E+04	+3.881E+03	+8.770E+01	ε_x^0
N_y	+3.881E+03	+7.063E+03	+8.770E+01	ε_y^0
N_{xy}	+8.770E+01	+8.770E+01	+3.998E+03	γ_{xy}^0

Thickness Normalized Homogenized Bending Matrix

M_x	-1.145E+03	+1.368E+03	+3.550E+01	κ_x
M_y	+1.368E+03	+1.141E+01	+3.550E+01	κ_y
M_{xy}	+3.550E+01	+3.550E+01	+1.379E+03	κ_{xy}

Thickness Normalized Homogenized Coupling Matrix

N_x	+2.633E+04	+9.522E+03	+2.151E+02	κ_x
N_y	+9.522E+03	+1.742E+04	+2.151E+02	κ_y
N_{xy}	+2.151E+02	+2.151E+02	+9.809E+03	κ_{xy}

Final Lamiante Zone 20:

Laminate Matrices

[ABD] Matrix

N_x	+3.376E+05	+1.320E+05	+3.013E+03	-4.671E+05	+6.780E+05	+1.737E+04	ε_x^o
N_y	+1.320E+05	+2.233E+05	+3.013E+03	+6.780E+05	+1.649E+05	+1.737E+04	ε_y^o
N_{xy}	+3.013E+03	+3.013E+03	+1.358E+05	+1.737E+04	+1.737E+04	+6.849E+05	γ_{xy}^o
M_x	-4.671E+05	+6.780E+05	+1.737E+04	+6.674E+07	+2.583E+07	+5.883E+05	κ_x
M_y	+6.780E+05	+1.649E+05	+1.737E+04	+2.583E+07	+4.446E+07	+5.883E+05	κ_y
M_{xy}	+1.737E+04	+1.737E+04	+6.849E+05	+5.883E+05	+5.883E+05	+2.657E+07	κ_{xy}

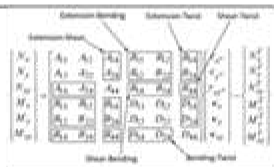

$[ABD]^{-1}$ Matrix

ε_x^o	+4.479E-06	-2.884E-06	-3.438E-08	+1.070E-07	-1.197E-07	+1.264E-10	N_x
ε_y^o	-2.884E-06	+6.486E-06	-7.762E-08	-1.210E-07	+9.023E-08	+3.276E-10	N_y
γ_{xy}^o	-3.438E-08	-7.762E-08	+8.465E-06	+1.499E-10	+3.047E-10	-2.181E-07	N_{xy}
κ_x	+1.070E-07	-1.197E-07	+1.264E-10	+2.247E-08	-1.423E-08	-1.771E-10	M_x
κ_y	-1.210E-07	+9.023E-08	+3.276E-10	-1.423E-08	+3.226E-08	-3.876E-10	M_y
κ_{xy}	+1.499E-10	+3.047E-10	-2.181E-07	-1.771E-10	-3.876E-10	+4.327E-08	M_{xy}

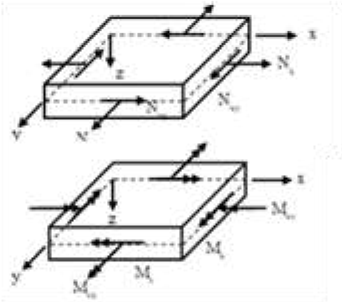

Engineering constants

	E_x	E_y	E_z	G_{xy}	G_{xz}	G_{yz}
In-plane	+7.156E+03	+4.942E+03		+3.786E+03		
Bending	+1.758E+04	+1.225E+04		+9.132E+03		
Zero-Curvature	+8.318E+03	+5.501E+03		+4.352E+03		

	ν_{xy}	ν_{yx}	ν_{xz}	ν_{zx}	ν_{yz}	ν_{zy}
In-plane	+0.644	+0.445				
Bending	+0.633	+0.441				
Zero-Curvature	+0.591	+0.391				

Homogenized Matrices

Thickness Normalized Homogenized Membrane Matrix

N_x	+1.082E+04	+4.232E+03	+9.658E+01	ε_x^o
N_y	+4.232E+03	+7.157E+03	+9.658E+01	ε_y^o
N_{xy}	+9.658E+01	+9.658E+01	+4.353E+03	γ_{xy}^o

Thickness Normalized Homogenized Bending Matrix

M_x	-9.597E+02	+1.393E+03	+3.568E+01	κ_x
M_y	+1.393E+03	+3.389E+02	+3.568E+01	κ_y
M_{xy}	+3.568E+01	+3.568E+01	+1.407E+03	κ_{xy}

Thickness Normalized Homogenized Coupling Matrix

N_x	+2.637E+04	+1.020E+04	+2.324E+02	κ_x
N_y	+1.020E+04	+1.757E+04	+2.324E+02	κ_y
N_{xy}	+2.324E+02	+2.324E+02	+1.050E+04	κ_{xy}

Final laminate Zone 21:

Laminate Matrices

[ABD] Matrix

N_x	+4.047E+05	+1.166E+05	+2.563E+03	-2.228E+06	+1.033E+06	+2.730E+04	ε_x^0
N_y	+1.166E+05	+2.508E+05	+2.563E+03	+1.033E+06	-4.979E+04	+2.730E+04	ε_y^0
N_{xy}	+2.563E+03	+2.563E+03	+1.206E+05	+2.730E+04	+2.730E+04	+1.037E+06	γ_{xy}^0
M_x	-2.228E+06	+1.033E+06	+2.730E+04	+8.123E+07	+2.357E+07	+5.185E+05	κ_x
M_y	+1.033E+06	-4.979E+04	+2.730E+04	+2.357E+07	+5.031E+07	+5.185E+05	κ_y
M_{xy}	+2.730E+04	+2.730E+04	+1.037E+06	+5.185E+05	+5.185E+05	+2.437E+07	κ_{xy}

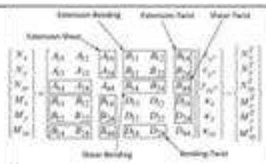

$[ABD]^{-1}$ Matrix

ε_x^0	+5.817E-06	-3.923E-06	-3.657E-08	+2.837E-07	-2.562E-07	-1.151E-09	N_x
ε_y^0	-3.923E-06	+6.904E-06	-5.130E-08	-2.554E-07	+2.070E-07	-1.264E-10	N_y
γ_{xy}^0	-3.657E-08	-5.130E-08	+1.308E-05	-1.159E-09	-1.167E-10	-5.565E-07	N_{xy}
κ_x	+2.837E-07	-2.562E-07	-1.151E-09	+2.905E-08	-1.968E-08	-1.817E-10	M_x
κ_y	-2.554E-07	+2.070E-07	-1.264E-10	-1.968E-08	+3.456E-08	-2.567E-10	M_y
κ_{xy}	-1.159E-09	-1.167E-10	-5.565E-07	-1.817E-10	-2.567E-10	+6.474E-08	M_{xy}

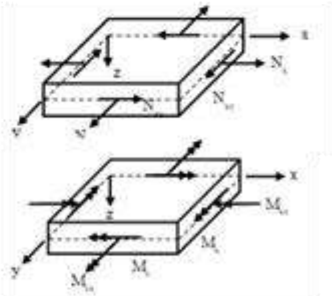

Engineering constants

	E_x	E_y	E_z	G_{xy}	G_{xz}	G_{yz}
In-plane	+5.440E+03	+4.584E+03		+2.420E+03		
Bending	+1.309E+04	+1.100E+04		+5.874E+03		
Zero-Curvature	+1.109E+04	+6.873E+03		+3.817E+03		

	ν_{xy}	ν_{yx}	ν_{xz}	ν_{zx}	ν_{yz}	ν_{zy}
In-plane	+0.674	+0.568				
Bending	+0.678	+0.569				
Zero-Curvature	+0.465	+0.288				

Homogenized Matrices

Thickness Normalized Homogenized Membrane Matrix

N_x	+1.281E+04	+3.691E+03	+8.112E+01	ε_x^0
N_y	+3.691E+03	+7.938E+03	+8.112E+01	ε_y^0
N_{xy}	+8.112E+01	+8.112E+01	+3.818E+03	γ_{xy}^0

Thickness Normalized Homogenized Bending Matrix

M_x	-4.462E+03	+2.068E+03	+5.468E+01	κ_x
M_y	+2.068E+03	-9.973E+01	+5.468E+01	κ_y
M_{xy}	+5.468E+01	+5.468E+01	+2.078E+03	κ_{xy}

Thickness Normalized Homogenized Coupling Matrix

N_x	+3.089E+04	+8.962E+03	+1.972E+02	κ_x
N_y	+8.962E+03	+1.913E+04	+1.972E+02	κ_y
N_{xy}	+1.972E+02	+1.972E+02	+9.267E+03	κ_{xy}